INTELLIGENT EDDY CURRENT CRACK DETECTION SYSTEM DESIGN BASED ON NEURO-FUZZY LOGIC

Baoguang Xu

A thesis
in
The Department
of
Mechanical & Industrial Engineering

Presented in Partial Fulfillment of the Requirements
For the Degree of Master of Applied Science
Concordia University
Montréal, Québec, Canada

September 2014
© Baoguang Xu, 2014

Concordia University
School of Graduate Studies

This is to certify that the thesis prepared

By: **Baoguang Xu**

Entitled: **Intelligent Eddy Current Crack Detection System Design Based on Neuro-Fuzzy Logic**

and submitted in partial fulfillment of the requirements for the degree of

Master of Applied Science

complies with the regulations of this University and meets the accepted standards with respect to originality and quality.

Signed by the final examining commitee:

_____ Chair

Mamoun Medraj

_____ Examiner

Henry Hong

_____ External Examiner

Lopes, Luiz A.C.

_____ Supervisor

Wenfang Xie

_____ Co-supervisor

Martin Viens

Approved _____
Chair of Department or Graduate Program Director

_____ 20 _____ _____
Dean of Faculty

Abstract

Intelligent Eddy Current Crack Detection System Design Based on Neuro-Fuzzy Logic

Baoguang Xu

The purpose of this study is to develop an artificial intelligent eddy current crack detection system in collaboration with 6-Degree-of-Freedom (DOF) robotic arm in order to provide the end users with reliable crack information.

In this particular study, the main focus is on data fusion which includes signal filtering, signal feature extraction, feature recognition, and final decision making. Various features such as the amplitude, phase angle and width of the loop from the measured differential eddy current test (ECT) signals are extracted to represent the changes of the electrical impedance of the ECT probe due to crack presence. Furthermore, a data base has been built for the extracted features from the known notch cracks purchased from Olympus. An adaptive neuro-fuzzy inference engine is trained to map the complex and nonlinear relationship between the extracted features and the crack information. The experimental tests show that not only the developed intelligent system is able to extract signal features and provide the user with 1. defect presence, 2. predict the depth of unknown crack based on the trained fuzzy logic engine. In addition, in terms of experimental setup, a data acquisition system implemented with 6 DOF robot arm for ECT is established. Extra works such as coordinate calibration, prototype probe holder design, on-line crack position location detection has also been carried out.

Acknowledgments

First of all, I would like to express my gratitude to Concordia University and CRIAQ (Consortium for Research and Innovation in Aerospace in Qubec) which provide me with such a good opportunity be part of this project and also my supervisor Dr. Wenfang Xie my co-supervisor Dr. Martin Viens, who mentored and inspired me with their patience, enthusiasm, and academic professional.

In addition thanks to École de technologie supérieure, Polytechnique Montreal, Laval University, NRC Aerospace Manufacturing Technology Centre with their laboratory equipment and training, also my teammates from individual universities. I also appreciate the support and guidance from our industry partners: L3 communications, Pratt & Whitney Canada.

Finally thanks to my family, especially my parents. Nothing would have happen without their unconditional love and support!

Baoguang Xu Montreal Canada

Contents

List of Figures vii

List of Tables x

List of Symbols and Abbreviations xi

1 Introduction 1

1.1 Non-Destructive Test 1
1.2 Eddy Current Test 4
1.3 Project motivation and work plan 5
1.4 Contribution of thesis 5
1.5 Thesis outline 6

2 Background knowledge and Literature Review 8

2.1 Introduction 8
2.2 Digital signal processing 8
2.3 Eddy current test principle 12
2.4 Factors Influencing ECT 16
2.4.1 Frequency 16
2.4.2 Configuration of testing probe 18
2.4.3 Surface geometry 22
2.4.4 Electrical conductivity of testing material 23
2.4.5 Ferromagnetic 23
2.5 Neuro-Fuzzy Logic 24
2.5.1 Fuzzy Logic 24
2.5.2 Fuzzy sets and membership functions 25

2.5.3 Fuzzy rules and fuzzy set operation 28
2.5.4 Neuro-Fuzzy Logic 31
2.5.5 ECT related Literatures 33
2.6 Conclusion 35

3 Eddy Current Signal Processing and Fuzzy Logic Implementation 36
3.1 Introduction 36
3.2 Design Diagram 36
3.3 Signal noise removal and filter design 37
3.4 Signal feature extraction 48
3.5 Fuzzy logic implementation 53
3.6 Fuzzy logic training 56
3.7 Conclusion 58

4 Experimental Setup Design 59
4.1 Introduction 59
4.2 ECT equipment and data acquisition system 59
4.3 ECT testing method and YASKAWA MOTOMAN SV3X Robot . . . 61
4.4 Probe holder design 68
4.5 Interface software design 79
4.6 Conclusion 81

5 Experimental results 83
5.1 ECT data aquired from crack pendicular to scan surface 83
5.1.1 Data analysis and fuzzy decision making results 87
5.2 ECT data aquired from crack with angle to scan surface 90
5.3 Conclusion 99

6 Conclusion 101
6.1 Summary of research work 101
6.2 Future work 102
6.3 Acknowledgements 103

Bibliography 103

List of Figures

1.1 Radial cracks around a rivet hole in airplane structure [1] 2
2.1 Measurement of certain depth [2] 10
2.2 Highpass fliter [2] 11
2.3 Lowpass fliter [2] 11
2.4 Eddy current generation [3] 13
2.5 Finite elements of eddy current in a coil [4] 14
2.6 ECT depth of pentration [5] 18
2.7 ECT absolute probe(a), ECT absolute probe crack signal (b) 19
2.8 ECT differential probe(a), ECT differential probe crack signal (b) . . 20
2.9 Scan orientation vertical to crack (a), parallel to crack (b) 21
2.10 Fuzzy logic interface [6] 25
2.11 People's height identification using classic crisp 26
2.12 People's height identification using fuzzy crisp 27
2.13 Fuzzy logic membership functions 28
2.14 Fuzzy set 29
2.15 Union of fuzzy sets 29
2.16 Intersection offuzzy sets 30
2.17 Complement offuzzy sets 31
2.18 Neuro-Fuzzy structure [7] [8] 32
3.1 Overall system diagram 37
3.2 Mallat wavelet transform 39
3.3 Multi-layer Mallat wavelet transform 39
3.4 Functions of Biorthogonal Wavelet bior 6.8 40
3.5 Biorthogonal wavelet filter design using matlab 41
3.6 ECT signal on x-axis before applying wavelet filter 42
3.7 ECT signal on x-axis after applying wavelet filter 42

3.8 ECT signal on y-axis before applying wavelet filter 43
3.9 ECT signal on y-axis after applying wavelet filter 44
3.10 ECT signal on xy-axis before applying wavelet filter 45
3.11 ECT signal on xy-axis after applying wavelet filter 45
3.12 Signal affected by Lift off 46
3.13 Crack signal fetch principle 47
3.14 (a) x-axis signal fetch result, (b) y-axis signal fetch result 47
3.15 x-y axis signal fetch result 48
3.16 Impedance of eddy current test 49
3.17 Typical crack signal from differential probe 50
3.18 "8" shaped signal generation 51
3.19 Feature extraction flow chart 52
3.20 Result of feature extraction 53
3.21 Flow chart of fuzzy logic 54
3.22 Neuro mapping structure 55
3.23 Fuzzy rules samples after training (part of) 56
3.24 ANFIS training (MFs and number of MFs selection) in matlab . . . 57
3.25 ANFIS training interface 57
4.1 Flow chat of robot communication 62
4.2 x (or y) axis sinusoid ECT signal 64
4.3 Flow chart of average value calculation algorithm 65
4.4 Total area calculation of a curve plot 66
4.5 Issue of overlap after on/off delay function 67
4.6 Simulink function for data average 68
4.7 Probe holder initial design (a), and robot arm stem (b) 69
4.8 Robot tool teaching [9] 70
4.9 User coordinate identification [9] 71
4.10 Calibration error results in scan path tilt 72
4.11 Ball bearing slider 74
4.12 Concept of spring loaded design 75
4.13 (a) Original holder grip design, (b) Double grip design for new holder 76
4.14 Spring load holder 3D assembly drawing 77
4.15 Spring loaded holder with probe installed 78

4.16 Spring loaded holder installation with robot arm and ECT equipment 79
4.17 ECT user friendly interface 80
4.18 User interface function group1 81
4.19 User interface function group2 81
5.1 Angled crack sample spec. 90
5.2 10 degree with test frequency of 0.1MHz. 91
5.3 10 degree with test frequency of 0.5MHz. 91
5.4 10 degree with test frequency of 1.5MHz. 92
5.5 20 degree with test frequency of 0.1MHz. 94
5.6 20 degree with test frequency of 0.5MHz. 94
5.7 20 degree with test frequency of 1.5MHz. 95
5.8 40 degree with test frequency of 0.1MHz. 97
5.9 40 degree with test frequency of 0.5MHz. 97
5.10 40 degree with test frequency of 1.5MHz. 98
A.1 UniWest US-454 [10] 109
A.2 Olympus Nortec 500S [11] 110
B.1 National Instruments NI PCI-6229 [12] 112
B.2 National Instruments NI USB-6009 [13] 113
C.1 SV3X robot arm axis [14] 114
C.2 SV3X robot arm operation area1 [15] 115
C.3 SV3X robot arm operation area2 [15] 115

List of Tables

4.1 Spring loaded mechanism options 73
5.1 ECT signal features of sample 1 with frequency from 0.4Mhz to 0.8MHz 84
5.2 ECT signal features of sample 1 with frequency from 0.9MHz to 2.0MHz 85
5.3 ECT signal features of sample 2 with frequency from 0.4Mhz to 0.8MHz 86
5.4 ECT signal features of sample 2 with frequency from 0.9MHz to 2.0MHz 87
5.5 Fuzzy logic decision making results 89
5.6 Fuzzy logic decision making result with width 90
5.7 ECT signal features of angled sample (10degree) with different frequencies 93
5.8 ECT signal features of angled sample (20degree) with different frequencies 96
5.9 ECT signal features of angled sample (40degree) with different frequency 99

List of Symbols and Abbreviations

$f(t)$	Signal function over time
t	Time
T	Total time period
n	Total amount of f functions
A	Dynamic Bayesian Networks
D	Electric flux density
B	Magnetic flux density
E	Electric field
H	Magnetic field
J	Current density
ρ	Electric charge density
ε	Permittivity
μ	Permeability
σ	Conductivity
Z_i	Impedance
A_i	Magnetic vector potential
r_i	Radius of circular loop

I_S	Impressed current
Z	Total impedance
R	Resistance of coil
X_L	Reactance of coil
L	Inductance
f	Frequency
δ	Skin depth
ω	Excitation frequency
C	Wavelet coefficient
(x_0, y_0)	ECT signal center point
(x_{max}, y_{max})	ECT signal peak point
k	Slope ratio of peak point and center point
ABS	Acrylonitrile butadiene styrene
ANFIS	Adaptive-Network-Based Fuzzy Inference System
DAQ	Data acquisition
DOF	Degree-Of-Freedom
DSP	Digital Signal Processing
ECT	Eddy current test
FIR	Finite Impulse Response
FPI	Fluorescent Penetrant Inspection
HPF	High pass filter
LPF	Low pass filter

MF	Membership function
MISO	Multiple-inputsingle-output
NDT	Non-destructive Testing
NRC	National Research Council
UT	Ultrasonic Testing
ORG	Original point
PE	Polyethylene
SS	Stainless steel

Chapter 1

Introduction

In aircraft engine manufacturing and aircraft maintenance industries, eddy current testing (ECT) is widely used to detect surface or subsurface crack. However, most of the ECTs in maintenance, are currently conducted by human inspectors, whose individual experiences may yield to differences in results interpretation. In addition, manpower assigned to such tasks results in significant recurrent costs and is time consuming. In order to stay in the leading and competitive position in aerospace industry, two Canadian aerospace companies P&W and L3 communications, need an automatized ECT detection solution to help them improve their efficiency, reduce man power and product costs which lead to this study.

In this chapter, a brief introduction about aerospace Non-destructive Testing (NDT), eddy current test applications, and work motivation and the purpose of using automated robot operation system will be given.

1.1 Non-Destructive Test

Non-destructive testing (NDT) is a group of techniques used in science and industry for evaluating the properties of materials, components, systems, without causing damage. As one of the quality control methods, NDT has been applied in many areas including process control, metal detection and parts inspection and maintenance etc. In aerospace industry particularly, NDT is not only necessary but also crucial, since life can be at risk with presence of certain imperfection. There are mainly two categories of aircraft defects: manufacture defect caused by the manufacture procedure

such as casting, welding, molding and aircraft assembly, and failures created during the application, such as fatigue, corrosion, fretting and impact induced damages, which have more complicated defect geometry. Despite there are numerous explanations of fatigue failure generation, the main reason behind the phenomena is because aircraft components as well as airplane structures are designed to withstand certain load. Under such circumstance where the components are under high stress relative to its material strength, with environment factor acting as a catalyst such as heat, acid, and humidy, flaws such as crack and corrosion are created and could propagate quickly [16]. For instance, in fatigue failure, early detection of defects such as corrosion and fatigue cracks leads to preserving the fuselage structure of airplanes from damages. Shown in Figure 1.1, inflation and deflation of aircrafts as a result of pressurizing and depressurization causes several kind of damages such as surface cracks, radial cracks around rivets beneath the heads of rivets and bolts, delamination of skin membranes and sub surface cracks in structural components. Through inspection of known problem areas by applying predetermined programs of periodic inspection for each aircraft, skin defects can be detected well before reaching a hazardous size. As a result, crack and corrosion are the most common problems that aerospace industries are facing and to which most NDT is aimed for.

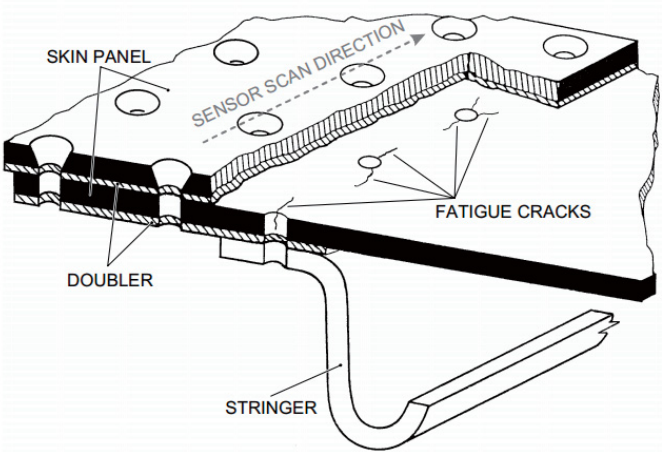

Figure 1.1: Radial cracks around a rivet hole in airplane structure [1]

There are many NDT technologies that are available for aircraft inspection. The most common method is visual and optical testing. Over 80 percent of the NDT

inspections are directly or indirectly related to visual exam [16]. This method can be performed by the trained inspectors or by the images acquired via camera and processed by human inspector or computer image recognition program. But the limitation of visual inspection is that the flaw must be accessible and the indication should be on the surface and visible.

Another of the NDT methods is Fluorescent Penetrant Inspection (FPI) that is based on visual inspection and has been applied widely in aerospace industry. The procedure of this method is illustrated as follows. First, the whole clean surface of examined area is covered by fluorescent solution. Due to the capillarity of liquid, the penetrant is able to fill into, and stay inside the opening of crack. Second, the penetrant is removed from the surface, and the proper enhance procurer such as developer is applied to draw the penetrant out of the defects to make it more obvious. Finally, the test piece is put into dark room with ultraviolet light to make indications visible for the trained inspector to identify and locate the defect indications. However, due to the size of indication, the cleanness of the surface and inspector's personal experience, the result of inspection can be different. To obtain an objective inspection results, the industry resorts to an automated FPI technique to improve FPI process. For example Pratt & Whitney has developed an automated FPI system which utilizes the FPI procedure via automated stations and can automate the first two steps of FPI procedure [17]. However, they still need human inspector to make the final decision in the last step. To automate this step, one of our teammates has developed an advanced automatic inspection system for aircraft parts based on fluorescent penetrant inspection analysis. Such system can detect and sort the defect by processing the images taken under the ultraviolet light [18]. The obtained crack results from FPI can give us the information of the rough location of the crack. The main problem of FPI is that it does not give information about the depth of a surface crack. In addition, it does not detect sub-surface cracks. And detected defect information is very rough and not very reliable due to the low resolution of the image and various illumination of the ultraviolet light or UV light. The industrial partners would like to use ECT to scan the region of the indication from FPI and obtain more accurate defect information which is the main motivation of this project.

1.2 Eddy Current Test

ECT is one of the NDT methods that are widely used for conductive material inspection. It can be used for crack detection, thickness and conductivity measurement [19]. Compared to other NDT methods such as FPI and ultrasonic test (UT), the advantages of ECT are listed as follows. 1. The equipment is portable and easy to use. 2. It provides quick access to inspection result (almost simultaneously). In ECT, two main kinds of probes, absolute and differential probes, are used for different purposes. The advantage of using differential configuration for crack detection is that it is able to eliminate gradual variation on or underneath surface. Whereas, the signal generated from the absolute probe is normally contaminated by the other information such as surface coating, conductivity and thickness shifting. Hence, the signals generated via differential probe are mainly based on crack indication. Another advantage of using differential probe is that the signal of crack indication appears in "8" shape, which is unique and distinctive compared to the curve line shape obtained using an absolute probe. In this project, the differential probe is used specifically for crack detection.

ECT is extensively used in the aerospace industry. For example, in Pratt & Whitney Canada, ECT is performed using a 6 Degree-Of-Freedom (DOF) robotic system for the components with known geometry and size. In this case, ECT is used to detect the presence of crack, i.e., if there were one crack detected, the component would be discarded. In L-3 Communications, the portable ECT equipment is used for aircraft maintenance. The maintenance work mainly focuses on finding and fixing the cracks with certain depth or shape, which may have the potential of propagation. As a result, it is important and necessary to know the size of the crack and it is preferred that the shape of the crack can also be revealed since certain shape and size do not require or require minimum maintenance depends on the location and orientation of the crack, in a heavily stressed (critical) part or not. However, the robotic or automated ECT system in P&W cannot be used for aircraft maintenance purpose due to complexity of surface geometry and the size of robot (some maintenance work require to go inside airplane for ECT scan which is nearly impossible for the bulky 6DOF robot to maneuver). The current maintenance work is mainly carried out by the human inspectors and the inspection accuracy largely depends on the human inspectors experience. Hence, to accelerate the inspection process and improve the inspection accuracy, a robotic ECT inspection system with intelligent

ECT crack detection is sought by the aerospace industry. In this thesis, the main focus is on developing an intelligent ECT detected crack signal analysis, which is the central part of the robotic ECT inspection system. The developed algorithm can be used in both engine manufacturing and aircraft maintenance industries.

1.3 Project motivation and work plan

To develop an intelligent ECT detected crack signal analysis algorithm, the first step is to build a theoretical model to describe the probe impedance using Maxwell equation [4], [20]. Then based on the model, the relationship between the detected impedance and the crack could be established. In [4], [20], both analytical and numerical modeling for ECT phenomena has been developed. Based on numerical model, finite element solution is used to predict eddy current probe impedance variation. However, although many theoretical models have been developed using crack feature mapping the ECT signal [21], [22], [23], due to the complexity of crack plus the lack of detailed coil specification, it is difficult to solve the reverse issue which is to use ECT signal to predict the size and shape of crack. In order to establish such relationship, solutions resort to the advanced software computing techniques such as fuzzy logic and neural network [24], which can be trained by known data to map the relationship.

1.4 Contribution of thesis

In this thesis, ECT signal processing system has been developed on analyzing and identifying some crack features based on the trained fuzzy logic engine. The main contributions are listed as follows:

- An ECT signal processing system has been developed including signal filtering, signal, feature extraction, and final decision making.

- New feature (original) has been extracted, and utilized to train the fuzzy logic and taken into consideration as a feature in terms of representing certain feature of crack.

- A user friendly interface has been developed to enable non-specialized signal processing personnel to load the signal, to apply the signal processing and to obtain crack characteristics from fuzzy logic.

- A data acquisition system as well as a 6 DOFs robot based scan system has been developed to collect the ECT data. A prototype of spring loaded probe holder has been designed and produced using 3D printer.

1.5 Thesis outline

The thesis is organized as follows.

- In Chapter 1, thesis background information, project introduction, project objectives, motivations as well as the thesis outline are introduced.

- In Chapter 2, a background knowledge and literature review of signal processing, ECT principles, as well as neuro fuzzy logic is provided.

- Chapter 3, introduces ECT signal features, the algorithm of feature extraction, filter design and processing result. The ECT data is acquired and processed based on two types of known samples: 1. visible aluminum artificial notch crack normal to surface; 2. visible aluminum artificial notch crack with angle to surface. Fuzzy logic training using ANFIS and test results is presented based on the trained fuzzy logic engine.

- Chapter 4 introduces the robot arm scan system as well as its working environment. The hardware information and software setup for data collection are provided. The introduction on the probe holder design, hands-on installation and design adjustment are also given.

- Chapter 5 provides the experimental result as well as research conclusion.

- Finally, Chapter 6 concludes the thesis and indicates its future work.

Chapter 2

Background knowledge and Literature Review

2.1 Introduction

This chapter will review some of the theoretical knowledge with regard to this research. An analog to digital signal data acquisition is used in this study to acquire ECT signal. The basic signal processing procedures based on ECT signal are acquired such as signal filtering, feature extraction, fuzzy logic training etc. This chapter begins with basic introduction of digital signal processing including analog to digital transform, signal properties, noises, and filter options. Then a brief introduction of ECT principle and fuzzy logic which plays a critical role in this research will be presented. The fundamental fuzzy logic concepts are given, and the difference between fuzzy and classic logic is demonstrated. Furthermore, the application of using fuzzy logic in ECT signal processing is reviewed.

2.2 Digital signal processing

Signal processing, also known as DSP (Digital Signal Processing), is one of the most powerful and universal technologies influencing our daily life in a great deal. With the development of computer science during 1980s, DSP has been applied not only in its initial application domains: military, oil exploration, space exploration and medical application, but also in various profitable areas and disciplines such as entertainment

(high quality sound and visual effects), mobile communications and industry management etc.[2]

Basically DSP includes data signal acquisition, converting data from analog into digital, signal filtering and information extraction. The analog signal exists in natural or the real world, such as sound of birds, the speed of a vehicle, and voltage in circuit which is continuous with regard to its parameter (time, frequency etc.). Before the computer was invented and people entered into the digital era, the analog signals were recorded continuously via certain media such as phonograph, magnet tapes and films or by certain electro component. The advantage of analog data is that it represents the full scale of the original signal yet also inherits all the noises and disturbances from the "mother signal". Moreover the analog data acquisition itself also gives birth to noises which add a lot of errors in terms of signal interpretation. Furthermore, because of the property of analog signal, it is difficult to perform scientific analysis, and not mentioning it is hard to duplicate identical replica. Even for signal filtering, the analog signal largely depends on electro elements which is time taking, lack of reliability, and sometimes expensive compared to digital filtering.

When converting into digital signal, the continuous analog signal becomes discrete due to the fact that the data is collected on each sample time. Because there are too many samples in very short sample duration in digital signal converting, it might seem to be continuous when displayed in graphic plot. Such feature concludes that digital signal is just a portion of the actual signal and there is always information lost from analog to digital conversion. The increase of sample rate could cause the increase of the rate at which the digital represents the analog signal. However, the cost will be higher and the equipment becomes more sophisticated.

Another important aspect in DSP is the relationship between the signal and underlying process [2]. Although signal is close to the natural phenomenon, their relationship is still unclear in terms of signal interpretation. For instance, considering flipping a coin, the chance of getting either head or tail is 50% statistically. However, in real life, the data could be constituted as 3 times head and 3 times tail. If only acquire the first 3 experiments as analysis signal, the result could be completely wrong. Even when carry out experiment with a large amount of data such as flip 1000 times, still the result based on actual data could be different (50.1% or 49.9%). In DSP, this irregularity found in data collection is called statistic noise [2].

In terms of signal interpretation, precision and accuracy is also a key factor that could influence the DSP result in a great deal. Accuracy reflects the ability of signal represents the TURTH of natural phenomenon. For example [2] histogram shown in Figure 2.1 for certain measurement, the mean is at the center of the distribution, which represents the best the best estimation. The gap between the mean and true value is the accuracy. Whereas, precision is how the signal value spread based on standard units which is shown in Figure 2.1 as the width of the distribution. Precision is also known as signal to noise ratio [2]. In this thesis, sophisticated commercial eddy current equipment made by leading companies is used In data acquisition process, a reliable data acquisition setup is built based on acuate data acquisition card with a input resolution of 14 bit, output resolution of 12 bit and max sample rate of 48 ks/s which is sufficient for this project. In this study, eddy current change is represented in ECT equipment screen as X-Y plot. And screen dot coordinates are available as analog output voltage ranging from +5vV to -5V. The ECT principle is introduced in the next section and the detailed ECT signal and equipment information will be introduced in Chapter 4.

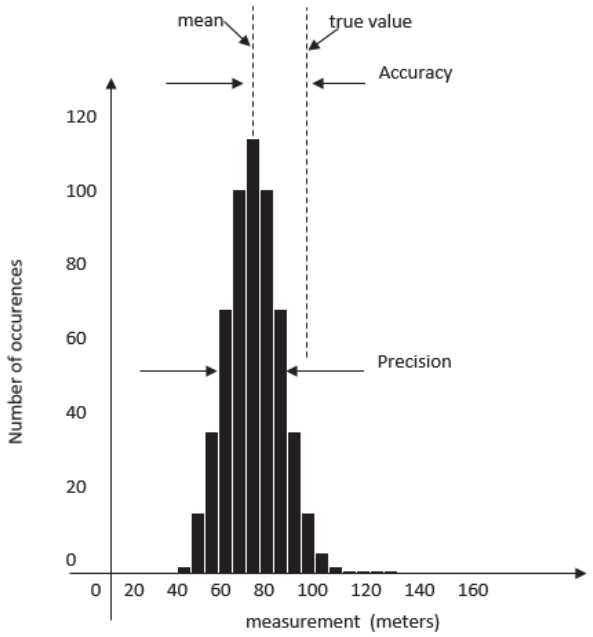

Figure 2.1: Measurement of certain depth [2]

In order to reduce noise of the signal, digital filter is used in this study. In DSP

there are a lot of filters that are available and choosing the right filtering parameters is one of the most important steps. One of the most fundamental and popular filter is high pass (HPF), low pass (LPF) band pass (BPF) and rejection band or band-stop filters (RBF). The function of low pass filter is to allow low frequency signal to pass and to hold high frequency signal. The high pass filter on contrary, allows high frequency to pass and holds the low frequency signal. Based on this, LPF can be transformed into many other filter types. For example, HPF can be considered as the whole signal minus LPF. In practice, many filters can be designed or assembled by several HPFs and LPFs, which will be introduced in Chapter 3.

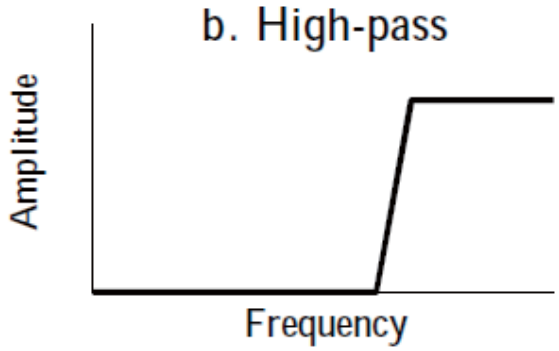

Figure 2.2: Highpass fliter [2]

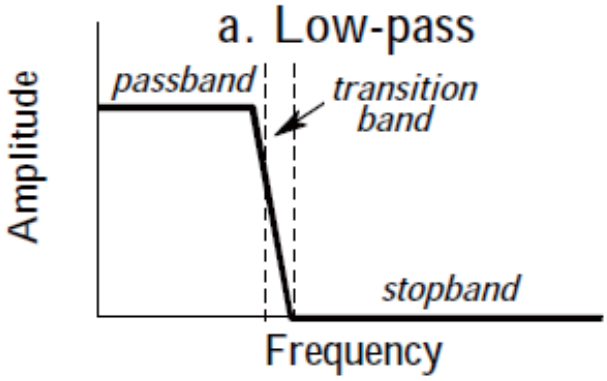

Figure 2.3: Lowpass fliter [2]

2.3 Eddy current test principle

The theory of ECT is reviewed in order to have a good understanding of signal interpretation. As mentioned in Chapter 1, besides crack detection, ECT is wildly used as one of NDT methods in metal and coating thickness measurement, electrical conductivity and magnetic permeability measurement, corrosion and erosion detection etc..

The principle of eddy current is based on electromagnetic induction, which can be explained via Maxwell equations [25]

$$\nabla \cdot \boldsymbol{D} = \rho \tag{2.1}$$

$$\nabla \cdot \boldsymbol{B} = 0 \tag{2.2}$$

$$\nabla \times \boldsymbol{E} = -\frac{\partial \boldsymbol{B}}{\partial t} \tag{2.3}$$

$$\nabla \times \boldsymbol{H} = \boldsymbol{J} + \frac{\partial \boldsymbol{D}}{\partial t} \tag{2.4}$$

where $\boldsymbol{E}$ is the electric field, $\boldsymbol{H}$ is the magnetic field, $\boldsymbol{D}$ is the electric flux density, $\boldsymbol{B}$ is the magnetic flux density, $\boldsymbol{J}$ is the current density, ρ is the electric charge density, and these parameters are related by the following equations.

$$\boldsymbol{D} = \varepsilon \boldsymbol{E} \tag{2.5}$$

$$\boldsymbol{B} = \mu \boldsymbol{H} \tag{2.6}$$

$$\boldsymbol{J} = \sigma \boldsymbol{E} \tag{2.7}$$

where ε is the permittivity, μ is the permeability, σ is the conductivity of the material.

The above Maxwell equations indicate that changing current produces changing magnetic field and changing magnetic field can also have impact on the changing current. If there were a coil with an altering current applied, because the varying current, the coil generates a corresponding altering magnetic field with its magnetic flux flowing and concentrated at the coil center which is known as primary magnetic field [26]. When the coil is approaching to a conductive material, the changing magnetic flux penetrates the material and generates circular current which is known as the eddy current, both on surface and inside the material [26]. Because the primary

magnetic field is altering, consequently the eddy current also alternates, which in return, produces a secondary magnetic field with a direction in opposition to the primary magnetic field of the coil. As a result, the strength of primary magnetic field is reduced. When there is variation near surface area of the test piece such as crack, apparent conductivity changes and intensity of eddy current will be reduced which leads to reduction of the strength of the secondary magnetic field and thus strengthening of net magnetic field passing through the coil. When the magnetic field in the coil changes, the equivalent electrical properties of the coil such as resistance and reactance will change accordingly. In order to monitor the changes of the test sample, the coil electrical properties is used as an indicator which is associated with the variation.

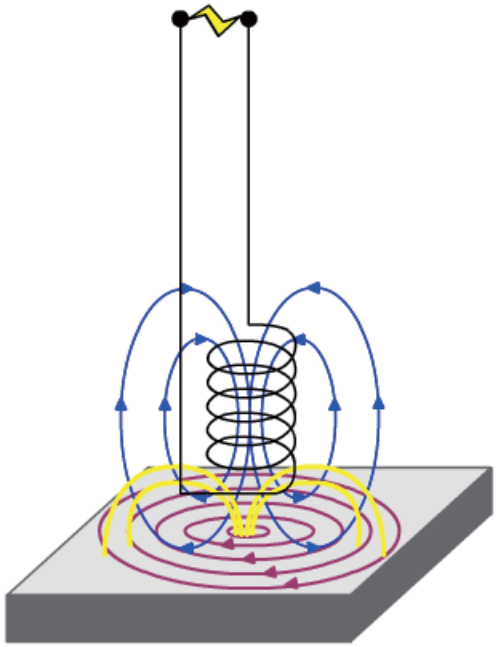

Figure 2.4: Eddy current generation [3]

In most ECT equipment, the impedance of coil or the impedance of probe is utilized to represent the test sample variation. According to the study of Lord, W. and Palanisamy's study [4] the numerical modeling (finite elements) of the impedance of a single turn coil of radius r can be expressed as Equation (2.8).

$$Z_i = -\frac{j\omega \oint A_i \cdot dl}{I_s} = -\frac{j\omega 2\pi r_i A_i}{I_s} \tag{2.8}$$

where Z_i is the impedance, A_i is the magnetic vector potential, r_i is the radius of circular loop, I_s is the impressed current.

For a coil with multiple turns the impedance can be expressed as:

$$Z_{coil} = -\frac{j\omega 2\pi N_s}{I_s} \sum_{j=1}^{N} r_{cj} A_{cj} \Delta_j \tag{2.9}$$

where N_s is the uniform turn density.

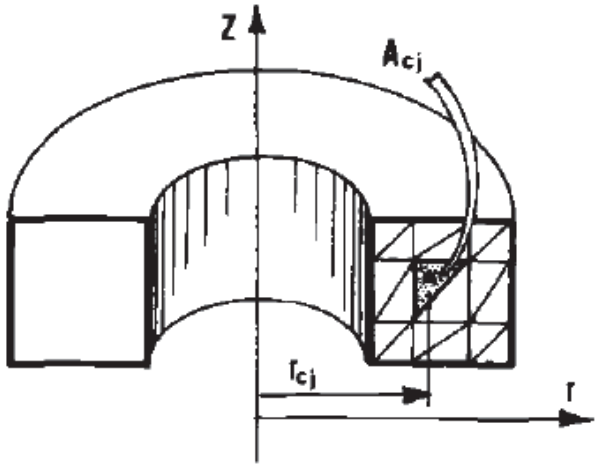

Figure 2.5: Finite elements of eddy current in a coil [4]

Many other researches have been done with regard to modeling ECT signal based on crack geometry.

Burrow (Auld and Moulder, 1999) [27] stated a quantitative expression for small ellipsoidal inclusions. Their theory was based on the induced magnetic field distribution by a fixed exciting current. This theory was immature but it was a major initial step in modeling of field/defect interaction. He postulated that the effect of small flaws can be represented by equivalent magnetic and electric dipoles. The resultant magnetic moments of inclusions, which were determined by their geometry, were evaluated in this mode.

Auld et al. (Auld, Muennemann and Winslow, 1981) [28] proposed a general theory for EC probe response to flaws for both high frequency (i.e. resonant) and low frequency probes. The formulations were presented for impedance of probe when inspecting a material including three dimensional and two dimensional surface cracks. They approximated the profile of three dimensional cracks by a section of circle in two dimensional models. The impedance of probe evaluated for the defects larger and smaller than standard penetration depth and some assumptions (e.g. plane waves and uniform field distribution in material) were used for evaluation of impedance variations.

In another work, Auld (Auld, Jefferies and Moulder, 1988) [23] used integration over the defect mouth. He assumed the crack dimensions are less than wavelength; therefore, he applied quasi-static regime to the field generated by probe. Magnetic field was represented by gradient of scalar potential inside the surface breaking. Finally, the impedance variation formulation was written in terms of scalar potential and subsequently calculated by finite difference method for rectangular and semi-elliptical shaped flaws.

Another research was presented by Auld and Moulder (Auld and Moulder, 1999) [27]. They mostly paid attention to the difference of field distribution in absence and presence of defect in material. This method alloweds them to find state changing impedance (ΔZ) formulation from subtraction of impedance values. Their impedance relation is built by applying Poynthings theorem and integration of magnetic and electric field over a surface enclosed the source. They generalized their theory for differential probes (i.e. their theory is independent of coil geometry).

The mathematical modeling is complicated whereas in ECT equipment the calculation of impedance has been done and the interpretation is straight forward as shown in Equation (2.10).

$$Z = \sqrt{R^2 + X_L^2} \tag{2.10}$$

where Z is the total impedance, R is is the resistance of coil, X_L is the reactance of coil.

Considered as total opposition of circuit acting on altering current, impedance is constituted with the sum of a real part which is the resistance and an imaginary part

which is reactance. The change of magnetic field will affect both the real part and the imaginary part. Therefore, by monitoring the change of the coils impedance certain nondestructive test can be performed.

Due to the physical principle of eddy current test, ECT is only applicable for conductive material which means it mostly works on metal parts. And it only works for surface or near surface defect detection.

2.4 Factors Influencing ECT

In ECT due to properties of magnetic induction, numerous elements act alone or together influencing the ECT result. In this study and practice applications, certain factors should be taken into considerations and the configurations of ECT equipment should be carefully adjusted according to specific usage. The following issues are the most common and important factors that influence the ECT result.

2.4.1 Frequency

Frequency determines the sensitivity of eddy current test especially for crack detection. Shown in Equation (2.11), the test frequency mainly affects the inductive reactance of coil.

$$X_L = 2\pi f L \tag{2.11}$$

where L is the inductance, f is the test frequency.

When the frequency is high, the changing of current goes high too, so it produces stronger primary magnetic field with more magnetic flux concentrated in the center of coil. When the charging coil getting closer to the test material with higher frequency, the additional magnetic flux increases the density of inducted eddy current. When eddy current encounters with any flaw, or discontinue, higher frequency corresponds to more eddy current interruption. Consequently, compared to low frequency, for the crack with the same size, higher frequency interrupts more eddy current, and thus causes more primary magnetic field increment and finally results in larger coil

impedance change. Thus in the ECT equipment, the crack signal will be more obvious than that with low frequency. For the small crack detection, one of the effective methods to improve accuracy is to increase the test frequency.

However, with the same eddy current probe applied on the same test sample, high frequency causes shallow penetration depth. The calculation of the penetration depth can be expressed as Equation (2.12).

$$\delta = \sqrt{\frac{2}{\omega \sigma \mu_o}} \tag{2.12}$$

where δ is the so-called skin depth which is the effective detection depth of ECT, μ_o is the magnetic permeability, ω is the excitation frequency and σ is the conductivity of the investigated material.

Eddy current phenomena exists not only on the surface but also inside the test sample as the primary magnetic field penetrates it. However there is a limitation of the penetration depth due to energy loss which is known as magnetic attenuation. In addition, the penetration depth is also limited by eddy current itself. As explained in 4.3, the direction of secondary magnetic field which is produced by eddy current opposes the primary field, thus it cancels the net magnetic flux and causing decrease of eddy current as the depth increases. Consequently, acting as a magnetic shield, the higher the test frequency goes, the stronger the eddy current gets, and the more overall magnetic field it cancels [5]. That is the reason why eddy current test for crack is mainly applicable on surface or near surface flaw detection. It is a dilemma in ECT between good sensitivity and good detective depth. So choosing a right frequency while performing ECT is very important. Thus the standard depth of penetration is introduced. The standard depth is the location where the eddy current decreases to 37% of its surface eddy current. When it gets deeper the variation of eddy current is too weak to be influential to the coils impedance. Multiple Frequency Techniques (MFT) is another method to solve this issue and improve eddy current test ability. By using different frequencies, ECT is able to test different depths simultaneously; different data can be compared or mixed in order to achieve more information of the test sample. For example, in tube inspection multi frequency is used to inspect the crack as well as monitor if the thickness of the tube is within its specification range.

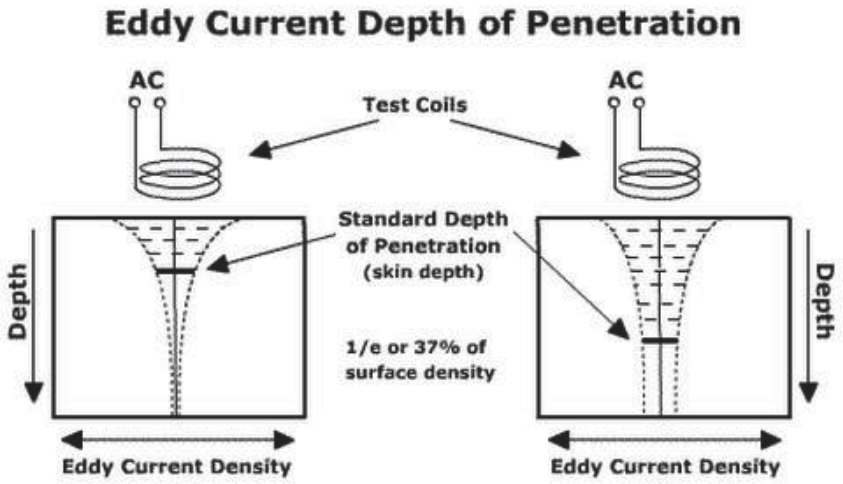

Figure 2.6: ECT depth of pentration [5]

Depending on different applications, frequency should be selected correspondingly. For electrical conductivity measurement purpose, same, frequency is applied on different testing samples, because the measurement is based on lift-off calibration of known materials, however, for crack detection, the frequency should be selected accordingly in order to exam the desired depth. Because the eddy current can penetrate the test sample for some distance, compared to other NDT method such as FPI, the ability of crack detection is more accurate. Moreover, eddy current is not only able to detect the flaw on surface but also can detect flaw below the surface.

2.4.2 Configuration of testing probe

For different ECT applications, different test probes are available to fulfill various tasks. And each type of probe produces different ECT signal. In this study, choosing the right probe and getting familiar with its signal are important.

Lift-off: lift-off occurs when there is distance in between probe and testing surface. Technically lift-off is the differenc between the probes impedance in the air and the probes impedance in touch or near the test piece. In some tests especially for crack detection, having a horizontal lift off line (a line formed when approaching ECT probe from air to test piece) is required in order to eliminate other indications on lift off direction. Ideally for propose of protecting the probe, it is preferred to have a little lift-off. However, the lift-iff distance should be kept the same when scaning on

different samples. As mentioned in Chapter 4 in this study, robot arm and spring loaded probe holder are used to control the distance of lift-off.

Absolute probe: absolute probe is one of the commonly used probes which has a single coil inside the structure and reflects absolute variation of the test sample. For this feature the absolute probe is suitable for electrical conductivity, coating and thickness measurement. Some crack detection is also available using absolute probe, however when an absolute probe been applied for crack detection, other variations such as thickness change of material, surface scratches, as well as small conductivity shifting due to metal thermal treatment, will affect test result. In other words, any factor which could disturb the coils impedance will be represented on ECT equipment impedance panel, furthermore for absolute probe the signal of crack and the signal of other variations is similar and hard to distinguish. Thus, absolute probe is hardly used in crack detection in practice.

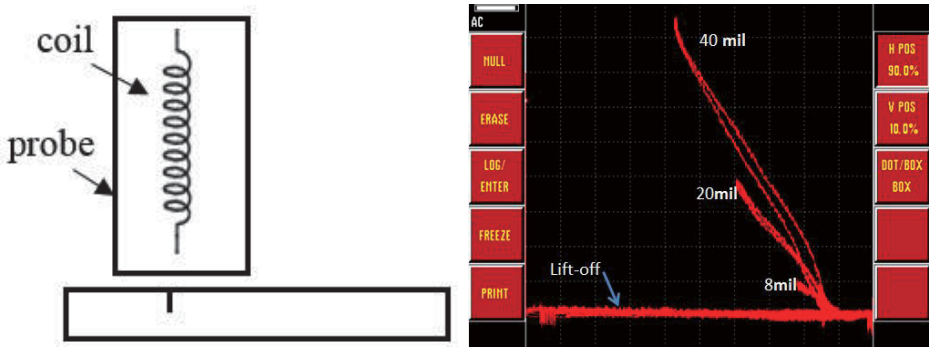

(a) (b)

Figure 2.7: ECT absolute probe(a), ECT absolute probe crack signal (b)

Differential probe: differential probe has two identical (ideally in theory) coils coupled in opposition, which means if both of the coil on top of the same material, the value of impedance is the same but with different directions, consequently, when using differential probe scan, if the variation is gradual, the signal will stay constantly approximate to zero because the coils are inspecting the same material however, when one coil is over a defect the other one is on top of good material a differential signal will be produced. As the probe moving forward, two coils will exchange their positions which means that the coil on top of the discontinue moves on to flawless region and the other coil moves from flawless region to meet discontinues. When both coils

pass the crack, the impedance comes back to zero again. After this procedure, it leaves on the impedance panel an "8" shaped indication which suggests the probe just passed by an imperfection. The differential probe is especially used for crack test since this configuration will eliminate gradual variation, such as conductivity or thickness change. Although high sensitivity is associated with high rate of noise, yet differential probes can provide relatively good performance due to small cracks need high sensitivity (high frequency) to detect. The differential probe itself not only is able to reduce a lot of noise (by cancelling the signal of each probe) but also the "8" shape signal generated by small variation such as crack contains a lot of crack information and is very unique to be recognized either by the inspector or programmable software which leads to the motivation of this study. But there are always exceptions of the signal shape, for example: when encounters with more complicated crack geometry, the signal will not be an "8" shape.

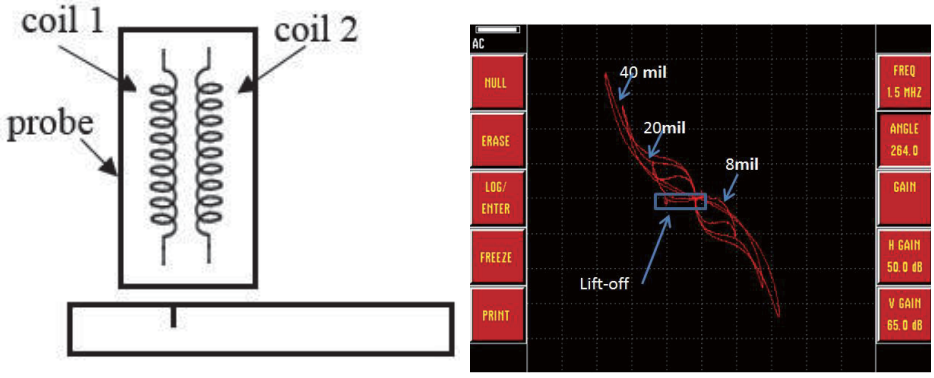

(a) (b)

Figure 2.8: ECT differential probe(a), ECT differential probe crack signal (b)

Unlike the absolute probe, the orientation of differential probe determines the crack detection ability. As shown Figure 2.9 (a), if the direction of crack is vertical to scan direction, the two coils are able to pass though crack one by one so as to create the differential signal. On contrary, if the direction of crack is parallel to scan direction which is shown in Figure 2.9 (b), both coils are scanning the crack at the same time. Thus, there will be no differential signal. For the unknown crack, it is mandatory to perform ECT at least twice: scan along one direction, rotate the probe for 90 degree then scan with the direction perpendicular to the first one.

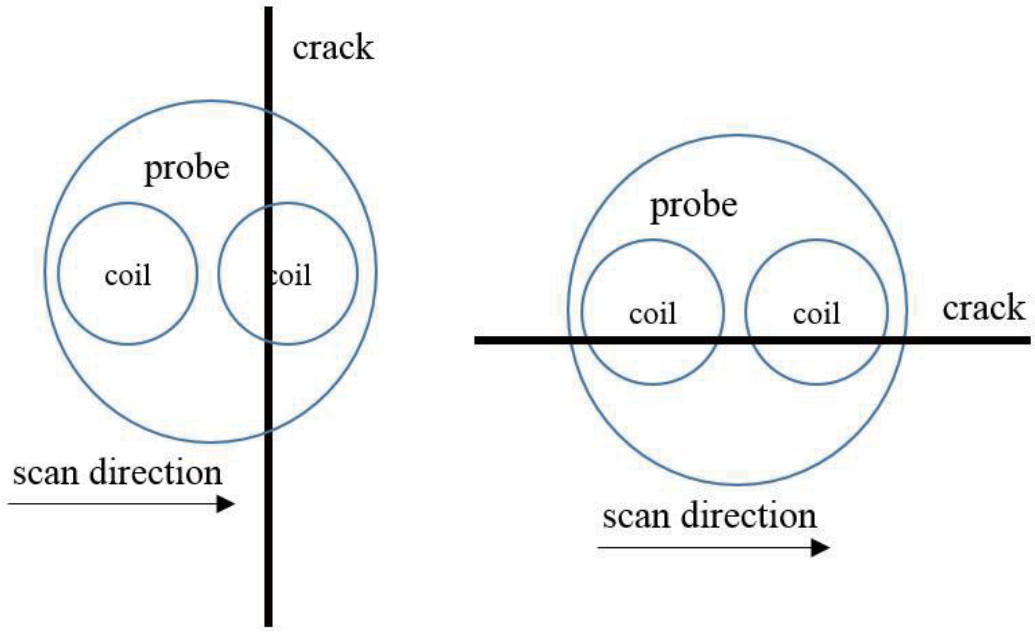

(a) (b)

Figure 2.9: Scan orientation vertical to crack (a), parallel to crack (b)

Reflection probe: In tube or cylinder inspection, the reflection probes are usually used. The reflection probe is like differential probe which has two coils to generate differential signal. However, different from differential probe, which both coils exams the testing piece, the coils of reflection probe have only one with current acting as a "stimulate coil" or "drive coil" to excite the eddy current, whereas the second coil's function is to receive the signal change from the first coil known as "pick up coil". The advantage of this arrangement is that each coil can be optimized individually. For example the drive coil can have a high frequency so as to have a strong and uniform magnetic flux. As for the pickup coil, it can be made very small in order to be sensitive to detect small cracks. Also for tube crack detection, if using conventional differential probe, it is time consuming to scan the whole tube. But for reflection probe design, the drive coil can be made big enough to embody the whole tube. It is especially useful for industry mass production and suitable to scan large and long tube parts.

2.4.3 Surface geometry

The surface geometry can affect the ability of eddy current test as well. There are three main kinds of surface variations which are difficult to scan or cause large noises: 1. Area near part edges or adjoining structure; 2. Metal thickness less than the effective depth of penetration of the material; 3. Excessive curvature of part surface. Edge effect occurs in Case 1 where a probe approaches the edge of testing sample. Under such circumstance, the shape of eddy current will be distorted because it cannot pass outside the edge of part. This eddy current distortion affects the test signal significantly, so avoiding scanning on the edges should always be taken into consideration when performing ECT. However in some particular cases where the defects are centered around the edge of the part, one solution is to use small diameter probe in order to minimize the edge effect. Small probes can also been applied in surface joint since it is hard for the big probe to get close enough to the corner which can result in too much lift-off.

As mentioned in 2.4.2, lift-off is preferred in ECT yet needs to be limited because too much lift-off also has a negative effect on test result. When the probe has been lifted too much above the test surface, the impedance will not change or change very little when the variation occurs in the test sample since the magnetic flux of eddy current is greatly reduced by air and becomes too weak to influence the coil.

Too much lift-off can also affect the sensitivity of the probe. Because in impedance panel the crack indication is related to lift off line. The so-called phase angle is the angle between lift-off line and the crack indication which is a main feature of crack signal. When the lift off is high, on the impedance panel the phase angle can be very small which makes it difficult to distinguish between real crack indication and signal noise. In Case 3 for curve surface which is also easy to have too much lift-off, the method to improve the crack detection ability is either to use small probe with spring load or to use flexible probe whose contact area can be distorted in order to adjust the curve surface. For conductivity test, because the test principle is based on lift-off and the result strongly depends on initial calibration, the surface of probe should have full contact with the testing surface to gurantee the accuracy. In this case, the instruments such as probe holder can be used to guarantee the lift off distance between probe and the test surface and also to ensure they stay perpendicular.

2.4.4 Electrical conductivity of testing material

Due to principle of ECT, it can be applied to test electrical conductivity. Meanwhile, the electrical conductivity can act backwards to affect ECT result. The impedance of coil is determined by its own resistance and inductive reactance. When the conductivity of the material being tested increases, the resistance of probe increases which causes more energy loses. The inductive reactance of the probe will be reduced more because more conductivity produces stronger secondary magnetic field which plays a role of canceling magnetic field of the probe. Due to different probe configurations the conductivity affects the result accordingly. For absolute probe the shift of conductivity of test surface can be influential to test result as it represents absolute variation of the test piece. For differential probe the influence of gradual electrical conductivity variation can be reduced.

2.4.5 Ferromagnetic

Compared to non-ferromagnetic material, the inductive reactance of probe increases instead of decreasing while testing ferromagnetic material. In other words, on impedance panel the direction of signal generated by ferromagnetic material is opposite to that of non-ferromagnetic material. The reason is that the magnetic permeability of ferromagnetic material is greater than that of non-ferromagnetic material, when probe is approaching to a ferromagnetic test sample, its primary magnetic field will be enhanced, which leads to the enhanced inductive reactance. As introduced before for non-ferromagnetic material the inductive reactance of probe will be reduced because of the reduced secondary magnetic field. Whereas for ferromagnetic material, because the probe′s inductive reactance is enhanced, and the amount of inductive reactance added by ferromagnetic material itself is greater than that created by secondary magnetic field, the total inductive reactance of probe increases instead of decreasing. The resistance of the probe increases which is the same as in non-ferromagnetic material test due to the increased energy consumption by eddy current. As a result in impedance panel the impedance goes up instead of going down when the probe approaches ferromagnetic material. However, for ferromagnetic material the magnetic permeability is not constant and can vary a lot since it not only depends on the material itself but also interacts with the magnetic field acting upon it. Because eddy

current is induced by varying magnetic field, consequently the inspection of ferromagnetic material is more difficult than that of non-ferromagnetic material. Taking the crack detection for example, the small variation of permeability affects the eddy current test, since the variation of magnetic permeability can produce the signals very similar to the crack which results in false detection. In order to have good test result, constant magnetic permeability is required. Magnetic saturation can be used to overcome this issue. In this technique, a saturation coil is used along with inspection coil in order to fill test material with magnetic flux until the magnetic permeability reaches its saturation. Based on Equation 18 ferromagnetic material also affects the penetration depth of ECT because the magnetic permeability changes. Based on this theory, for probe design, ferromagnetic material can be used as a core inside the coil to improve the probes sensitivity, because it enhances the primary magnetic field.

2.5 Neuro-Fuzzy Logic

2.5.1 Fuzzy Logic

In the real world there are some human experiences that are blurry or vague based on individual experience. Such as the weather is cold, it is late, the food is good. Mathematical tools or traditional logic term such as 0 (false) or 1 (true) seems too rigid to describe fuzzy cases. In order to find a scientific way of interpretation, fuzzy logic is introduced. A fuzzy system is a rule based system [6]. Its constituted by fuzzy sets, a set without well-defined boundaries; membership functions, a curve or a plot line indicates how input is mapped into a value between 0 and 1 [29]; so-called IF-THEN rules based on human experiences, natural phenomena, or mathematical equations. In addition, fuzzifier and defuzzifier are used to transform fuzzy input and output between linguistic terms and real values.

Fuzzy logic is known as an artificial intelligence tool which is used to describe complicated physical phenomena and to anticipate the linear or nonlinear results based on collected input and output data [6]. It has been largely used in control system, signal processing, communication, etc. A lot of research works have been carried out on processing eddy current signal by using artificial intelligence methods such as fuzzy logic or neural network or both to sort or predict flaw size. In [36], the crack sizing algorithm using fuzzy logic based on the signal features of amplitude

and phase angle has been developed and some promising results on crack detection have been achieved. In [41] an EDDYAI diagnostics expert system is developed by utilizing fuzzy logic as crack decision maker and neural network to predict the size of crack. In [36] and [41], the researchers only use amplitude and phase angle of the loop and ignore the width of the signal, which contains some important information of the crack.

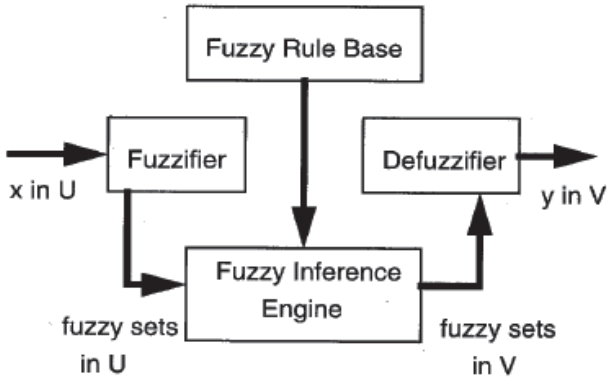

Figure 2.10: Fuzzy logic interface [6]

2.5.2 Fuzzy sets and membership functions

Fuzzy sets are the sets constructed by its elements with certain degree of membership. It was first introduced by Lotfi A. Zadeh (1965) as an extension of crisp set [30]. A good example to explain the differences between classic crisp set and fuzzy set is the height of group of people [29]. For example a group of people has the height from 4 to 6 feet. In class logic, if setting the standard of tall people as the height above 6 feet. Consequently, a person in the group who is taller than 6 feet is considered as 1, whereas the rest are considered as 0. But the problem of traditional logic is that, based on our experience, 5.9 feet is also somehow tall, its not definitely tall as can be considered as 1, but it is not supposed to be as short as 0. The flexibility of fuzzy logic is that its membership function is no longer as in classic logic which is either 1 or 0. Instead, the fuzzy logic membership mapping the value of input using every value between 1 and 0. Which means, 5.9 feet can be considered as 0.9, 5 feet could be considered as 0.5.

For classic crisp set if considering a persons height (x) is in the set of Tall the membership function $\mu_A(x)$ is denoted by either 0 or 1:

$$\mu_A(x) = \begin{cases} 1 & \text{if } x \geq 6 \\ 0 & \text{if } x < 6 \end{cases} \tag{2.13}$$

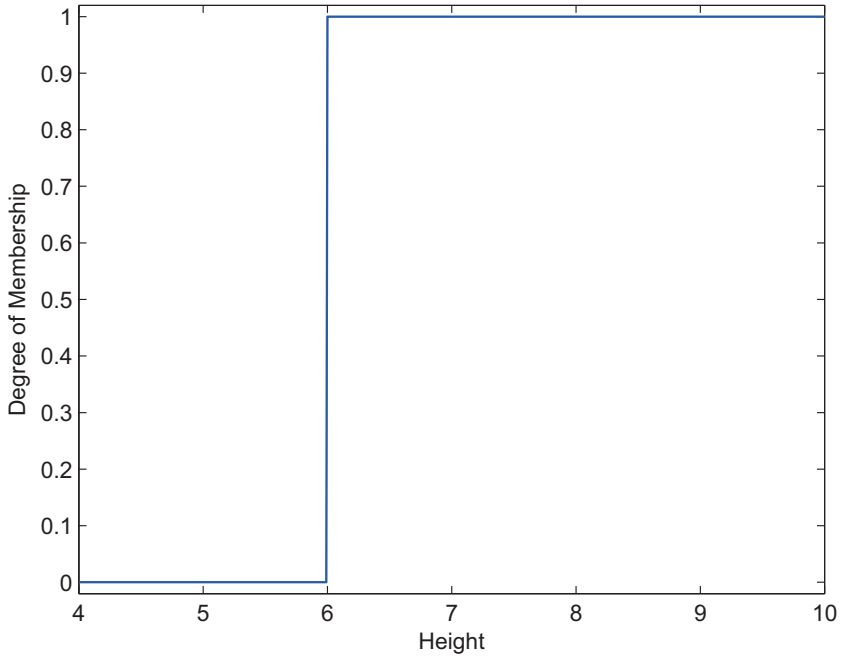

Figure 2.11: People's height identification using classic crisp

For fuzzy set if the persons height (x) is in the set of Tall the membership function $\mu_A(x)$ is denoted between 0 and 1:

$$0 \leq \mu_A(x) \leq 1 \tag{2.14}$$

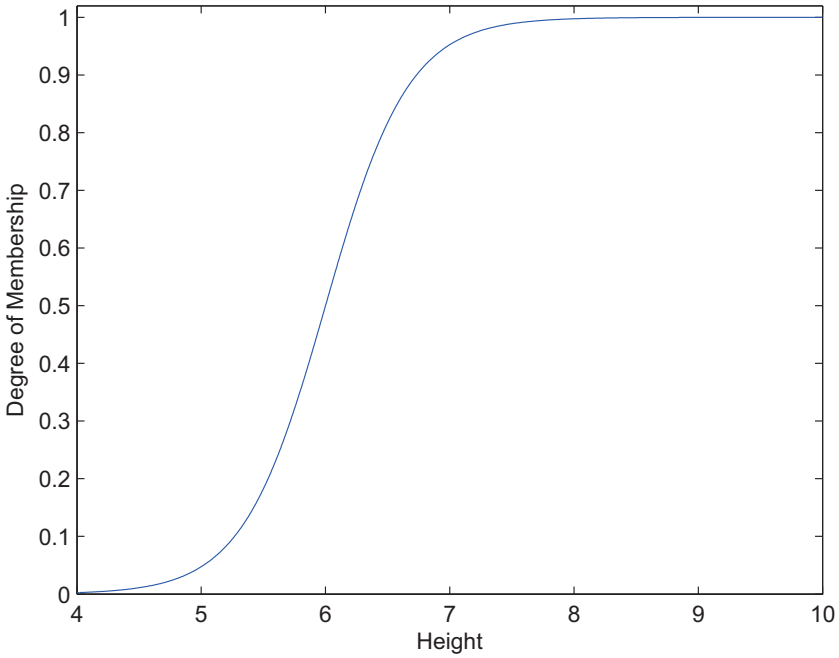

Figure 2.12: People's height identification using fuzzy crisp

In order to map the input into certain membership value, membership function (MF) is employed. The selection of membership functions is based on expertise in consideration of efficiency, convenience and application. Figure 2.13 demonstrates some of the common MFs for fuzzy logic implementation.

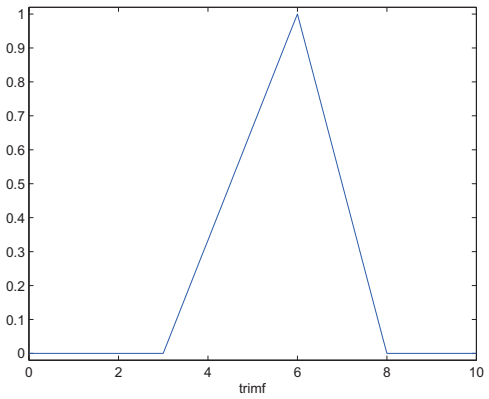

(a) Triangular-shaped membership function

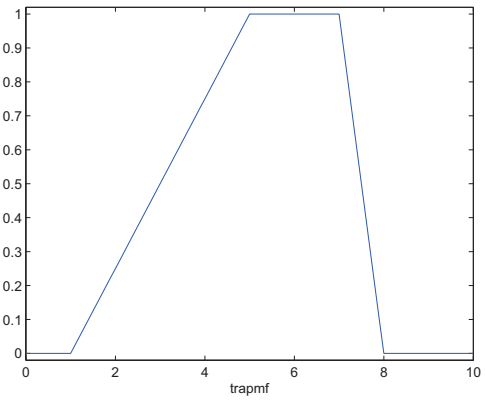

(b) Trapezoidal-shaped membership function

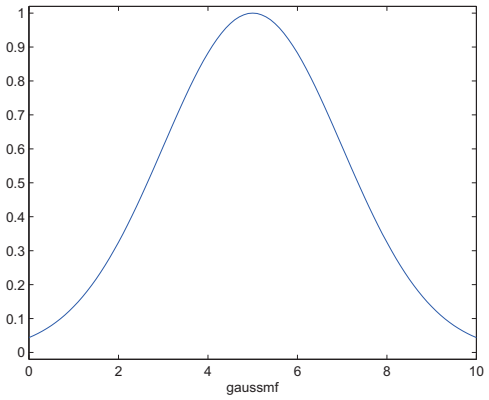

(c) Gaussian curve membership function

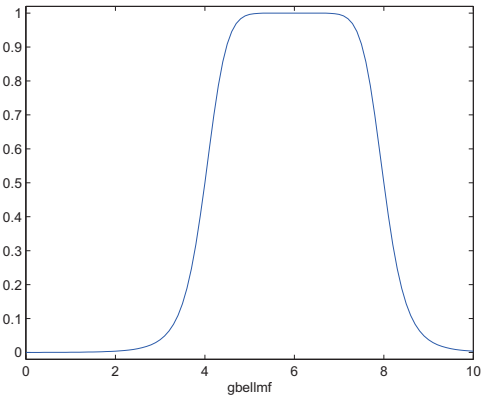

(d) Generalized bell-shaped membership function

Figure 2.13: Fuzzy logic membership functions

2.5.3 Fuzzy rules and fuzzy set operation

Fuzzy logic linguistic variables was first introduced by Professor Lotfi Zadeh in 1975 [31]. Value of variable is formed by linguistic statement rather than numerical number. For fuzzy logic expression, the linguistic statement can be conducted using IF-THEN rules, which consist of two parts, the condition part (IF part) which makes up the statement and the action part (THEN part) which indicates the consequence. In 1965, Zadeh introduced fuzzy rule operations [30] which are intersection (AND), union (OR), and complement (NOT). The rules of each operation are demonstrated as below:

Denote A and B as two fuzzy sets with their membership function $\mu_A(x)$ $\mu_B(x)$,

which shown as Figure 2.14

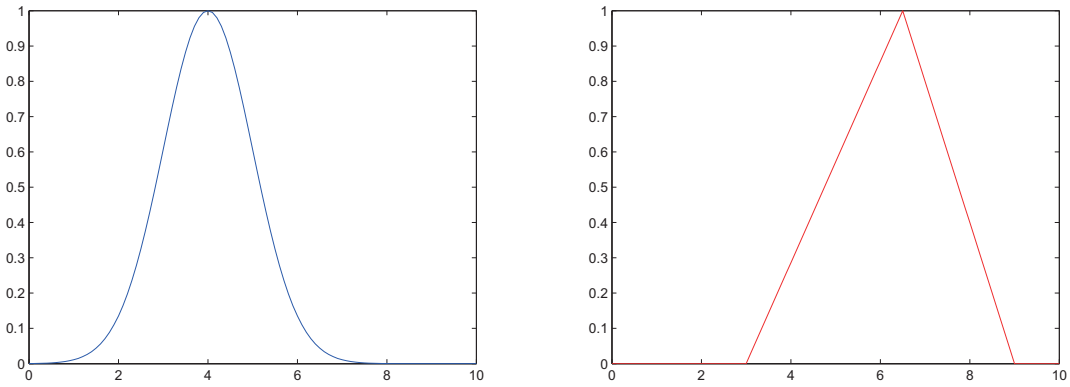

(a) Fuzzy set A (b) Fuzzy set B

Figure 2.14: Fuzzy set

The union of fuzzy set A and Fuzzy set B is defined as equation(2.15), shown in Figure 2.15

$$\mu_{A \bigcup B} = max(\mu_A(x), \mu_b(x)) \tag{2.15}$$

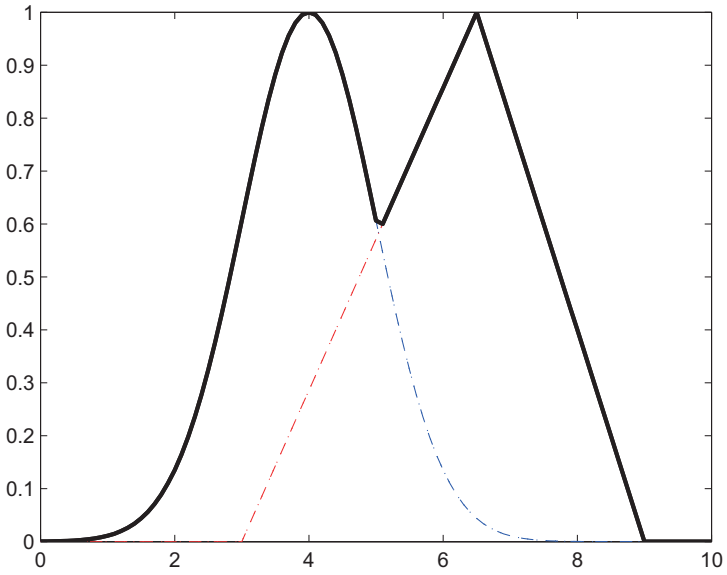

Figure 2.15: Union of fuzzy sets

The intersection of fuzzy set A and Fuzzy set B is defined as (2.16), shown in Figure 2.16

$$\mu_{A \bigcap B} = min(\mu_A(x), \mu_b(x)) \tag{2.16}$$

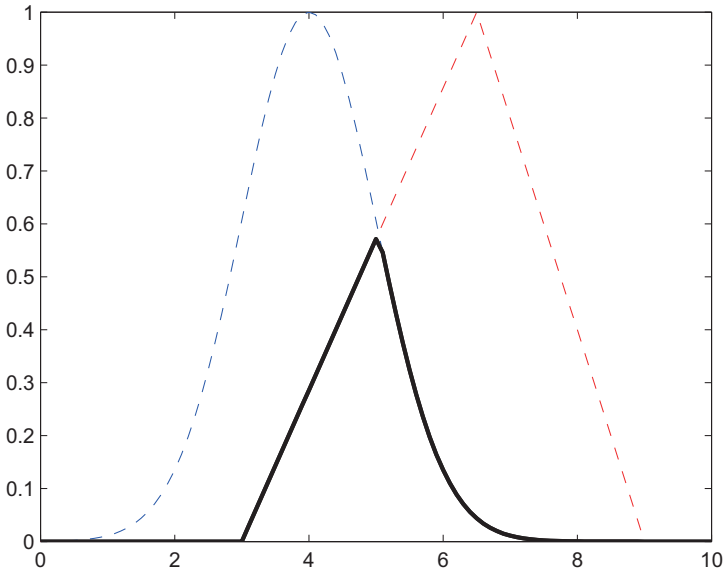

Figure 2.16: Intersection offuzzy sets

The complement of fuzzy set A is defined as (2.17), shown in Figure 2.17

$$\mu_{\bar{A}}(x) = 1 - \mu_A(x) \tag{2.17}$$

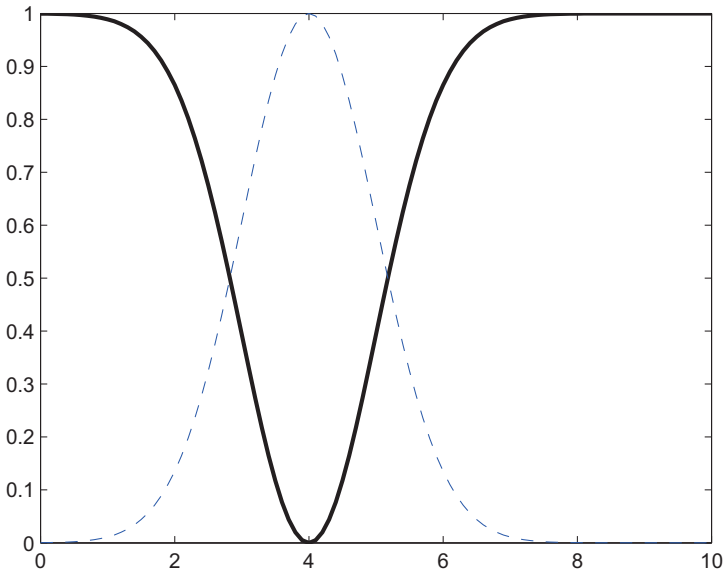

Figure 2.17: Complement offuzzy sets

2.5.4 Neuro-Fuzzy Logic

In order to adapt different data set and have a tuned fuzzy logic interface, a neuro-based fuzzy logic training method is used in this research. Neuro-based fuzzy logic is inspired by neural network, similar to that of neural network which constitutes input and output mapping via their membership functions and related parameters [8]. It has been applied in abundant areas such as control system, data analysis, and theoretical molding

There are numerous ways in terms of neural network and fuzzy logic implementation. But in general, they all belong to the following three categories (Nauck, 1997; Vieira et al., 2004) [32]:

- Cooperative Neuro-Fuzzy System
  Cooperative system is the simplest model. Based on training data neural network determines the fuzzy logic membership functions and/or fuzzy rules. Once the fuzzy logic parameters are set, neural network goes to the background.

- Concurrent Neuro-Fuzzy System
  In concurrent system, neural network is used for input parameter definition or

to change the output. This learning process will not change the parameters of the fuzzy logic system.

- Hybrid Neuro-Fuzzy System
  Through pattern processing like neural network, hybrid system is able to determine the fuzzy systems parameters. An ANFIS system is one of the hybrid systems.

Based on work of (Jang & Sun, 1995)[8]. There are 5 layers for ANFIS architecture which is shown in Figure 2.18:

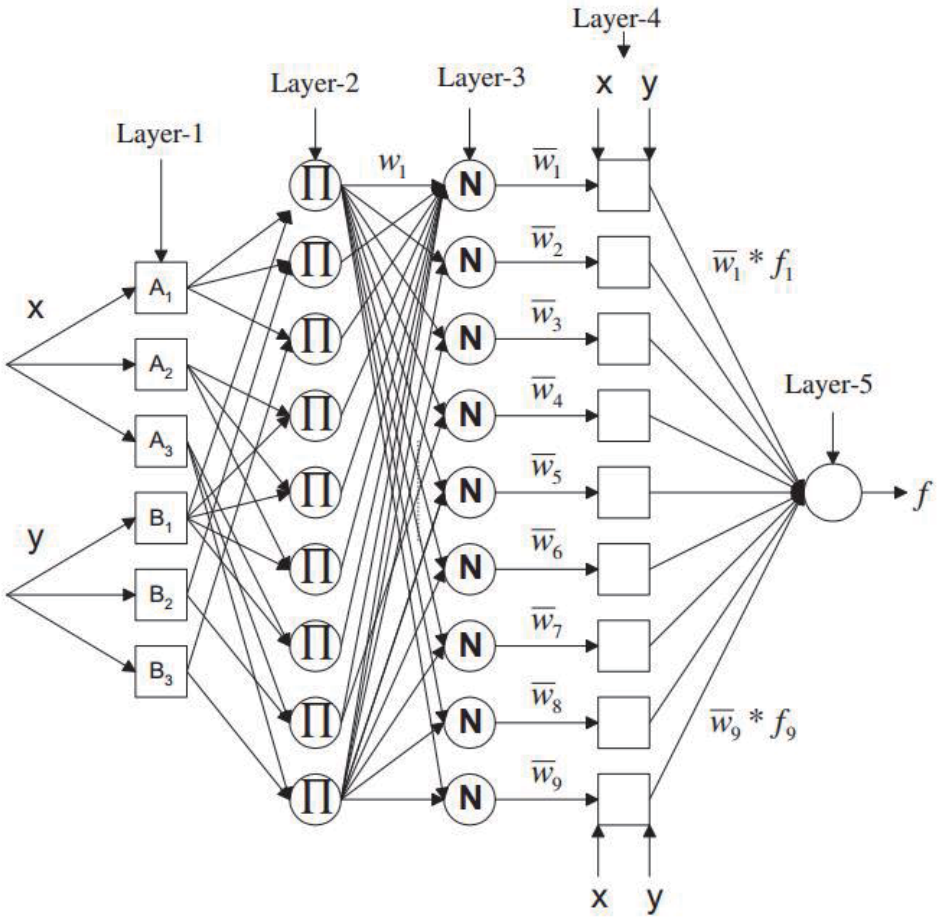

Figure 2.18: Neuro-Fuzzy structure [7] [8]

Layer1: every node i in this layer is a square with a function

$$O_i^1 = \mu_{A_i}(x) \tag{2.18}$$

Layer2: every node i in this layer is a circle note, marked as $\prod$. The function of this part is to multiple the incoming signals and send the processed signal out.

$$w_i(x) = \mu_{A_i} \times \mu_{B_i}, i = 1, 2 \tag{2.19}$$

Layer3: every node i in this layer is a circle note, marked as N. The function of ith node is to calculate the ith rules firing strength. The sum of the total rules firing strength is:

$$\bar{w_i}(x)\frac{w_i}{w_1 + w_2}, i = 1, 2 \tag{2.20}$$

Layer4: every node i in this layer is a square note, the function is shown as follows.

$$O_i^4 = w_i f_i = \bar{w_i}(p_i x + q_i y + r_i) \tag{2.21}$$

Layer5: node in this layer is a circle note, marked as $\sum$, it calculates the overall output based on pervious steps.

$$O_i^5 = overalloutput = \sum_i \bar{w_i} f_i = \frac{\sum_i w_i f_i}{\sum_i w_i} \tag{2.22}$$

2.5.5 ECT related Literatures

Based on AI technology, a lot of research has been done by many researchers with regard to using AI tool for eddy current modeling or inverse problem solving.

Grimberg, R and Savin, A and Iancu, L and Chifan, S [2000], [33] used fuzzy logic inference to quantify material discontinuities of wire via eddy current sensors. The eddy current was created by transducer and the study was based on using fuzzy logic to solve inverse problem of dyadic Greens functions which is an analytical model describing Rotating Magnetic Field of Transducer. The result shows for wire discontinues the fuzzy logic interface is able to provide accurate result.

Sikora, Ryszard and Baniukiewicz, Piotr [2006], [34] used fuzzy logic based system to solve eddy current inverse problem by analyzing the sensors electromagnetic field. This research provides a fuzzy logic learning algorithm which overcomes the issue of neural based inverse model which is insufficient in terms of training process because

it demands a large set of training set. In addition, based on their algorithm, the simulated crack geometry in both 2D and 3D has been presented.

Song, Sung-Jin and Shin, Young-Kil [2000], [35] used finite element method to model ECT flaw signals in case of axisymmetric crack geometry. The simulation result is verified via experimental signal. Neural network is used as an automated characterization tool based on features extracted from simulated signal. In this study, signal itself is symmetric and originate from zero point (0, 0), the signal features is extracted from upper loop of the differential signal. The neural system is realized by probabilistic neural networks for flaw classification and back propagation neural networks for flaw sizing.

Lopez, Luiz Antonio Negro Martin and Ting, Daniel Kao Sun and Upadhyaya, Belle R [2007], [36] used features of actual differential eddy current signal as data base to design a fuzzy logic crack recognition software. In this study, signal processing for eddy current is applied and a user interface is developed. Because the noise of actual signal, more accurate and precise acquisition signal methodology is needed as a future work.

Chady, Tomasz and Enokizono, Masato and Sikora, Ryszard [2000], [37] used dynamic neural network models (with moving window) for eddy current multi-frequency system simulation and flaws identification. The result demonstrates a promising research direction in terms of inverse problem solution. There are two inverse schemes where one is called direct inverse model which could be applied on signal with normal noise disturbance, another is called optimized forward model which is used for high noise signal modeling and more applicable for practise purpose.

Yusa, Noritaka and Cheng, Weiying and Chen, Zhenmao and Miya, Kenzo [2002], [38] also worked on using neural network approach to solve the inversion problem of real cracks. One of the significant contribution is that their inverse model is applicable for conductive cracks, which is more accurate to estimate the cracks that are created in natural environment. 2D crack reconstruction is created based on this study. However verification of the reconstructed crack needs to be done as a future work in order to test the systems reliability.

In most of the above research, eigher simulated signal or the eddy current signalis with a relatively ideal situation (absolute signal, symmetric differential signal, etc.) is used. This research is inspired by Lopez, Luiz Antonio Negro Martin and Ting,

Daniel Kao Sun and Upadhyaya, Belle R [2007], [36]. Besides just using amplitude and phase angle of the loop as crack feature, the width of the signal which contains some important information of the crack is used to train the fuzzy logicusing nero-fuzzy logic trainning method.

In this project, fuzzy logic is applied as a decision making tool for developing the intelligent ECT crack detection system. The data is mainly based on practical signal which is manually collected. Also, the width of loop has been used as fuzzy inputs together with amplitude and phase angle. By tuning so-called IF THEN rules and choosing the right membership functions (MFs) and numbers of MFs, the accurate results on crack information (depth, width etc.) can be obtained

2.6 Conclusion

In this chapter, the fundamental background principles of DSP, ECT and Neuro-Fuzzy logic are presented. The thorough literature reviews on these topics are conducted. The reason of using neuro-fuzzy logic to design intelligent ECT crack detection system is given. The literature reviews demonstrate that the research on intelligent ECT crack detection is very rare, and yet the developed system is a sought-after NDT technology in aerospace industry.

Chapter 3

Eddy Current Signal Processing and Fuzzy Logic Implementation

3.1 Introduction

In this chapter research work on ECT signal processing is introduced. The detailed DSP method especially for ECT differential signal processing such as filter design, feature extraction methodology and most importantly the design of fuzzy logic system are given. The testing samples information and experimental results and conclusions will also be presented accordingly.

3.2 Design Diagram

As shown in Figure 3.1, the designed intelligent ECT crack detection system mainly contains: signal feature extraction, de-noise, fuzzy logic training and fuzzy decision making. The whole process consists of two parts. One part is signal training process and the other one is called decision making process. The two processes share some similar functions such as the ECT signal filter, feature extraction function, yet distinguish each other in terms of fuzzy logic implementation. In training process, ANFIS (Adaptive-Network-Based Fuzzy Inference System) is used to train the fuzzy logic whereas in decision making process the trained fuzzy logic is used to predict the crack features.

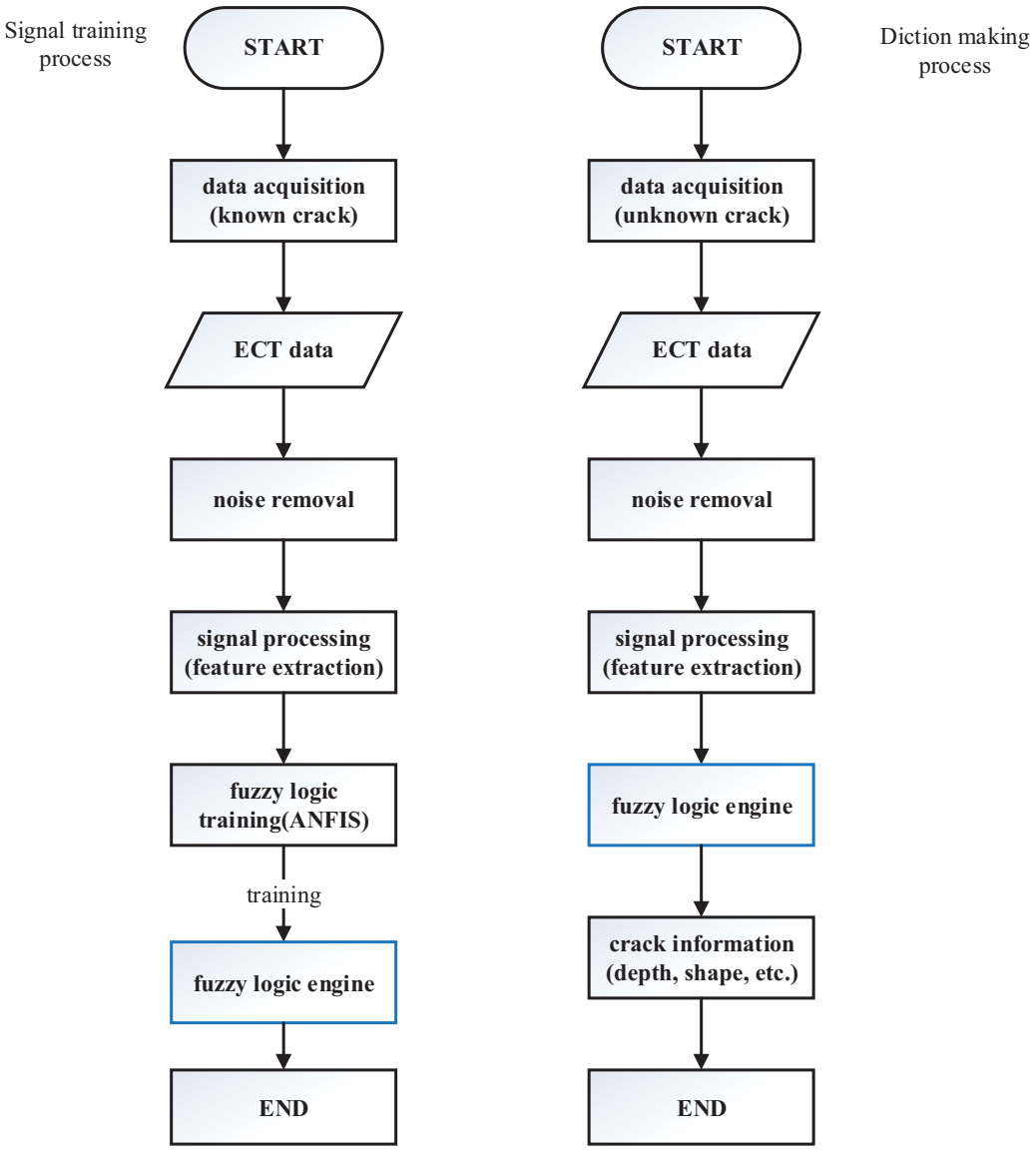

Figure 3.1: Overall system diagram

3.3 Signal noise removal and filter design

The design of intelligent detection system starts with the signal noise removal for the collected data of ECT. The collected signal data sometimes contains the noises especially for manual operation, which influences the feature extraction measurement

and reduces the accuracy of fuzzy logic judgment. It is very important to remove these unwanted noises before applying signal processing.

The high pass filter (HPF) and low pass filter (LPF) are not used individually in this study since the frequency threshold is hard to select since different scan method will have different noise associated with different threshold frequency. In this study a universal filter is needed for all ECT signal. In signal processing, another most common tool for signal analysis and noise removal is Fourier analysis which decomposes the signal into the components of sinusoids. In other words, Fourier analysis transforms the signal from time domain into frequency domain [39]. Fourier analysis is very useful when dealing with stationary signal which does not change too much over time. However, in eddy current test, it is very important to know when the signal commences to change. In order to cope with this, wavelet analysis is used for noise removal. In wavelet transform, the wavelets of different scales and positions are used to approximate the signal. For continuous wavelet transform, it is defined as the time of signal multiplied by scaled, changed versions of wavelet function ψ [39]:

$$C(scale, position) = \int_{-\infty}^{\infty} f(t)\psi(scale, position, t)dt \tag{3.1}$$

where C is wavelet coefficient, *f(t)* is the signal function over time.

The solution of the equation is the wavelet coefficient C which is function of scale and position. The noise is separated via the wavelet transform and by modifying the right coefficient C so that the noise can be reduced to minimum. The wavelet signal de-noise involves three steps: 1. Decompose signal into wavelet components (in which case noises are been separated). 2. Define the right wavelet C coefficient in order to minimize or remove noises. 3. Reconstruct the processed signal by defining C coefficient [40].

The mathematical wavelet transform is very complicated and generates a lot of data [39]. An efficient way of to simplify the calculation work is to use Mallat algorithm which applies filters to decompose the signal. Figure 3.2 and 3.3 shows Mallat wavelet transform and Multi-layer Mallat wavelet transform [39], where A is approximation coefficients, and D is detail coefficients.

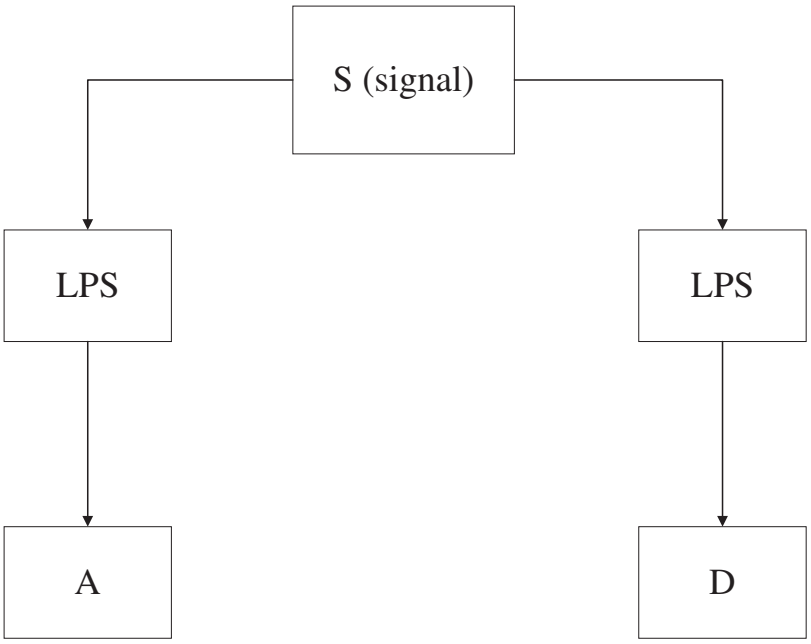

Figure 3.2: Mallat wavelet transform

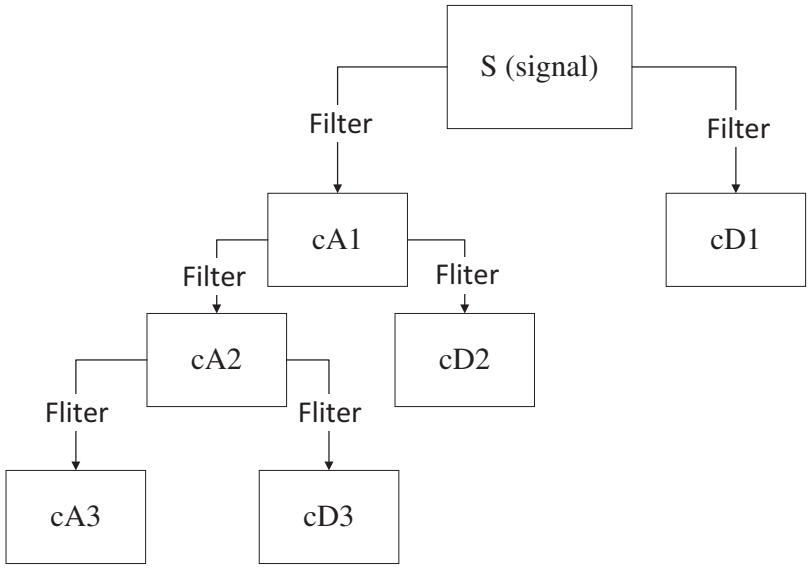

Figure 3.3: Multi-layer Mallat wavelet transform

As shown Figure 3.5 for this study, biorthogonal wavelet with FIR (Finite Impulse Response) filter is used to preform wavelet analysis.

Biorthogonal wavelets have the property of linear phase, which is suitable for signal reconstruction. Shown in Figure 3.4, different scaling functions, wavelet functions, as well as HPF LPF are used for signal decomposition and reconstruction.

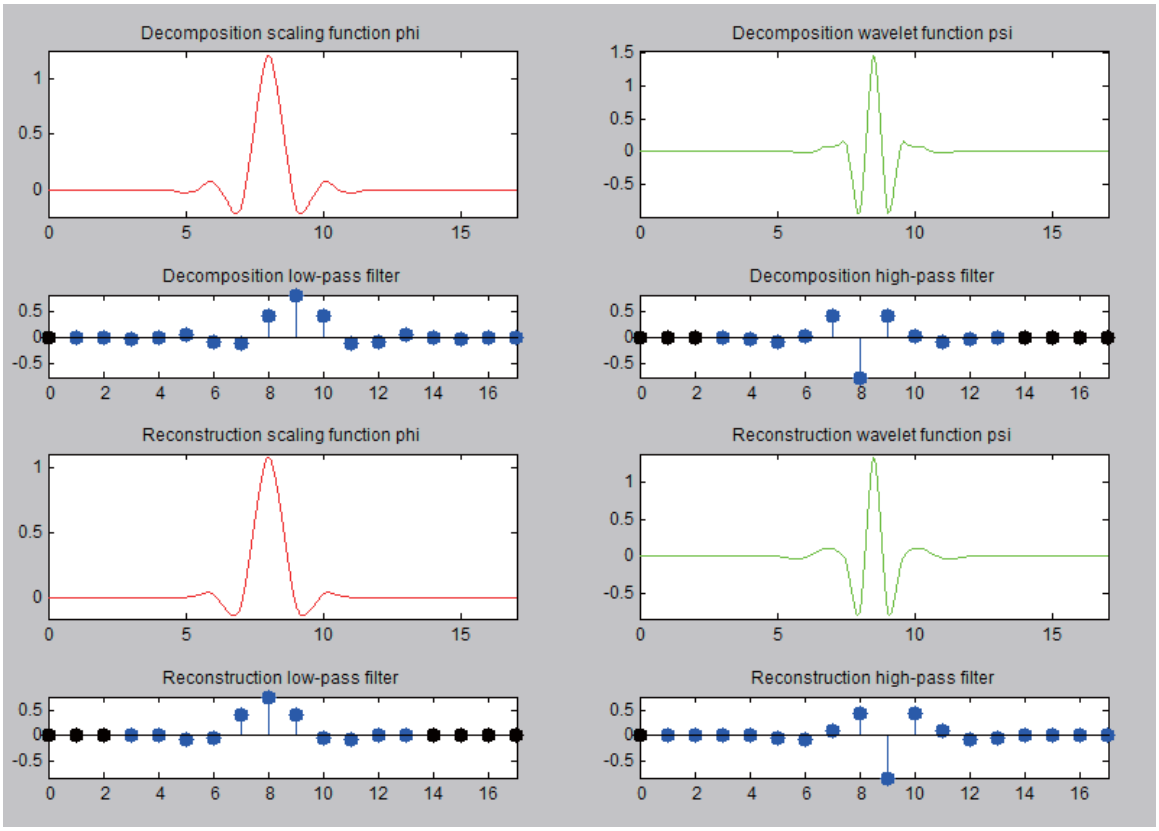

Figure 3.4: Functions of Biorthogonal Wavelet bior 6.8

In this study 1-D Wavelet Analysis Tool and its built-in bior 6.8 wavelet function is used for signal denoise. 12 levels of decompose is sellected in order to separate more noise from the original signal. There are also 7 types of built-in threshold method available which are: Fixed form, Rigourous SURE, Heuristic SURE, Minimax, and Penalize(high, medium, low) by feeding ECT signal into these thresholds, Penalize medium is used because it has the best result. For thresholing type, we also need to choose between soft and hard thresholding. the differences is that for hard thresholding, the wavelet coefficients remains in the result in in signal reconstruction, whereas

for soft holding the coefficients will be eliminated. The soft thresholding provides user with more smooth signal and it is important in some signal processing, such as image processing. However in our study both hard and soft thresholding have good performance.

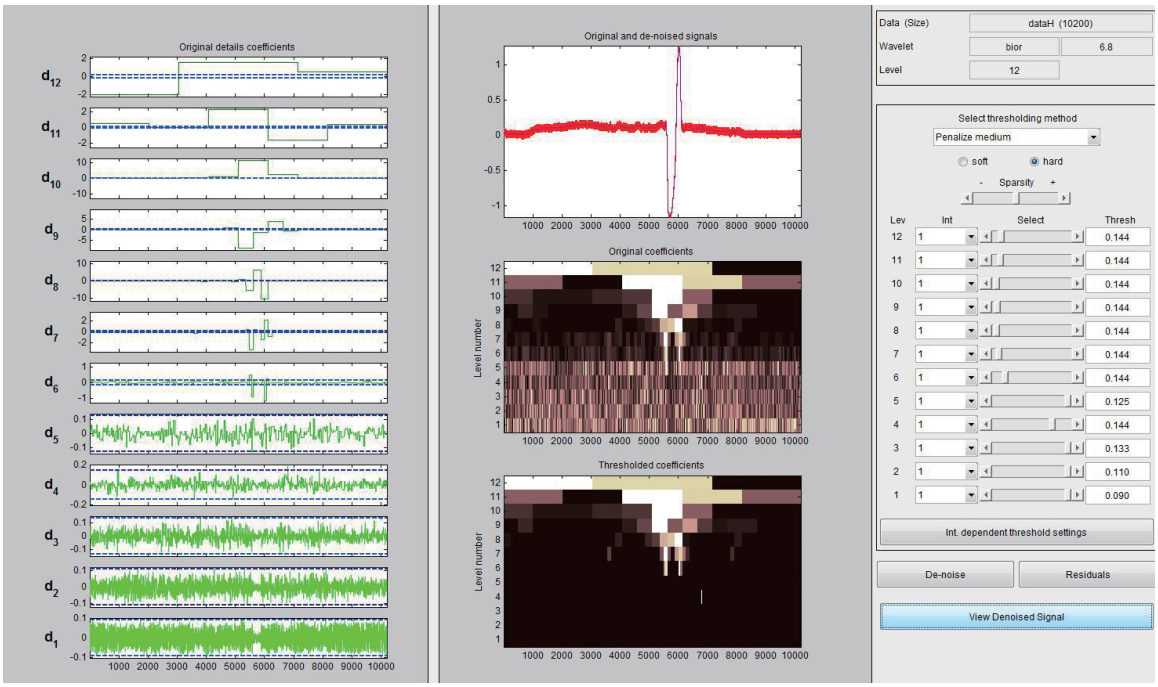

Figure 3.5: Biorthogonal wavelet filter design using matlab

As shown Figure 3.6 and 3.7, the data from x-axis before and after de-noise demonstrates a good noise removal result.

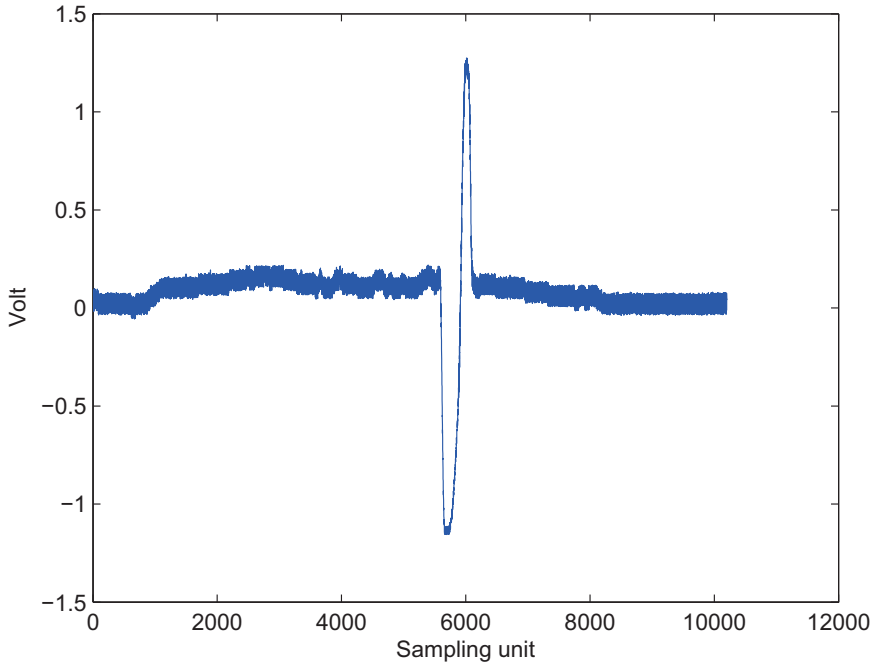

Figure 3.6: ECT signal on x-axis before applying wavelet filter

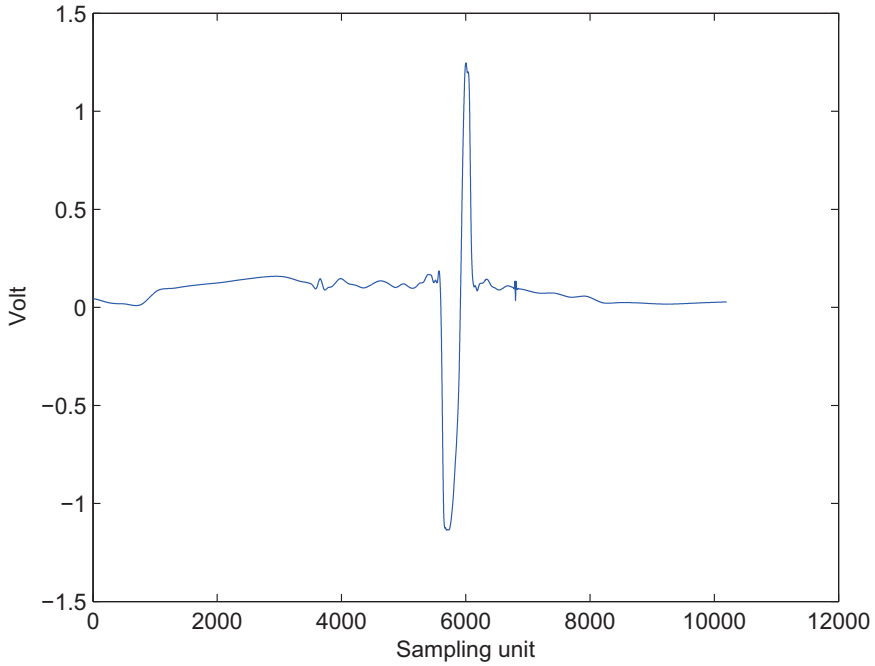

Figure 3.7: ECT signal on x-axis after applying wavelet filter

As shown Figure 3.8 and 3.9 data from y-axis before and after de-noise demonstrates a good noise removal result.

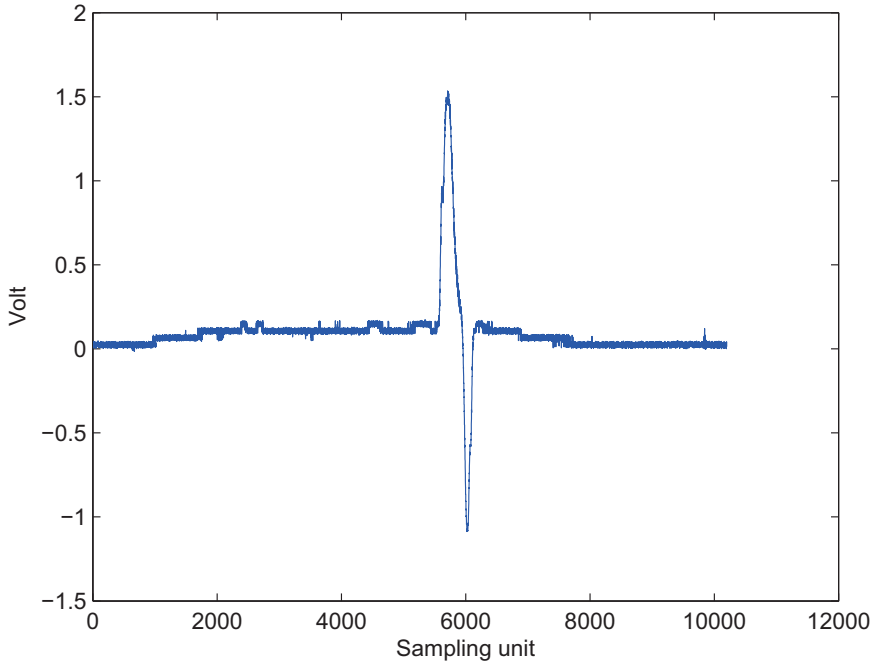

Figure 3.8: ECT signal on y-axis before applying wavelet filter

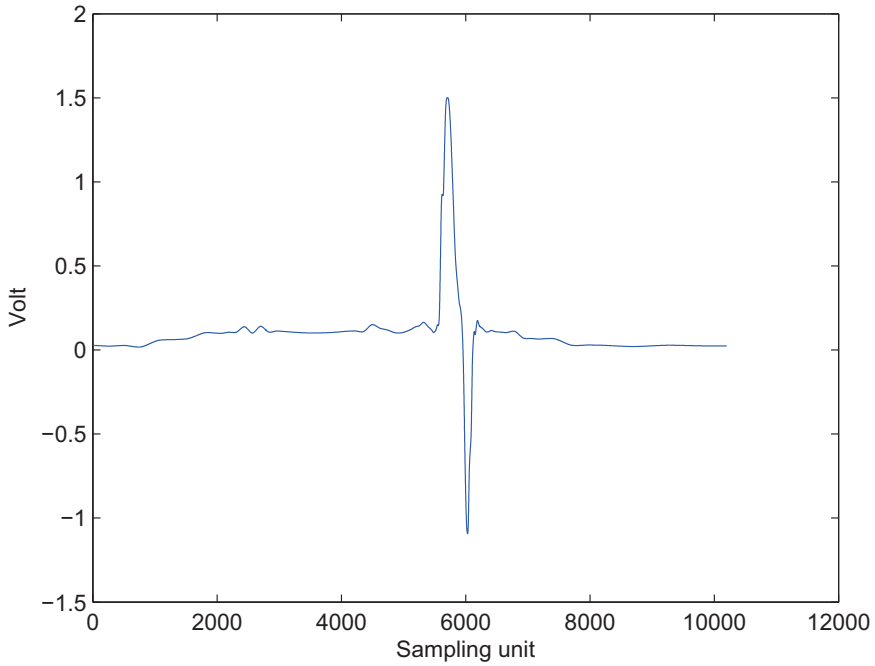

Figure 3.9: ECT signal on y-axis after applying wavelet filter

Figure 3.10 and 3.11 show the data from x-y plot before and after de-noise. The results demonstrate a good noise removal performance.

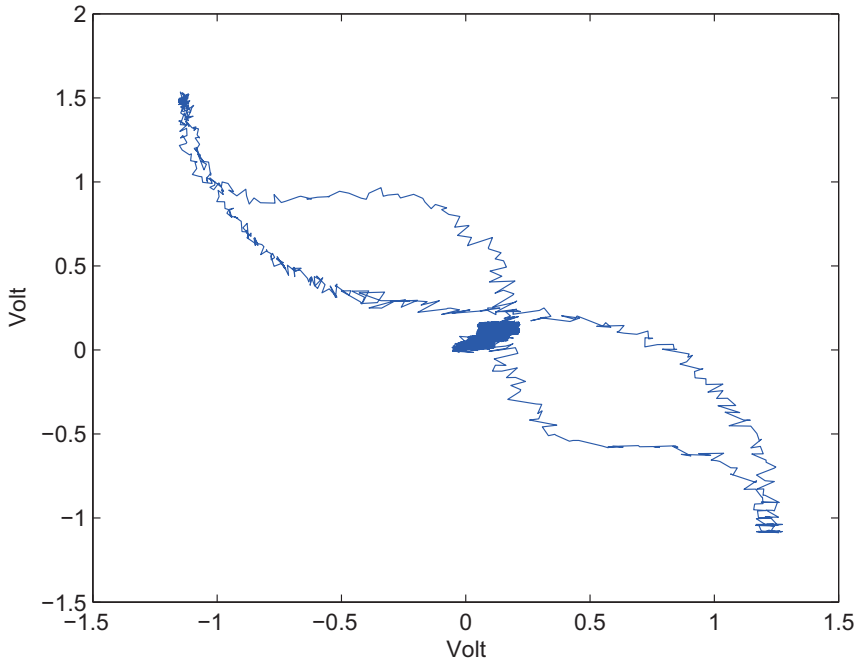

Figure 3.10: ECT signal on xy-axis before applying wavelet filter

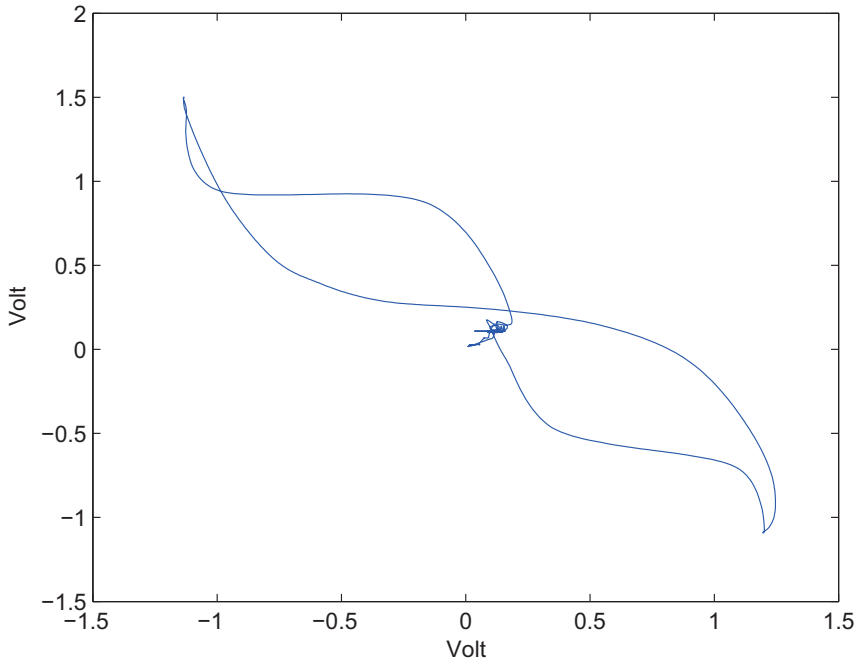

Figure 3.11: ECT signal on xy-axis after applying wavelet filter

Another issue with regard to signal noise is how to eliminate the useless signal around the center point due to lift-off. A shown in Figure 3.12, the lift-off can affect the calculation of the signals width.

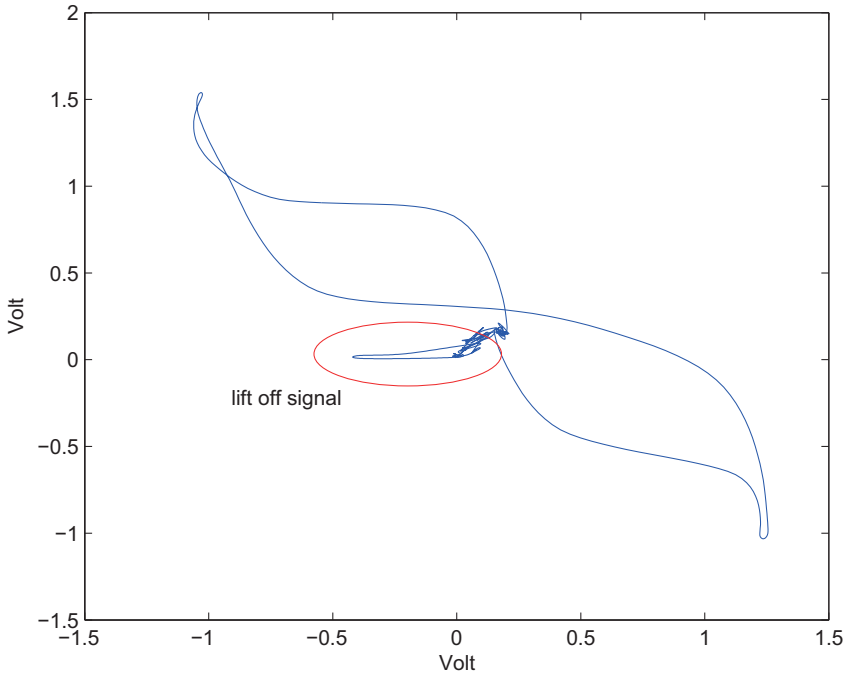

Figure 3.12: Signal affected by Lift off

The algorithm of eliminating this kind of signal is to get the signal which represents the crack only. The steps are described as follows: as shown in Figure 3.13 the first step is to find the peak points of the individual x-axis or y-axis signals shown in *. Then calculate the maxim and minim value of the entire signal which is shown in dot. The last step is to calculate the angle between each peak points and the maxim and minim value. The location of smallest angle indicates the point where the signal begins to have major shift. The signal within this range is considered as the "crack signal".

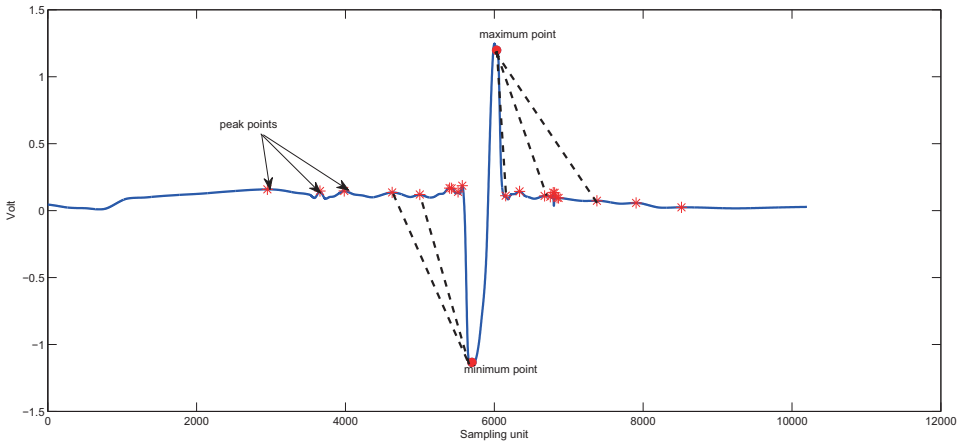

Figure 3.13: Crack signal fetch principle

Figure 3.14 shows x axis and y axis plot. The solid line indicates the fetched signal which is caused by crack and the dashed line represents unwanted signal irrelevant to crack.

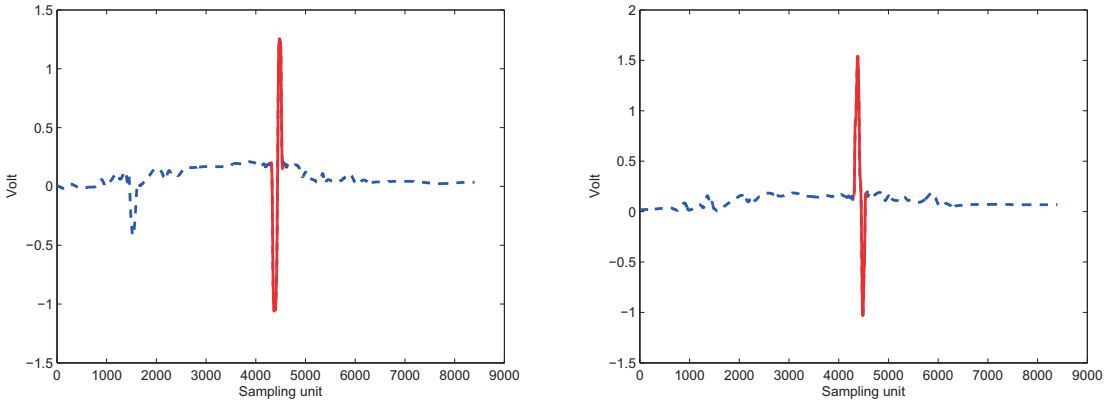

(a) (b)

Figure 3.14: (a) x-axis signal fetch result, (b) y-axis signal fetch result

Figure 3.15 shows the result of x-y plot. The solid line indicates the fetched signal which is caused by crack and the dashed line represents unwanted signal irrelevant to crack.

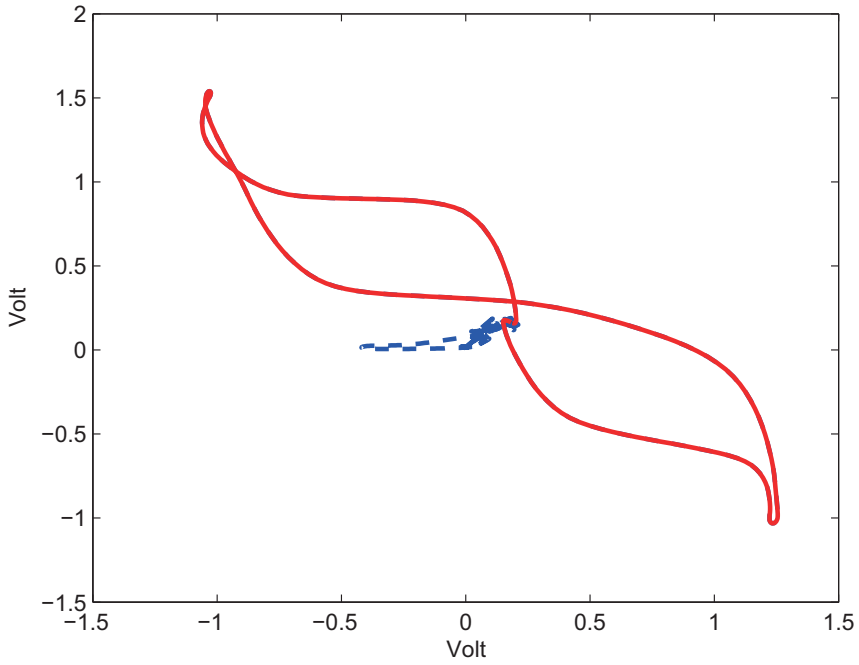

Figure 3.15: x-y axis signal fetch result

Comparing between Figures 3.12 and 3.15, it is shown that the unwanted signal due to lift-off has been removed. The processed signal is ready for the subsequent feature extraction.

3.4 Signal feature extraction

When eddy current coil interacts with testing samples, the changing of material property causes the changing of coil impedance. The coil impedance can be expressed as a two dimensional variable [19]

$$Z = R + jX_L \tag{3.2}$$

where R is the resistance of the coil (y axis), jX_L is the reactance of coil which can be influenced by testing frequency (x axis).

As shown in Figure 3.16, in eddy current equipment display, the signal is redefined as normalized R_{cn} and X_{cn} using voltage as output data. In impedance panel

the “amplitude” and “phase angle” represent the degree of impedance shifting which corresponds to the variation of examining sample.

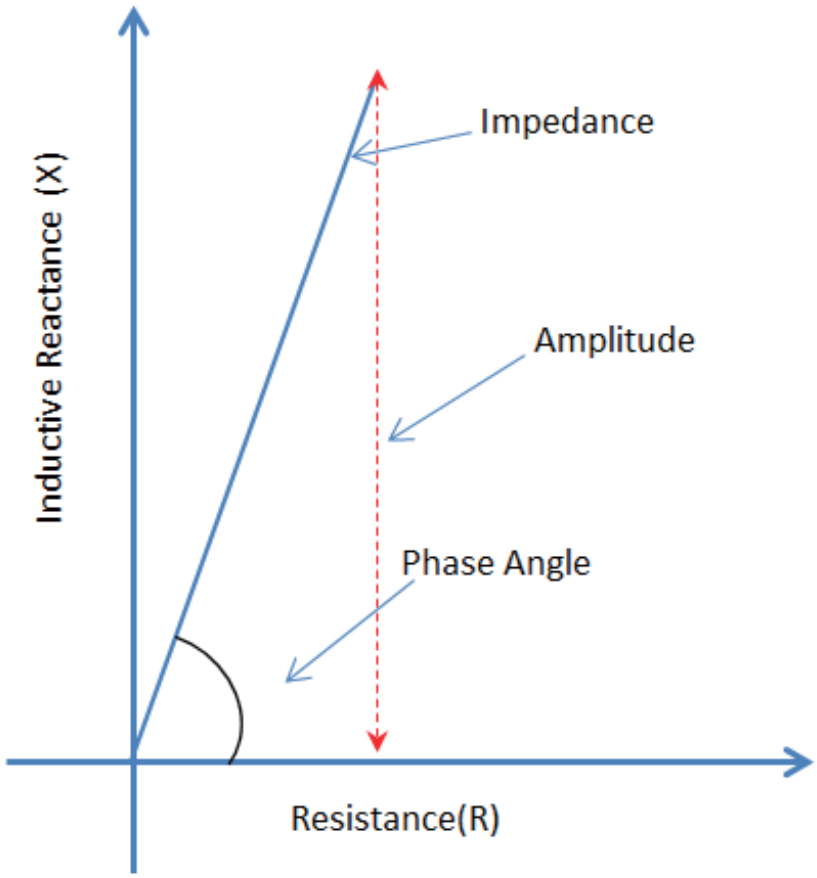

Figure 3.16: Impedance of eddy current test

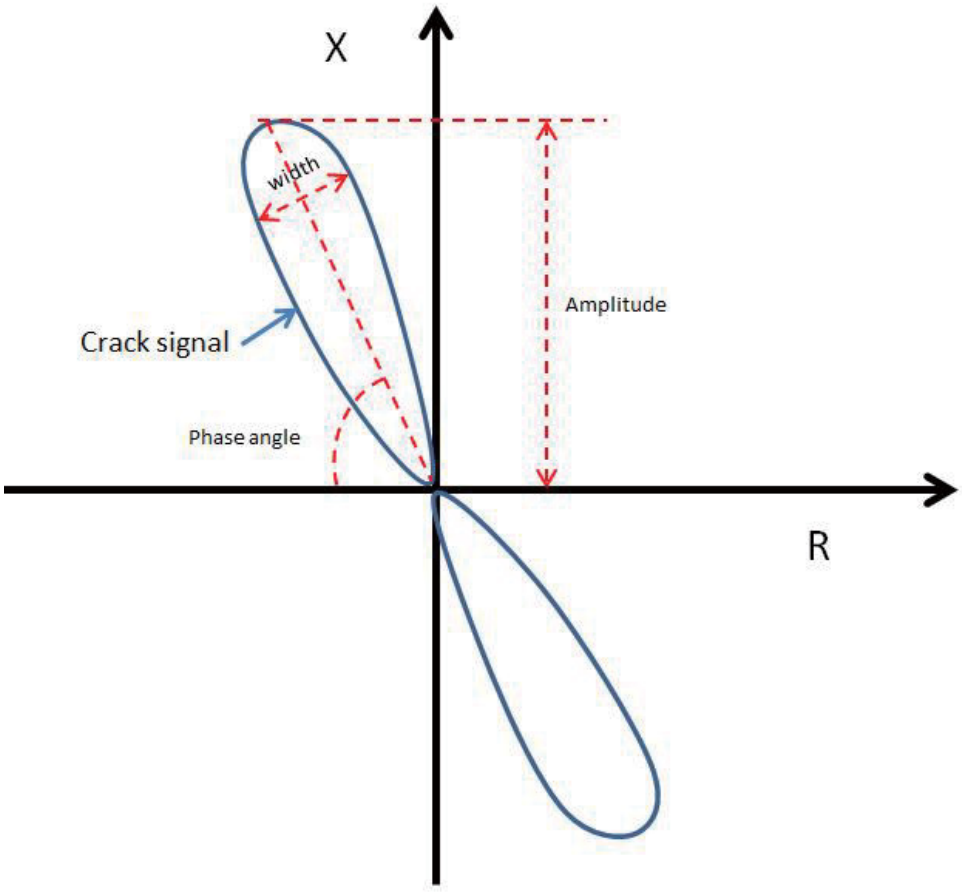

Figure 3.17: Typical crack signal from differential probe

For differential probe applied in crack detection, the signal is in "8" shape as shown in Figure 3.17. From the perspective of eddy current test inspectors, the high amplitude and large phase angle indicates the crack with large size. In this work "phase angle" and "amplitude" are calculated and utilized to determine the depth of crack. Another feature "width" will also be taken into account for crack sizing. It is observed that all these features from the "8" shaped signal are directly related to the crack information. Hence, to detect the crack and further find out the size and shape of the crack, some signal features which represent the important information of the crack need to be extracted.

As mentioned in Section2.4.2, Figure 3.18 demonstrates the differential signal generated with respect to the coil position over crack location. The data collected from eddy current equipment is plotted in x-y coordinate (volt). Each individual (x, y)

combination represents the impedance at certain time. Under ideal circumstance, the "8" shape signal is symmetric starting from the origin point (0, 0). But in reality, especially in manual operation the center point is not always on the origin (0, 0). In addition, the "8" shape may be asymmetric due to the asymmetric shape of probe coil.

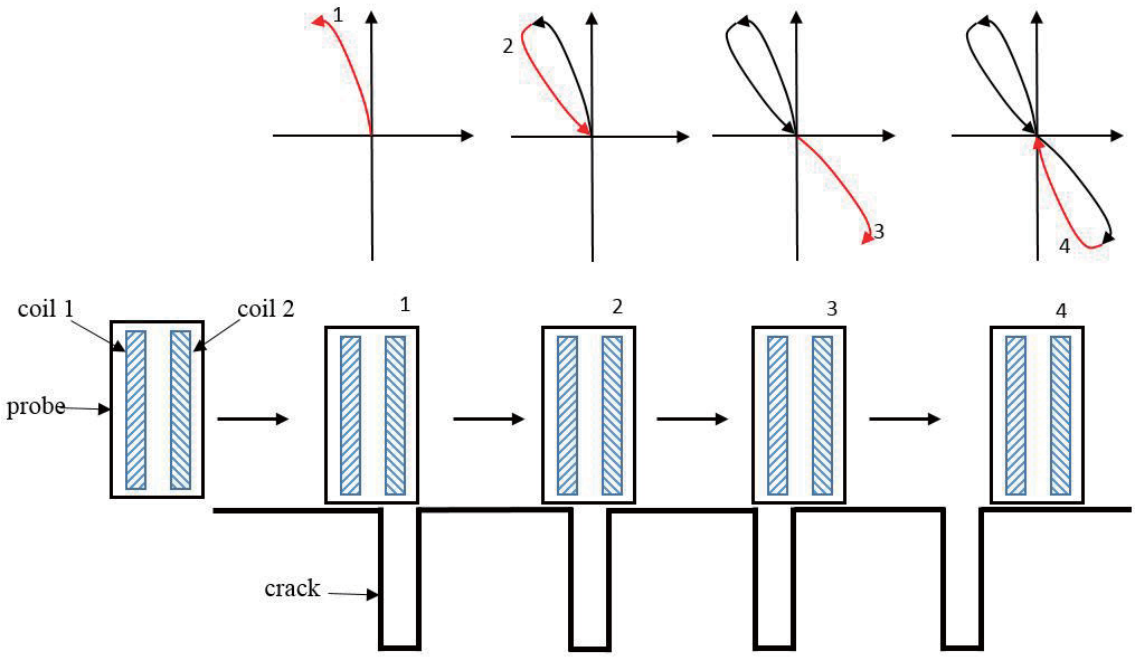

Figure 3.18: "8" shaped signal generation

The feature extraction algorithm is designed as shown in Figure 3.19. The following steps are developed to extract the desired signal features.

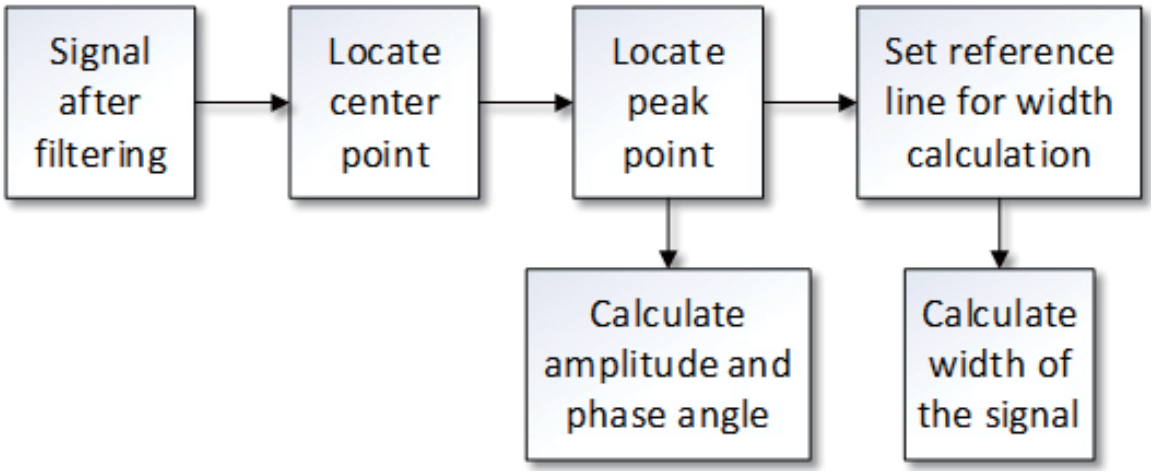

Figure 3.19: Feature extraction flow chart

1) Find the actual signal center point which is the point where the signal is originated. Ideally the signal generated from coordinate (0, 0), however in practice, espially for manual scan the origin point can be shifted which is dennoted as (x_0, y_0) and then compute the distance between each x,y coordinates based on equation (3.3).

$$normal\,impedance = \sqrt{(x_0 - x_i)^2 + (y_0 - y_i)^2} \tag{3.3}$$

2) Locate the maximum normal impedance as peak point (x_{max}, y_{max}), calculate the slope ratio k and the phase angle.

$$k = \frac{y_{max} - y_0}{x_{max} - x_0} \tag{3.4}$$

$$phase\,angle = arctan(k) \tag{3.5}$$

3) Based on the peak point and center point, a reference line is formed. For any point (x_i, y_i), the calculation of width of the upper and down loop for the "8" shape signal is to locate the maximum vertical distance (d) between each individual point and the reference line.

$$d = \frac{|(x_{max} - x_0)(y_0 - y_i) - (x_0 - x_i)(y_{max} - y_0)|}{\sqrt{(x_{max} - x_0)^2 + (y_{max} - y_0)^2}} \tag{3.6}$$

The feature extraction results are shown in Figure 3.20, where □ indicates the center point, ∘ indicates the peak points in each loop, and * indicates the max width

of upper and downside loop.

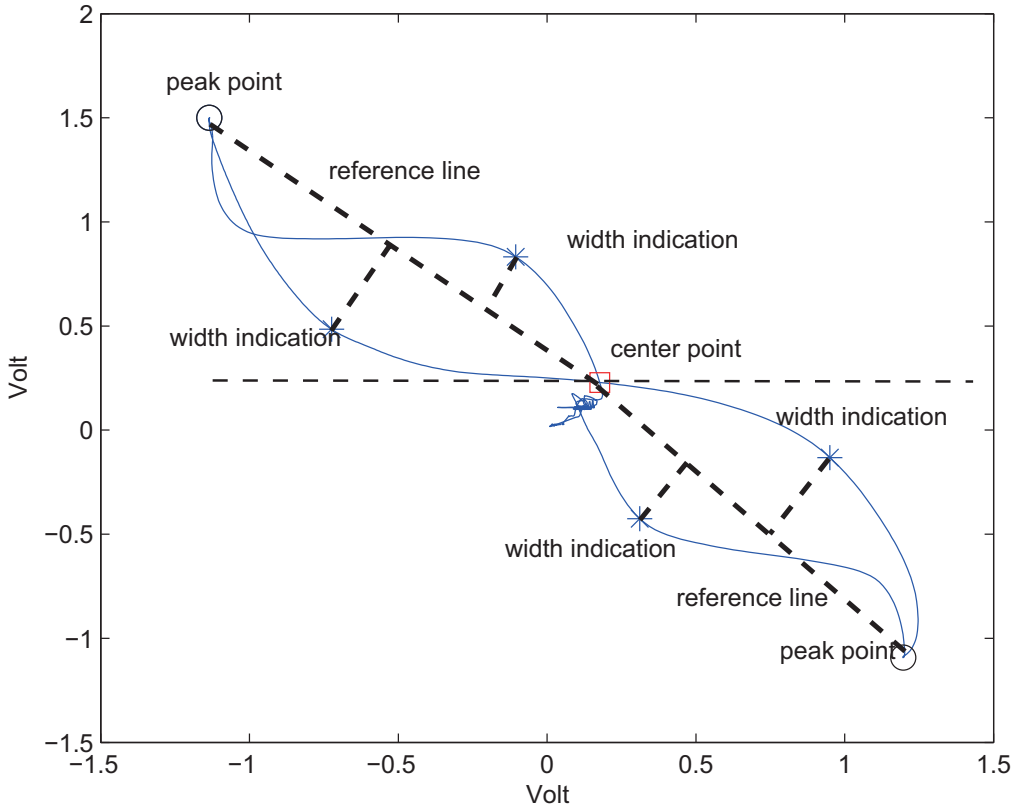

Figure 3.20: Result of feature extraction

The extracted features together with the known crack information are stored in the database for the fuzzy logic system training. It is observed that these features are related to the crack information and hence are used as the input to the fuzzy logic engine.

3.5 Fuzzy logic implementation

Fuzzy logic in this study is used as a decision maker, to provide the crack information based on extracted features: amplitude, phase angle, and width. This fuzzy based decision making system contains system input, system output, membership functions

(MF) and IF THEN fuzzy rules. The inputs are the features of crack such as amplitude, phase angle and loop width. The output of the system is the actual crack information such as depth, width and shape.

As shown in Figure 3.21, each input is related to one fuzzy set and each fuzzy set has its corresponding MF. The MF responds to the degree of each fuzzy set as a member in the membership in scale of 0 to 1 [6]. The fuzzification is performed in order to associate fuzzy set with MFs. Fuzzy rules are stated in IF-THEN linguistic sentences, which describe the relation between input and output for instance: IF the amplitude (input) is high THEN the crack depth is deep (output). Finally, because more than one fuzzy rule has been applied, and also the execution result is linguistic (deep), a defuzzification process is needed to transfer the linguistic variables into numerical crisp values [6] [41]. The flow chart of fuzzy logic is shown in Figure 3.21.

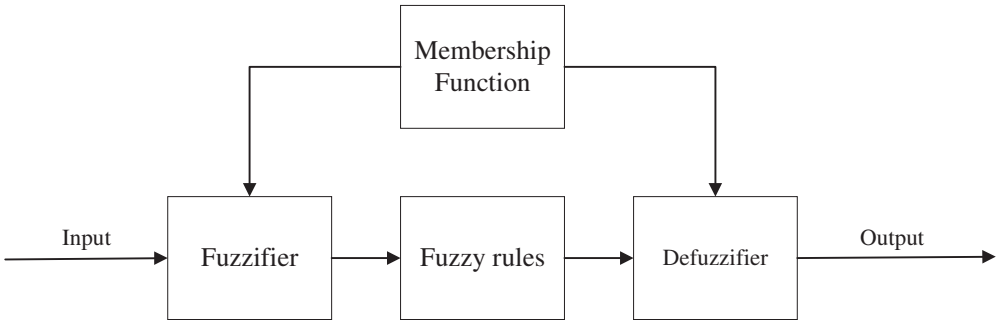

Figure 3.21: Flow chart of fuzzy logic

In this research, different frequencies are applied to exam the crack with different depths and shapes. For each MF, the numbers of MFs as well as the fuzzy rules should be developed independently according to different feature groups. In this work, ANFIS in Matlab is utilized as system learning process to obtain fuzzy logic system. Then this trained fuzzy logic engine is applied to predict the crack information based on the extracted features or the combination of the features.

Figure 3.22 shows the ANFIS mapping. The input features are: amplitude, phase angle and maximum width. The known output is the depth of the crack. By using

hybrid learning rule with linear output, Sugeno fuzzy logic system with multiple inputs single output (MISO) is generated 3.22. Figure 3.23 shows the trained fuzzy IF THEN rules.

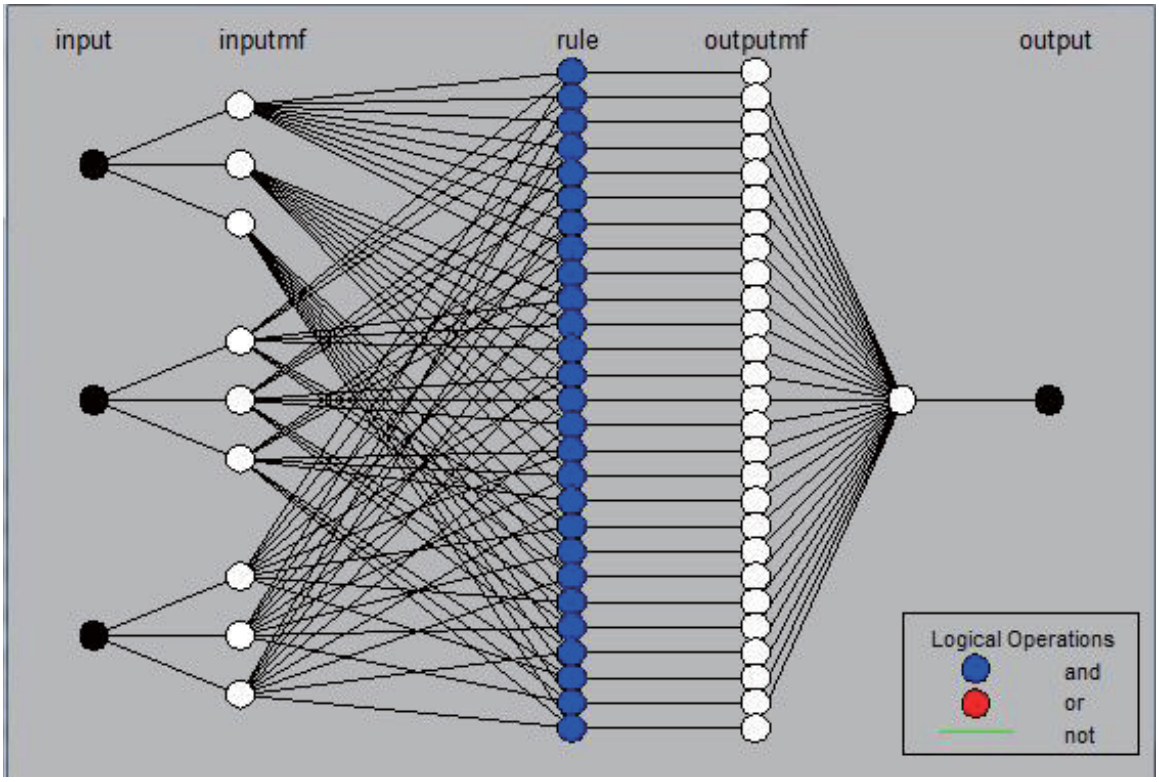

Figure 3.22: Neuro mapping structure

1. If (input1 is in1mf1) and (input2 is in2mf1) and (input3 is in3mf1) then (output is out1mf1) (1)
2. If (input1 is in1mf1) and (input2 is in2mf1) and (input3 is in3mf2) then (output is out1mf2) (1)
3. If (input1 is in1mf1) and (input2 is in2mf1) and (input3 is in3mf3) then (output is out1mf3) (1)
4. If (input1 is in1mf1) and (input2 is in2mf2) and (input3 is in3mf1) then (output is out1mf4) (1)
5. If (input1 is in1mf1) and (input2 is in2mf2) and (input3 is in3mf2) then (output is out1mf5) (1)
6. If (input1 is in1mf1) and (input2 is in2mf2) and (input3 is in3mf3) then (output is out1mf6) (1)
7. If (input1 is in1mf1) and (input2 is in2mf3) and (input3 is in3mf1) then (output is out1mf7) (1)
8. If (input1 is in1mf1) and (input2 is in2mf3) and (input3 is in3mf2) then (output is out1mf8) (1)
9. If (input1 is in1mf1) and (input2 is in2mf3) and (input3 is in3mf3) then (output is out1mf9) (1)
10. If (input1 is in1mf2) and (input2 is in2mf1) and (input3 is in3mf1) then (output is out1mf10) (1)
11. If (input1 is in1mf2) and (input2 is in2mf1) and (input3 is in3mf2) then (output is out1mf11) (1)
12. If (input1 is in1mf2) and (input2 is in2mf1) and (input3 is in3mf3) then (output is out1mf12) (1)
13. If (input1 is in1mf2) and (input2 is in2mf2) and (input3 is in3mf1) then (output is out1mf13) (1)
14. If (input1 is in1mf2) and (input2 is in2mf2) and (input3 is in3mf2) then (output is out1mf14) (1)

Figure 3.23: Fuzzy rules samples after training (part of)

3.6 Fuzzy logic training

For fuzzy logic training purpose, the best way to train the system is to use the data from real crack with theoretical modeling result and human inspectors experience. However, because the theoretical modeling is still developing and it is very time taking for us to collect data from the same human inspector. The only training data available currently is the ECT feature from DAQ.

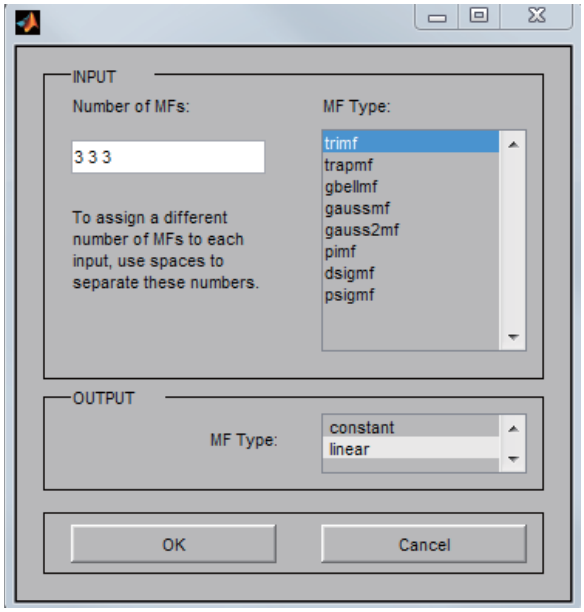

Figure 3.24: ANFIS training (MFs and number of MFs selection) in matlab

As shown Figure 3.24, there are a lot of combinations in terms of MF(membership function) and number of MF combination. It is very time consuming at the beginning of the project to find an accurate fuzzy logic training result just based only on ECT data. As shown in Figure 3.25 a user friendly interface is developed in order to accelerate the procedure. The main algorism is to generate all of the possible numbers for each MF. Then based on the training data and test data, best number for that specific membership function and the result will be given and the user can save the trained fuzzy logic for further use.

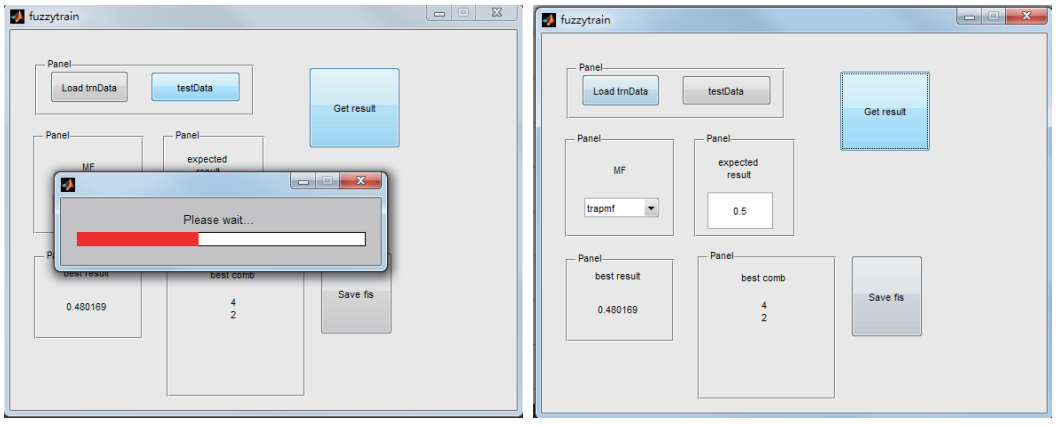

Figure 3.25: ANFIS training interface

3.7 Conclusion

In this chapter, an intelligent detection system based on Neuro-fuzzy has been developed including signal de-noise, signal feature extraction and crack decision making. The detailed design procedures for these three parts are presented. A user friendly interface is developed for the convenience of data input, fuzzy logic membership choosing and final detection display etc.

Chapter 4

Experimental Setup Design

4.1 Introduction

This chapter will give a brief introduction about equipment, data acquisition setup used in this study. The YASKAWA® motorman robot system is presented. In addition for practical experiment aspect, probe holder design is given as an extra duty related to this project. The software design of the interface of intelligent ECTsystem is given.

4.2 ECT equipment and data acquisition system

There are many ECT equipment from various companies available in the current market. Two of them are chosen for ECT experiment.

The first one is ECT equipment US-454 from UniWest® provided by industrial partner Pratt & Whitney Canada. It is a portable sophisticated ECT inspection instrument with accurate result as well as abundant test functions. The reasons of selecting this equipment are listed as follows: 1. rental is available from Pratt & Whitney Canada, to avoid additional purchase; 2. the acquired signal is the same as that in industrial practical application which could be used to compare human inspector's result with signal processing result; 3. various types of probes are available for more complex geometry ECT scan in the future; and 4. testing method and consultant are available from industrial NDT engineers.

The second one is ECT equipment Olympus® Nortec 500S provided by École de technologie supérieure (ETS). The reasons of choosing this equipment are listed as follows: 1. it is available from ETS lab ; 2. it comes with standard known notch cracks as well as other ECT test samples (conductivity, corrosion, etc.); 3. the equipment is accurate, easy to use and suitable for self-learning; 4. the ECT experimental results and testing consultant are available from ETS based on this equipment.

The objective of using two ECT equipment in this project is to establish a cross-comparison process on the same crack between two different equipment in order to help the team have a better understanding of eddy current interpretation as well as building up fuzzy based ECT crack signal archive based on these two ECT equipment. In this paper particularly studies are based on Olympus Nortec 500S.

For different ECT equipment, different data acquisition cards are used respectively. National instruments NI PCI-6229 is used for UniWest® US-454, and National instruments NI USB-6009 for Olympus® Nortec 500S.

National Instruments® NI PCI-6229 is a sophisticated PCI data acquisition (DAQ) card which performs high sample speed and low signal to noise ratio. To connect PCI-6229 to computer not only a connector block is required but also a 68-pin X Series to M Series high frequency cable is needed. Because this DAQ card have a relatively high performance and it is selected to acquire the data from ECT equipment UniWest US-454.

National instruments® NI USB-6009 on the other hand is a portable USB DAQ card which has a good performance and easy to use feature. Only USB cable is required to connect USB-6009 to computer. Unlike the cable used for PCI-6229 whose length is limited due to its high speed features, the USB cable can be prolonged as the experiment requires. It is also convenient to make analog input channel connection adjustment since all the I/O ports are available on the DAQ card. Because the ECT equipment is installed on robot arm which have many motions (up, down and rotation), a lot of hardware installation and configuration needs to be adjusted and revised. Experiments in this thesis is conducted via USB-6009 connected to Nortec 500S.

4.3 ECT testing method and YASKAWA MOTOMAN SV3X Robot

In this project two types of ECT scan are performed. The first one is based on the commonly used method of ECT operation which is manual scan. For notch and large crack, it is one of the simplest and the fastest ways. However, it generates certain amount of noise due to unstable of human handholding. The developed DSP filter can be used to remove such noises. In addition for aircraft maintenance purposes, most of ECT is performed manually. It is necessary to train the fuzzy logic based on data acquired manually.

Another way of ECT scan is for the small cracks, where case the scan frequency is high and the ECT signal is highly sensitive to small interruption. The robot arm is used not only to provide a stable scan process, but also to support other NDT method such as FPI in this project. The robot arm is YASKAWA® Motoman SV3X six axis robot arm with Motoman XRC controller in the lab of National Research Council (NRC). As mentioned before and shown in Figure 8, the YASKAWA®

Motoman SV3X robot arm has 6 axis which are: S-axis (turning ± 170); L-axis (lower arm +150, -45); U-axis (upper arm +190, -70); R-axis (wrist roll ±180); B-axis (wrist pitch/yaw ±135); T-axis (wrist twist ±350) [22]. Each axis processes capacity of high speed, accuracy and the ability of providing the robot arm with large range of operation area as well as excellent flexibility. It is able to perform complicated path operation with regard to component geometry [23]. The way to control the robot is to modify the coordinate of each axis accordingly to the motion objective through its programing language defined as robot job file. For safety consideration, robot arm simulation is required to be done before actual robot manipulation via Motosim software provided by YASKAWA®.

In addition in this study, the communication with robot controller is required which is proposed by industrial partners. The aim of adding this function into the scan system is to further utilize the robot in order to preform online crack coordinate recording so as to provide the DAQ system with the information to go back at the crack location after first time scan and do double check or detailed crack exam. As shown in Figure 4.1, according to the acquired data, the computer is expected to

send the controller a signal as ±12V when encounters with a possible crack indication online. Then according to the pulse signal, the controller is able to record its current coordinate and save it. When the scan is finished, the controller can control the robot arm to go back to crack indication for a double scan in order to verify the crack. Currently the dashed function is still under development by the other team member in this project.

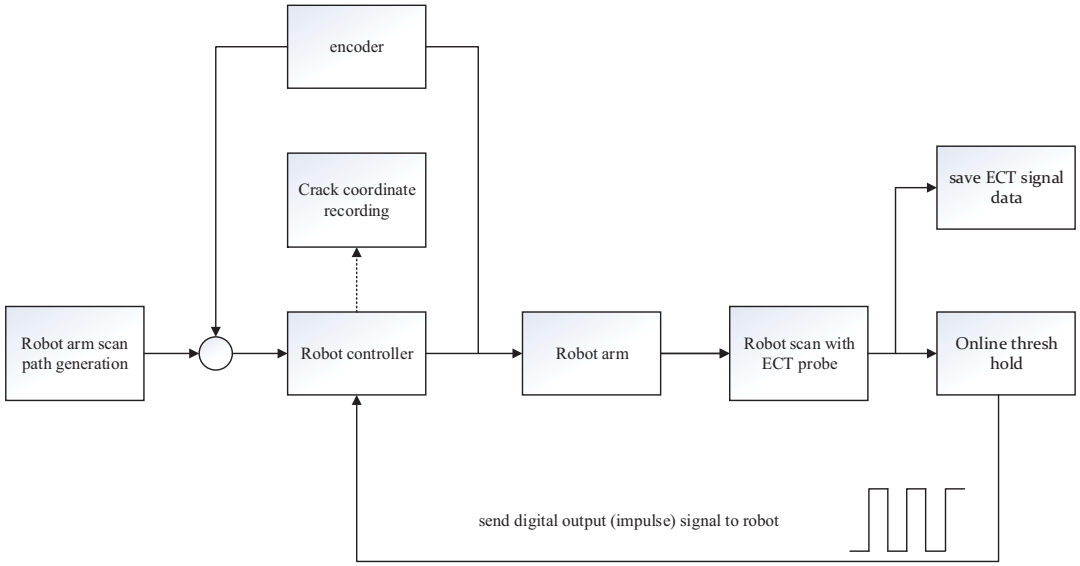

Figure 4.1: Flow chat of robot communication

Motoman XRC controller is a reliable and accurate robot controller based on powerful 32-bit microprocessor for its data processing. It is able to run up to 6 tasks at the same time and control 3 robots simultaneously. It also has built in digital I/O and analog output function [42]. There are three ways in terms of communication and command. The first one is using the teach pendant. This is the most common and convenient way to control the robot. Not only it has the function to control the robot arm to move around and load the job file which is the robot arm motion program, but also it allows certain interaction with the controller such as such reading the robot speed, and saving current position etc.. The second one is using SD memory card for robot communication. In current state of this project the communication to controller is based on using SD card to load and sending job file to the robot.

The procedures are given as follows: 1. A path generation program is written to define the robot motion. Then the motion program is copied to memory card then was loaded to the controller via teach pendent. This way is simple yet belongs to one way communication which is solely sending command to controller. In terms of interaction, what needs to be done is to establish a communication method between ECT signal and the robot controller so that the coordinate of crack indication can be automatically recorded. The third way of communication is through I/O ports of the controller. It enables the user to have access to the controllers general register so as to manipulate controller at a higher level.

The current study has been done with regard to processing ECT signal online and sending pulse signal based on crack indication. ECT output has two channels that represent the x and y-coordinate and as shown in Figure 4.2 the signal is a sinusoid when encountering with a crack. The online threshold is needed for signal progressing at each step, since the points exist all the time but it is hard to know when the peak value represents the real crack indication occurs. Thus it is challenging to determine such threshold to distinguish the peak values and the crack indication. An on-line threshold determination algorithm is proposed by saving the data within a first few seconds (user modifiable) of scan process before the crack is detected. Then the average values of the saved data is served as a reference. Finally this average value is used to compare with certain user defined threshold to determine whether the current signal is an indication of potential crack.

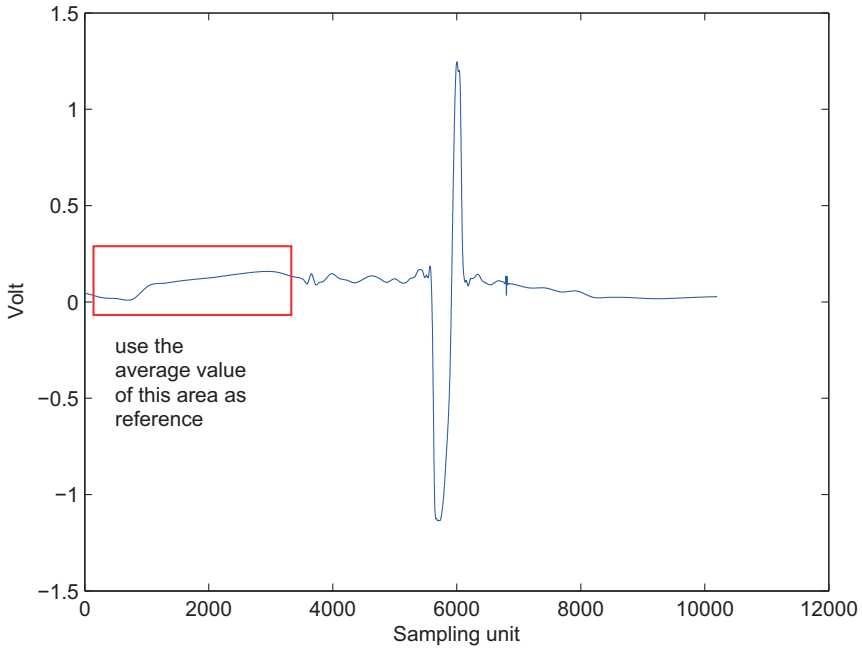

Figure 4.2: x (or y) axis sinusoid ECT signal

The online average calculation is carried out on matlab Simulink. In the process, it is noticed that using Simulink MEAN function introduces the delay of data collection since the sampling rate is 1000/s, so the data could be very large in a few minutes. To solve this problem, an alternative way to calculate the average value in a period of time is carried out. The principle is to use the integral of the signal over time described as in Equation (4.1).

$$Avg = \frac{\int_T^0 f(t)dt}{T} \tag{4.1}$$

where *f(t)* denotes the signal function over time t, T denotes the total time period The average value calculation algorithm is designed as shown in Figure 4.3.

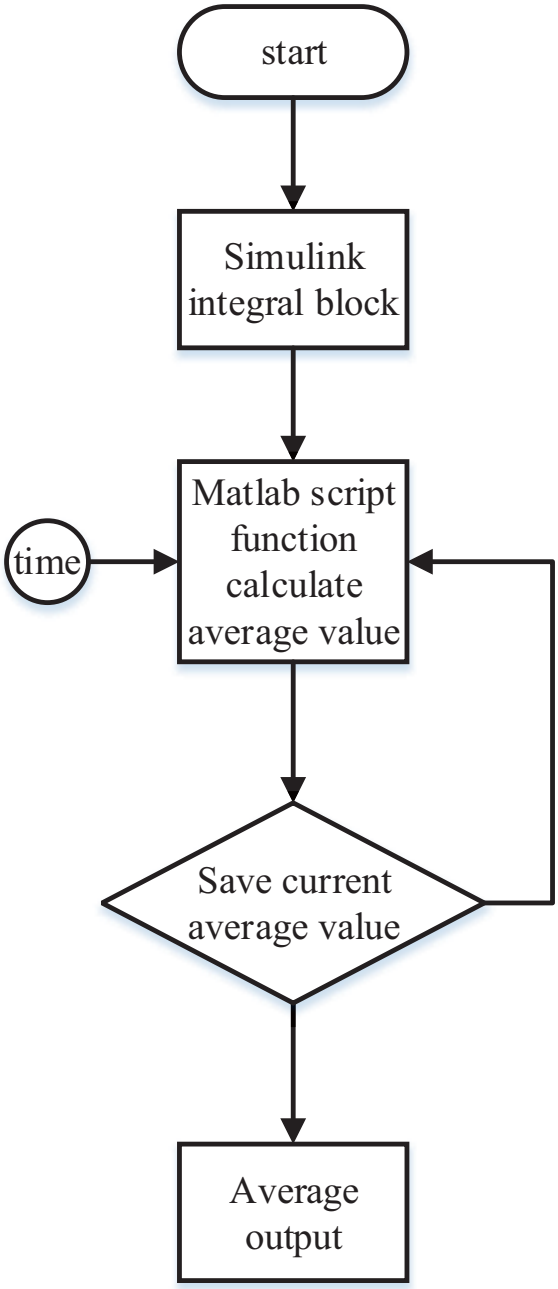

Figure 4.3: Flow chart of average value calculation algorithm

The following steps are the numerical implementation of Equation (4.1).

1) The mean value equals the total amount of f value over the amount number of f function shown as Equation (4.2)

$$Mean = \frac{|f(t_1) + f(t_2) + \cdots \cdot f(t_n)|}{n} \tag{4.2}$$

where n denotes the total amount of f functions

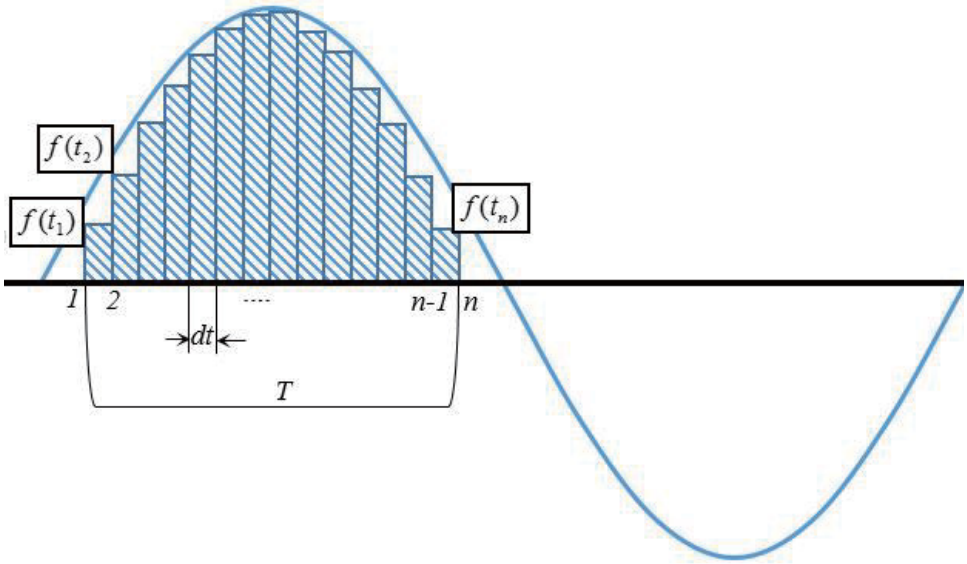

Figure 4.4: Total area calculation of a curve plot

2) As shown in Figure 4.4 A is the total area of a curve can be considered as the sum of infinite small rectangular, shown as Equation (4.3).

$$\sum_0^n A = \int_0^n f(t)dt = f(t_1)dt + f(t_2)dt + \cdots \cdot + f(t_n)dt \tag{4.3}$$

3) Since one has

$$T = ndt, \tag{4.4}$$

Equation 1 can be rewritten as Equation 4.5

$$Avg = \frac{\sum_0^n A}{T} = \frac{\int_0^n f(t)dt}{ndt} \tag{4.5}$$

Combining Equations 4.2 and 4.5:

$$Avg = \frac{[f(t_1) + f(t_2) + \cdots + f(t_n)]\cancel{dt}}{\cancel{n}\cancel{dt}} = \frac{|f(t_1) + f(t_2) + \cdots + f(t_n)|}{n} = Mean \tag{4.6}$$

Figure 4.6 shows the Simulink diagram. The calculated average value is compared with modifiable threshold value. When the incoming signal surpasses the threshold, a pulse of "high" signal will be sent out. In addition digital to analog converting needs to be done via adding converting module into the diagram. As shown in Figure 4.5 On/off delay module is added in order to prolong the duration of each pulse Because the initial time duration of crack indication pulse is too short for the relay to react. As a result, a 1 sec signal delay is added and output voltage is set as 12V. However, because of the on/off delay, if multiple cracks are detected, the overlap will affect the judgment. More hardware reconfiguration will be done in the future in order to solve the problem.

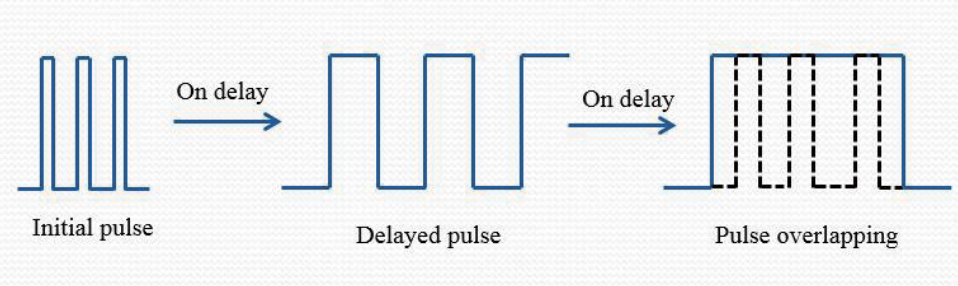

Figure 4.5: Issue of overlap after on/off delay function

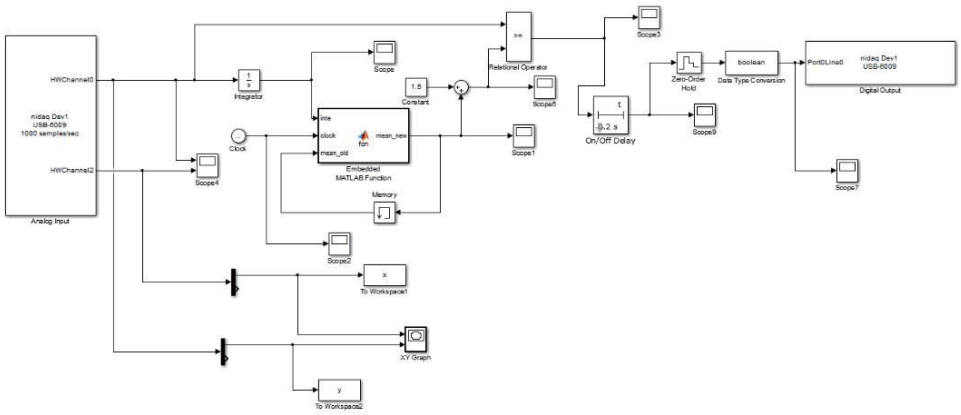

Figure 4.6: Simulink function for data average

4.4 Probe holder design

Another practical issue in this study is to connect the ECT probe to the robot arm. There are several aspects that should be taken into consideration when designing the probe holder. First, the probe holder should be easy to produce. Secondly, a simple but effective mechanism should be added in order to protect probe from damage such as collision. Finally, the grasp should not only be firm in high frequency when a little disturbance of probe has big effects on the entire testing result, but also fixable, in order to protect the probe. Hence, the rigid probe grip could slowly damage the probe when performing multiple scan tasks.

The first holder is designed in order to simplify the fitting with the robot arm stem whose specification is shown in Figure 4.7. The material is stainless steel (SS) which is the same as robot stem. A bolt is added at the grip section in order to adjust the force of griper by loose and tight the screw. But the issue is that stainless steel is time taking to machine as well as the hardness is too high compared to the material of the probe. This could be a potential risk factor even with an adjustable grip force. In addition, there is no mechanism to protect the probe from vertical impact.

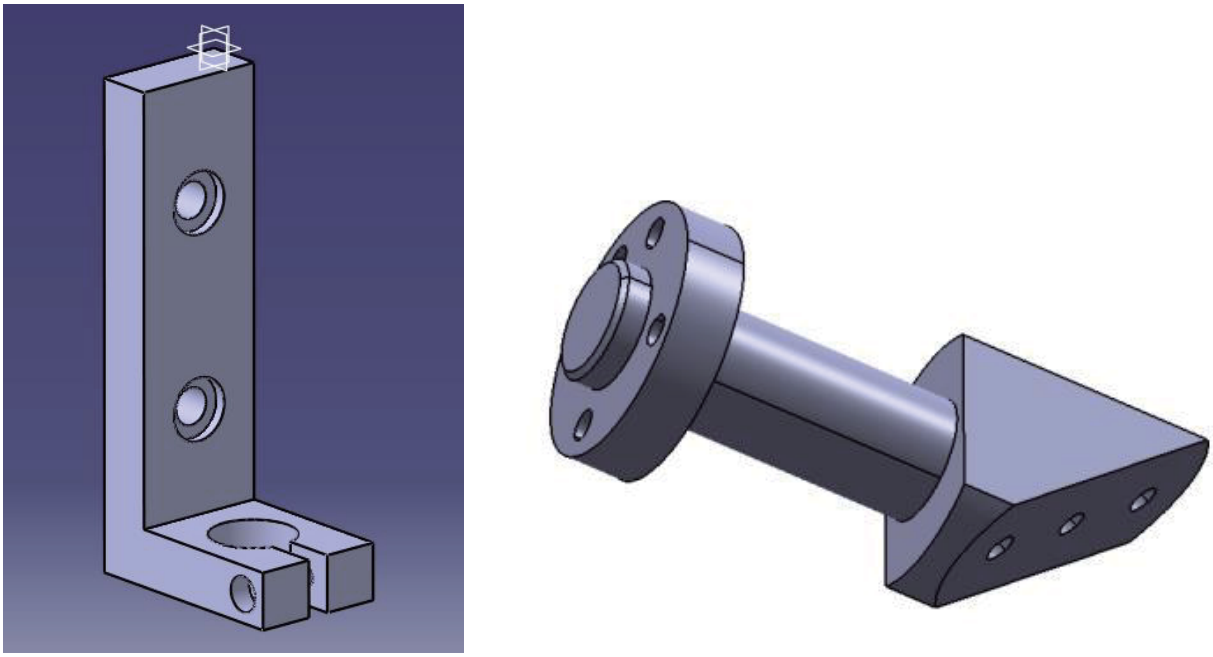

(a) (b)

Figure 4.7: Probe holder initial design (a), and robot arm stem (b)

Before the robot scan, calibration is required to ensure the robot arm is able to provide interpolation operations such as linear and curvature. There are two main calibrations needed for this project with regard to ECT. The first is the tool calibration also known as tool teaching process. As shown in Figure 4.8 [9], five different poses are processed with the tool center point as the reference. This process is to define the tool center so that the dimensional information is registered into robots coordinates. By touching the tip of tool to the center point, the robot is able to learn how to manipulate its 6 axis accordingly in order to reach anticipated position.

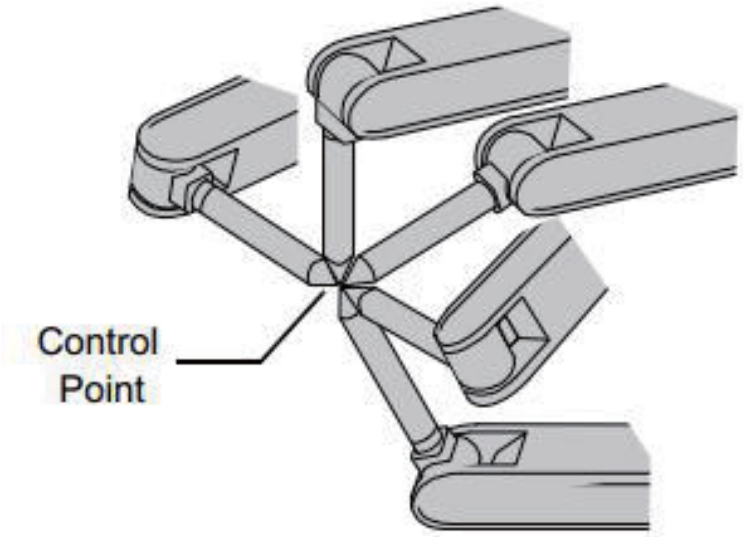

Figure 4.8: Robot tool teaching [9]

Another calibration is called user coordinates setting. In other word, this step is to teach the robot where the work platform is and where the job initial position is. As shown in Figure 4.9 [9] the working interface needs three points to calibrate, which are original point (ORG) where each job starts, also known as home point; X point, which is a point in X-axis, XY point which is on Y-axis side. The direction of Y and Z-axis is defined by point XY [9].

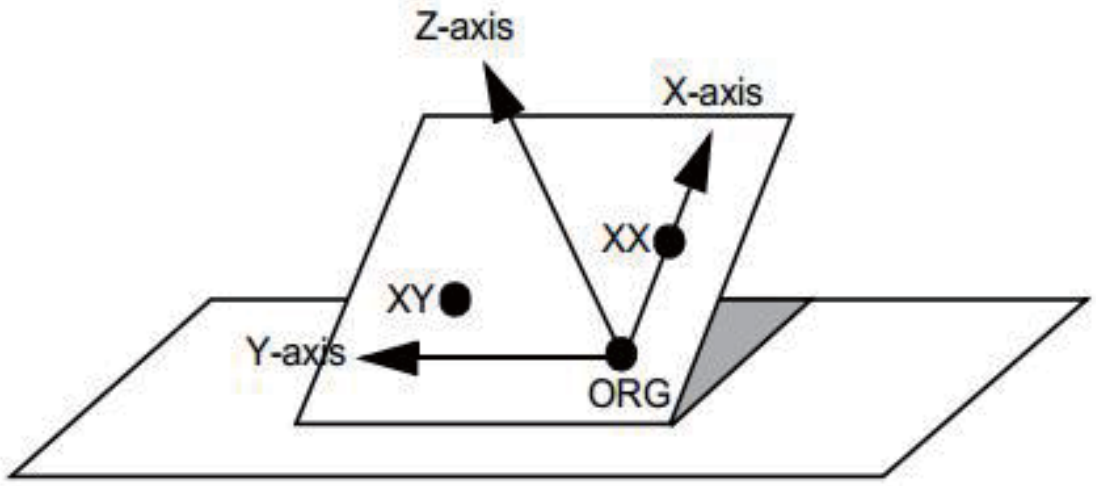

Figure 4.9: User coordinate identification [9]

In the process of user coordinate calibration, the ORG and XX point must be taught precisely. In reality when performing calibration, it is very challenge to utilize the robot to touch three points XY, XX and ORG precisely in the same surface. Therefore, calibration errors are inevitable especially on Z axis which is shown in Figure 4.10. The error caused by scan path tilt in Z-axis results in tilt in tool motion route. Although the error is very small and even cannot be visually observed, such error can cause the probe to have too much lift-off (from the scan surface) (refer to 2.4.2) or in another direction, tend to press too much against the surface, or result in damaging the probe since the probe is very sensitive to Z direction variation. Thus a spring load probe or probe holder is necessary and important to reduce the calibration error on Z axis.

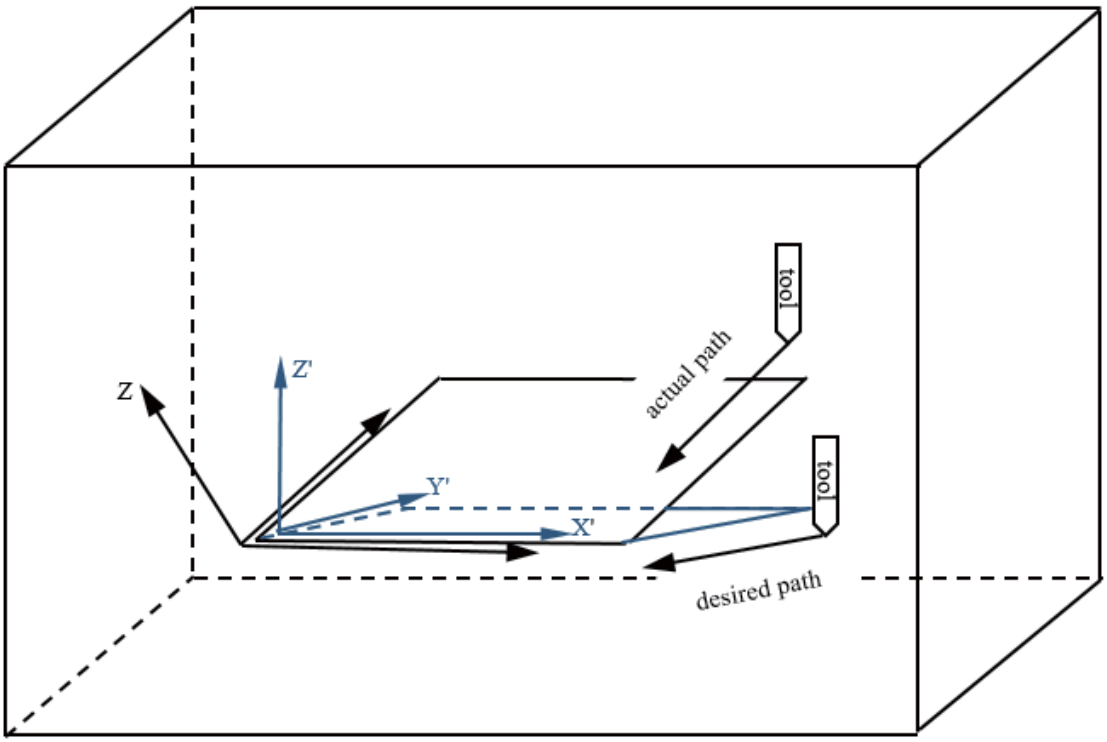

Figure 4.10: Calibration error results in scan path tilt

A spring loaded probe holder is needed for robot ECT not only to protect the probe but also to compensate the robot calibration error on Z axis. Several options are available: 1. ECT equipment supplier can support with customized spring loaded probe; 2. Pratt & Whitney Canada is able to provide spring loaded probe which could be used in US-454. But need to purchase cable. 3. Revise the current probe holder design to add spring into the holder.

As shown in Table 4.1, three options are listed on spring loaded mechanism and the third option is the most efficient in terms of time and cost. In addition, not only the structure of probe holder needs to be revised but also the material of the probe holdershould be changed. Hence, ABS (Acrylonitrile Butadiene Styrene) is used as an alternative softer material which is able to potentially protect the ECT probe, and 3D printing technology in the partner–Polytechnic University is used for the components manufacture.

Table 4.1: Spring loaded mechanism options

spring load options	**item needed**	**cost**	**estimated delivery time**	**addition point**
customized spring loaded probe	contact manfacture	CAD $1500	approximately more than 2 months	TBD
existing spring loaded probe	cable	USD $345	2 weeks	optional when use US-454 for ECT
spring loaded probe holder design	ABS	Very low cost of ABS	less than 1 week	design can be revised if needed
	low friction slide	CAD $110.83		
	compression spring	CAD $4.9		

Laboratory 3D printer is used for prototype and mock up sample production. Based on the designed digital 3D model, it is able to gradually deposit the materials down layer by layer into the desired position in order to form the needed shape. Although 3D printing is still a laboratory technology under development, in this case for producing the probe holder, it is a perfect candidate for manufacturing since the geometry of the part is not too complicated and the smooth surface requirement is not too high.

In order to provide a smooth and accurate vertical up and down movement for spring load function, a low friction slider is selected as shown in Figure 4.11, for vertical motion solution.

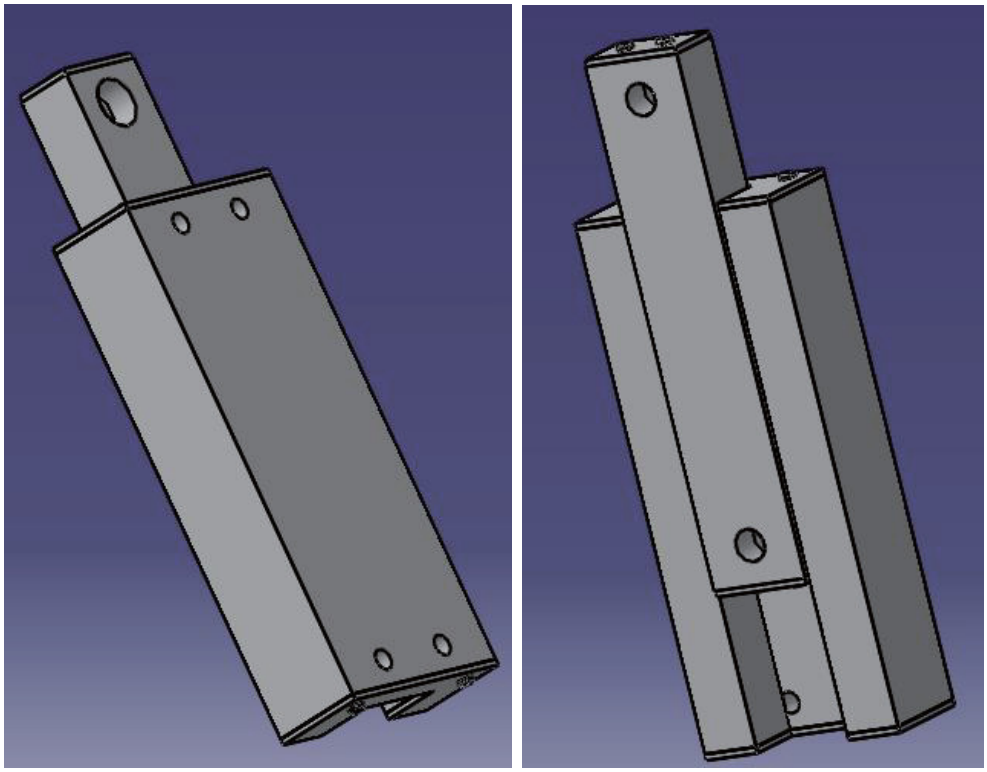

Figure 4.11: Ball bearing slider

The concept of designing the rest of the probe holder is to assemble the other parts on the slider. As shown in Figure 4.12, the other components are served not only to connect the probe with robot stem but also to assemble around ball bearing slider. On the top of the holder, two cylinder grooves are made for spring installation.

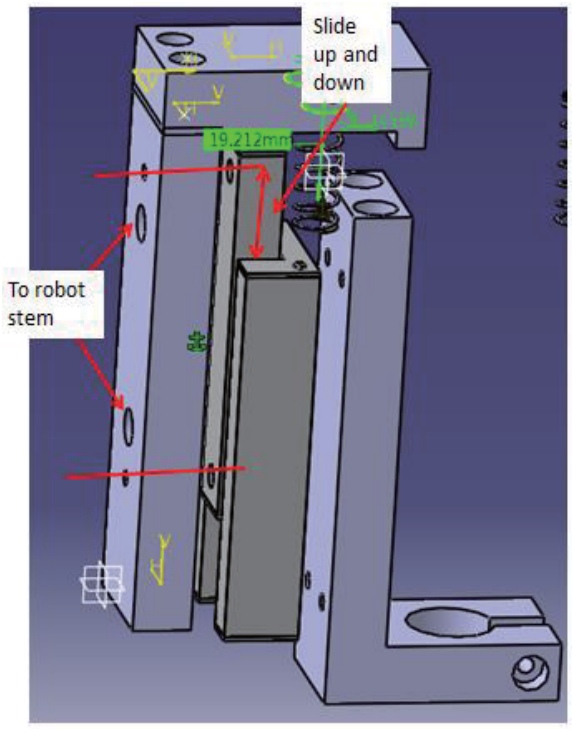

Figure 4.12: Concept of spring loaded design

After trial tests of the initial design, an issue is found out with regard to the probe holder's griping part because the probe is not been held steady enough. There are two main reasons. First, because the flexibility of ABS is not as good as that of stainless steel, even when the bolt is tight the contact of the gripper and the probe is not as firm. Secondly the contact area of the gripper with probe is not sufficient big to prevent the probe from slight tilting when the force is applied horizontally (robot moving direction) and vertically (spring load force) at the same time. As a result, in the experiment, the ECT signal shifts at the beginning and when the robot movement switches its direction. Again this very slight motion is hard to visually observed yet affects ECT signal due to the sensitivity of ECT probe itself. The higher frequency it is, the more sensitive the probe and the more tilting can affect the signal. In Figure 4.13 a new holder is designed using extra gripper in order to ensure the probe is held in its position

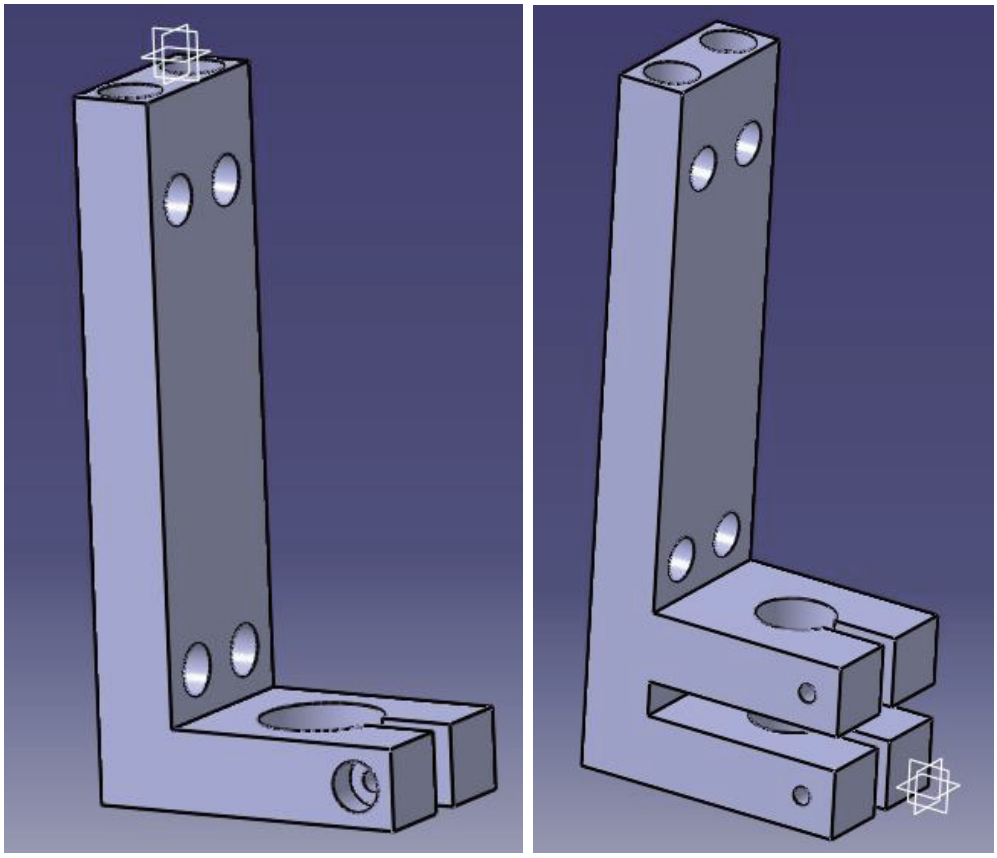

(a) (b)

Figure 4.13: (a) Original holder grip design, (b) Double grip design for new holder

As shown in Figure 4.14, 3D assembly of the spring loaded holder, it is able to overcome the previously mentioned issues and to perform a steady grip and yet fixable vertical motion.

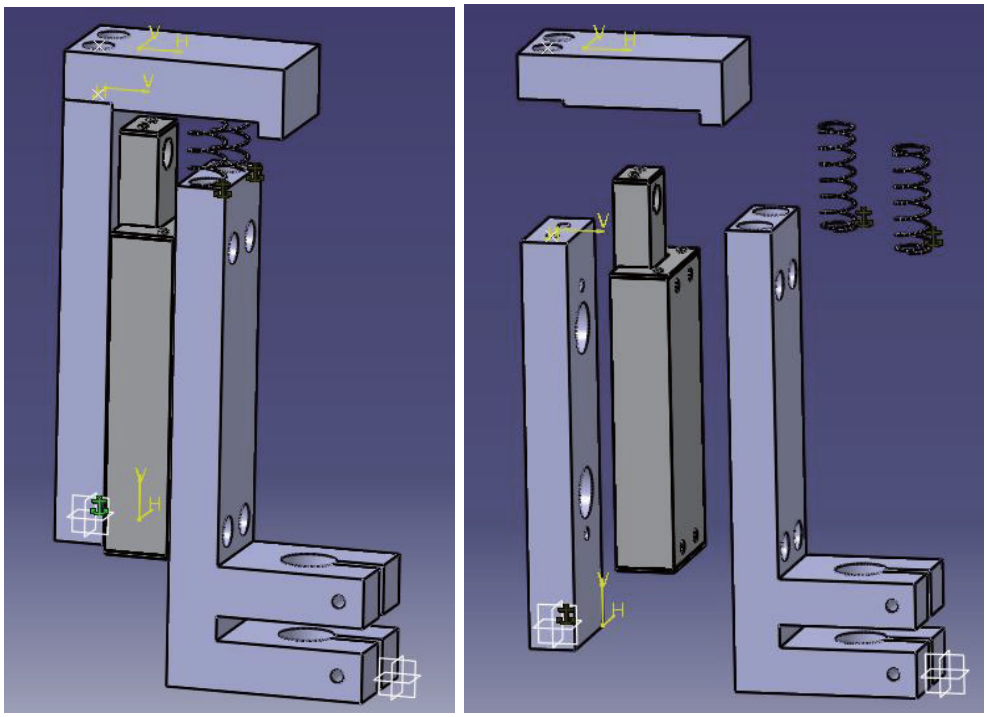

Figure 4.14: Spring load holder 3D assembly drawing

As shown in Figure 4.15 where the holder has been assembled onto the robot, another small adjustment is made in the griper. As mentioned before, because ABS is not as fixable as SS in terms of plastic deformation, using bolt to tight the gripper is less effective than using SS. A Polyethylene (PE) made sleeve is used to overcome the drawback of ABS.

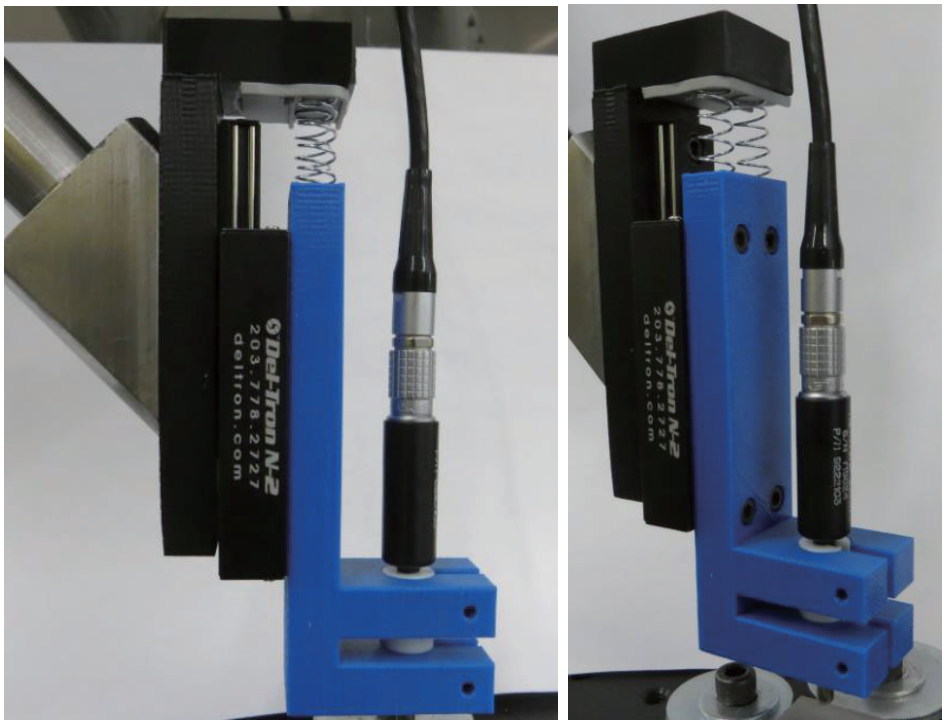

Figure 4.15: Spring loaded holder with probe installed

Figure 4.16 shows the assembly of robot and spring loaded probe holder together with the 6 robot arm. The current design is only for flat surface ECT scan, with further progress of the other team members in this project, the probe holder will be improved to accommodate the test parts with more complex geometry.

Figure 4.16: Spring loaded holder installation with robot arm and ECT equipment

4.5 Interface software design

Furthermore, a user friendly interface is developed which embeds the functions of data filtering, data plotting, feature extraction and crack depth prediction. The interface will be used as computer aid software to help inspectors.

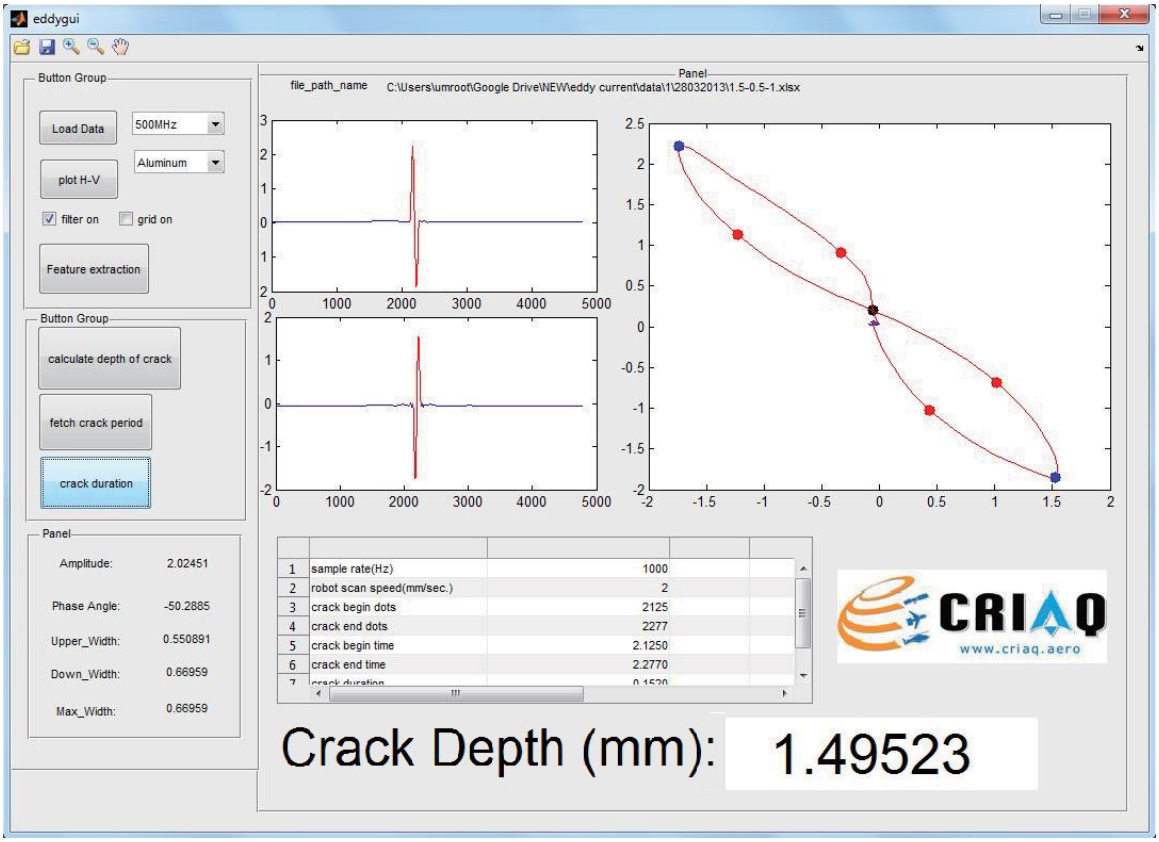

Figure 4.17: ECT user friendly interface

Shown in Figure 4.18 the first function group is data operation group. It enables users to load data, plot the data, and get data features. The two pop-up menus provide user the option to choose different test frequencies and sample materials. When they are selected, the program will switch to different trained fuzzy logic engine to process the signal. Also the user can turn on and off the filter and grid by clicking on respected check boxes. Finally the user can click feature extraction button to extract features of crack which will be shown on x-y plot with color coded feature indications.

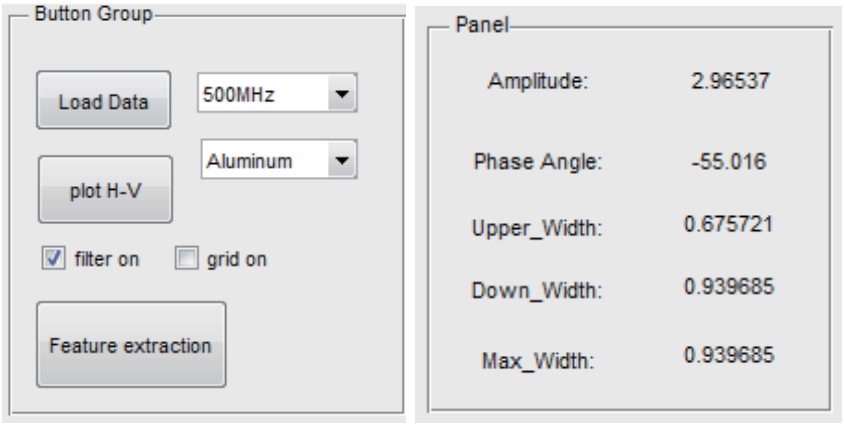

Figure 4.18: User interface function group1

As shown in Figure 4.19 the second function group provides signal processing operation. When click "calculate depth of crack" the program will process the signal based on extracted signal features via trained fuzzy logic engine. By clicking "fetch crack period" button, the program will eliminate the lift-off effect as mentioned in Chapter 3. By clicking "crack duration" and input sample rate and robot scan speed the program can calculate some useful information, such as the crack start time, end time, and whole crack duration (unit in second). These information can serve as extra reference data and could be used to assist robot scan.

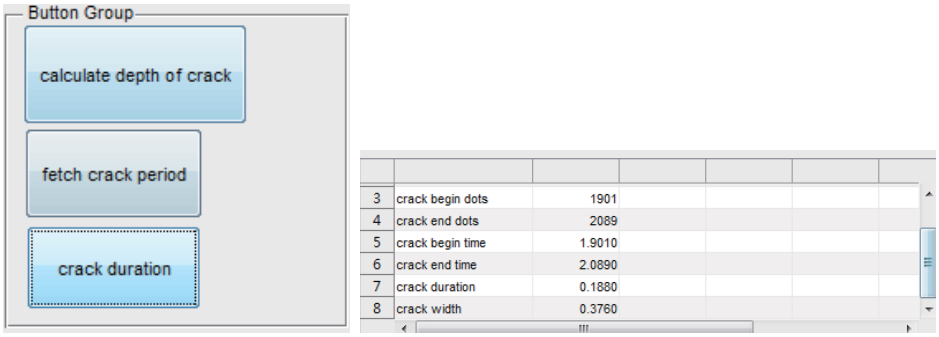

Figure 4.19: User interface function group2

4.6 Conclusion

In this chapter, an analog to digital ECT data acquisition system is built up for a 6-axis robot arm. The the system is capable of collecting the data and providing the

communication function between the computer and robot, which is sending 12V analog signal to the controller when a crack is encountered. The constraints on budget and time are taken in to consideration during spring loaded probe design and manufacture. Several adjustments according to structure design and material selection are carried out based on multiple experiments as well as the advice from team members. In addition, a user friendly software interface is developed with ECT signal processing functions. Future work includes programming the computer sending command to robot controller to record the coordinate based on crack pulse signal sent by data acquisition system via I/O port. And new probe holder design suitable for complicated component scan is expected to be delivered which is beyond the scope of this study.

Chapter 5

Experimental results

Various experiments of the developed intelligent ECT system are carried out on the known notch cracks with different depths. The eddy current equipment is Nortec® 500S testing unit from Olympus®, and the probe is differential reflection probe (PRL/500 kHz - 3 MHz/D). Eddy current scan is processed manually in order to simulate the industrial scan process. Extensive experiments have been performed to test the developed intelligent ECT system. The main results are presented on the three stages of intelligent system design: 1. Data acquisition with known notch cracks 2. Fuzzy logic engine training and 3 Fuzzy logic engine testing for crack detection. The test is performed using different frequencies. Six different depths of cracks are distributed in two aluminum samples as sample1:0.2mm, 0.51mm, 1.02mm and sample2: 0.8mm, 1.5mm, 2mm.

5.1 ECT data aquired from crack pendicular to scan surface

As shown from Table 5.1 to Table 5.4 different frequencies are used in the two notch crack samples. With the increase of depth crack features: phase angle, amplitude, and max width increase as well. For each set of collected data under different frequency, wavelet filter is used to remove the noise and extracted three key features: angle, amplitude and maximum width relating to the crack information.

Table 5.1: ECT signal features of sample 1 with frequency from 0.4Mhz to 0.8MHz

frequency (MHz)	**phase angle (volt)**	**amplitude (volt)**	**maxwidth (volt)**	**crack depth (mm)**
0.4	-36.56	0.50	0.47	0.8
	-49.54	1.46	0.63	1.5
	-54.07	2.15	0.69	2.0
0.6	-34.27	0.55	0.55	0.8
	-46.32	1.51	0.65	1.5
	-52.39	2.24	0.69	2.0
0.7	-43.70	0.79	0.47	0.8
	-52.80	1.93	0.52	1.5
	-55.96	2.61	0.60	2.0
0.8	-38.77	0.68	0.45	0.8
	-48.05	1.60	0.57	1.5
	-53.65	2.48	0.63	2.0

Table 5.2: ECT signal features of sample 1 with frequency from 0.9MHz to 2.0MHz

frequency(MHz)	**phase angle (volt)**	**amplitude (volt)**	**maxwidth (volt)**	**crack depth (mm)**
0.9	-45.02	0.89	0.45	0.8
	-53.21	2.03	0.49	1.5
	-56.00	2.72	0.51	2.0
1	-45.52	0.92	0.42	0.8
	-54.92	2.18	0.54	1.5
	-57.34	2.95	0.54	2.0
1.5	-43.83	0.96	0.49	0.8
	-51.34	2.11	0.55	1.5
	-54.17	2.84	0.67	2.0
2	-39.14	1.02	0.61	0.8
	-49.49	2.53	0.72	1.5
	-51.15	3.30	0.80	2.0

Table 5.3: ECT signal features of sample 2 with frequency from 0.4Mhz to 0.8MHz

frequency(MHz)	**phase angle (volt)**	**amplitude (volt)**	**maxwidth (volt)**	**crack depth (mm)**
0.4	-52.06	1.80	0.63	0.8
	-56.52	2.36	0.72	1.5
	-54.98	2.44	0.72	2.0
0.6	-46.98	1.54	0.60	0.8
	-50.10	2.04	0.63	1.5
	-52.59	2.52	0.69	2.0
0.7	-56.00	2.38	0.60	0.8
	-56.44	2.79	0.58	1.5
	-57.71	2.98	0.65	2.0
0.8	-50.80	2.04	0.55	0.8
	-53.56	2.59	0.59	1.5
	-52.47	2.63	0.67	2.0

Table 5.4: ECT signal features of sample 2 with frequency from 0.9MHz to 2.0MHz

frequency(MHz)	**phase angle (volt)**	**amplitude (volt)**	**maxwidth (volt)**	**crack depth (mm)**
0.9	-55.37	2.40	0.46	0.8
	-56.69	2.94	0.50	1.5
	-58.50	3.17	0.57	2.0
1	-56.15	2.57	0.48	0.8
	-58.03	3.22	0.63	1.5
	-58.34	3.24	0.59	2.0
1.5	-52.43	2.46	0.55	0.8
	-54.36	3.14	0.62	1.5
	-54.69	3.20	0.70	2.0
2	-50.51	2.95	0.64	0.8
	-52.68	3.42	0.65	1.5
	-51.94	3.58	0.67	2.0

5.1.1 Data analysis and fuzzy decision making results

By comparing the two samples, it is noticeable that the opening of the notch crack is different which indicates a possible hypothesis that the width of signal could be not only related with the depth of crack but also corresponding to the opening with of notch crack. However as a result of insufficient data, further theoretical work needs to be carried out in order to support experimental result.

After the feature extraction process, 5 sets of the features are used to train fuzzy

logic and one set is used to validate the training result. The training results using the amplitude and phase angle are shown in Table 5.5. A semi-auto MF and numbers of MF tuning program is developed to find the proper MF and the number of MF, which can be used for ANFIS training parameters. In Table 5.5, the verifying result is close to the actual depth of crack and the accuracy is shown by accurate rate. With adequate sets of data it is possible to find a universal MF as well as the numbers of MFs for data from fixed frequency. Whereas as shown in Table 5.5, due to lack of data (only 6), different MF as well as numbers of MFs are obtained via training program at the same frequency. The accuracy rate is calculated as follows.

$$Accuracy\,Rate = \frac{test\ data - |test\ data - actual\ data|}{actual\ data} \times 100\% \qquad (5.1)$$

Table 5.5: Fuzzy logic decision making results

test frequency	type of MF	numbers of MFs		depth of crack (mm)	fuzzy logic result	accurate rate
		input1	input2			
0.4MHz	trimf	6	3	0.5	0.53	94.40%
	gbellmf	3	9	0.8	0.79	98.93%
	trimf	3	3	1.0	1.00	100.00%
	trapmf	2	3	1.5	1.50	99.98%
0.6MHz	trimf	2	4	0.5	0.51	98.45%
		6	2	0.8	0.81	98.97%
	trapmf	4	2	1.0	1.08	92.43%
				1.5	1.56	95.86%
0.7MHz	gbellmf	4	4	0.5	0.52	95.70%
	trapmf	4	6	0.8	0.81	99.09%
		5	8	1.0	1.00	99.96%
	trimf	7	4	1.5	1.51	99.52%
0.8MHz	trapmf	4	2	0.5	0.48	96.34%
		9	2	0.8	0.81	98.86%
	trimf	7	6	1.0	0.99	99.36%
		7	5	1.5	1.50	99.90%
0.9MHz	trimf	3	8	0.5	0.51	98.56%
	gbellmf	5	5	0.8	0.79	98.85%
	trimf	9	3	1.0	1.01	98.66%
	trapmf	4	2	1.5	1.50	99.95%
1.0MHz	trimf	3	5	0.5	0.50	99.36%
	gbellmf	4	8	0.8	0.79	99.24%
	trimf	7	3	1.0	1.00	99.57%
		8	9	1.5	1.50	99.83%
1.5MHz	trimf	8	4	0.5	0.51	97.49%
	trapmf	6	2	0.8	0.79	99.08%
	trimf	8	7	1.0	0.96	96.31%
		2	6	1.5	1.49	99.20%
2.0MHz	trimf	8	4	0.5	0.51	97.49%
	trapmf	6	2	0.8	0.79	99.08%
	trimf	8	7	1.0	0.96	96.31%
	trapmf	8	2	1.5	1.51	99.33%

Because the two samples could have different notch opening, fuzzy logic training was carried out by dividing the signal features sample by sample, and adding width as a third feature. As shown in Table 5.6 due to insufficient training data the result

is not good and further investigation is need to be done in the future

Table 5.6: Fuzzy logic decision making result with width

sample1							
test frequency	type of MF	numbers of MFs			depth of crack (mm)	fuzzy logic result (mm)	accurate rate
		input1	input2	input3			
0.4MHz	gbellmf	2	2	2	0.5	0.56	87.71%
0.6MHz	trapmf	2	2	2		0.54	91.53%
0.7MHz	gbellmf	2	2	2		0.33	66.06%
0.8MHz	pimf	2	2	2		0.44	87.94%
0.9MHz	trimf	2	2	3		0.50	99.74%
1.0MHz	trimf	2	2	3		0.50	99.74%
1.5MHz	gaussmf	2	2	2		0.23	46.89%
2.0MHz	gbellmf	2	2	2		0.47	93.63%

5.2 ECT data aquired from crack with angle to scan surface

Another experiment is carried out by using the angled crack Figure 5.1.

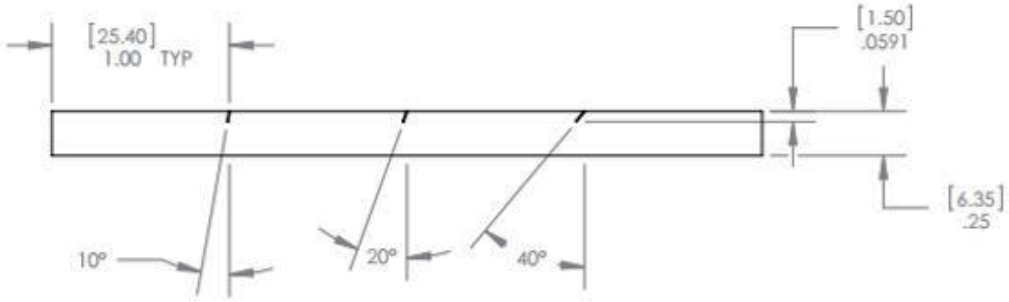

Figure 5.1: Angled crack sample spec.

The signal plots of the crack with 10 degree under frequency 0.1, 0.5, 1.5MHz are shown in Figure 5.2, Figure 5.3, and Figure 5.4 respectively. The corresponding signal features are shown in Table 5.7.

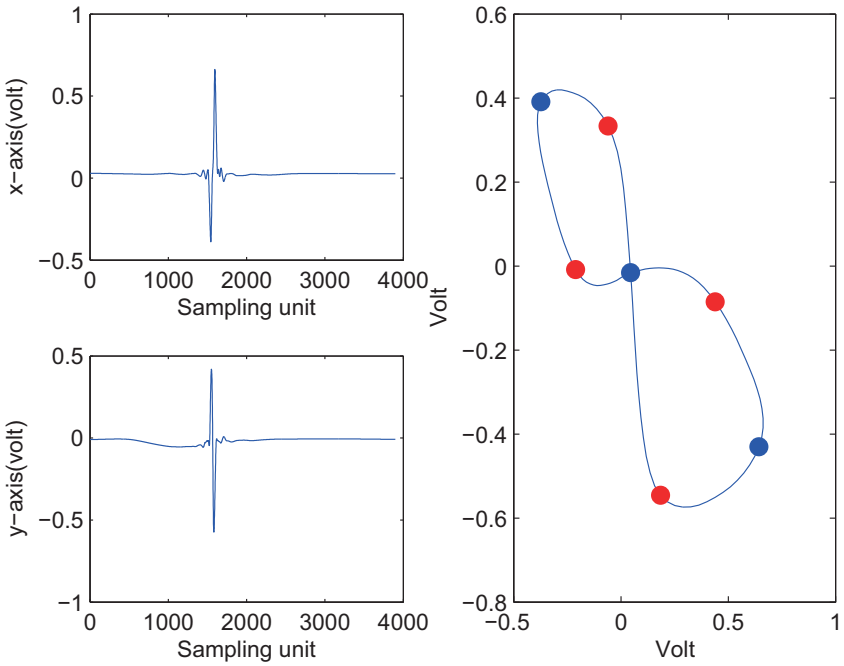

Figure 5.2: 10 degree with test frequency of 0.1MHz.

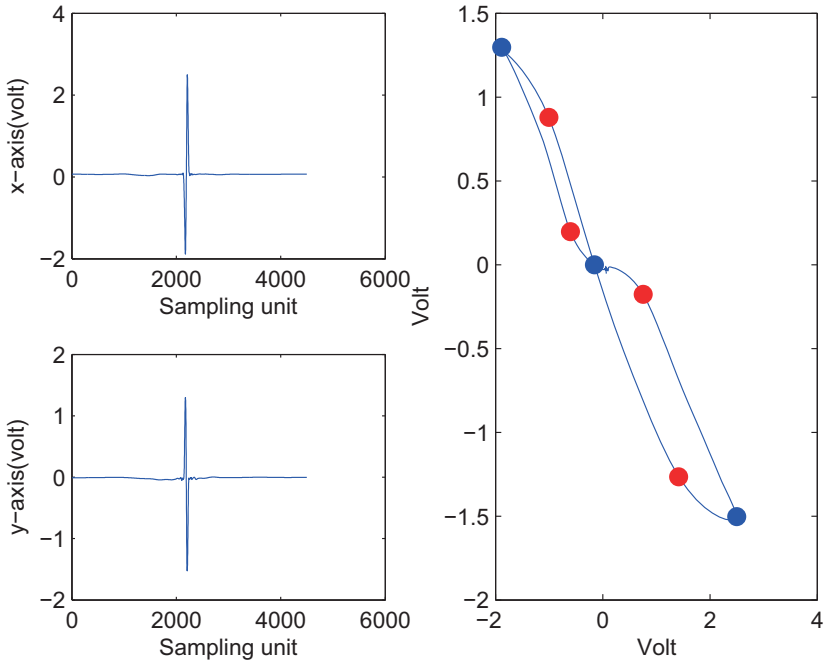

Figure 5.3: 10 degree with test frequency of 0.5MHz.

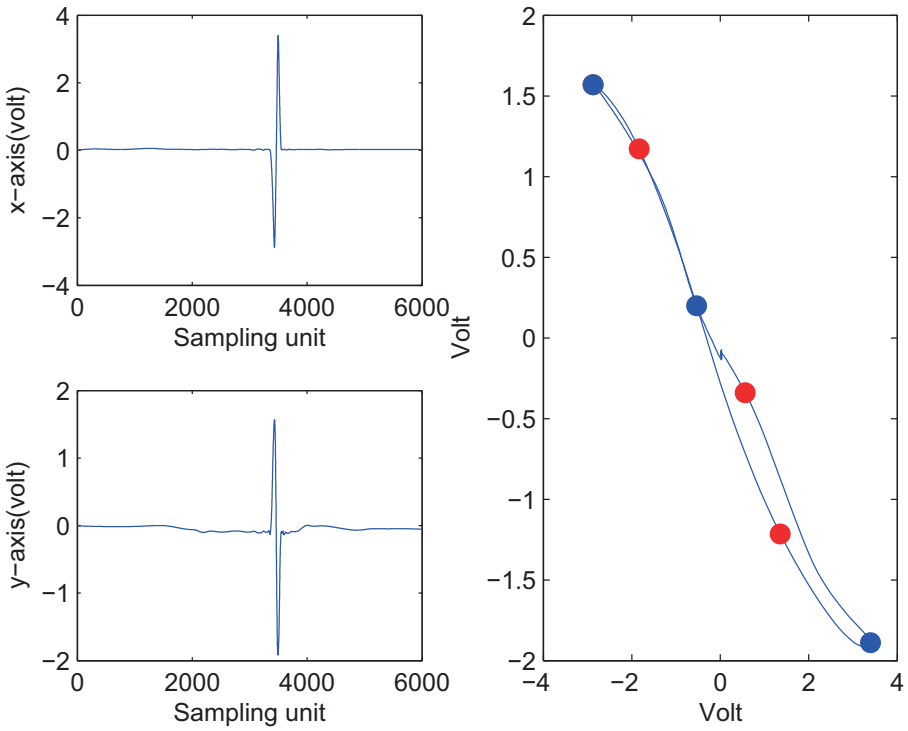

Figure 5.4: 10 degree with test frequency of 1.5MHz.

Table 5.7: ECT signal features of angled sample (10degree) with different frequencies

frequency(MHz)	**phase angle up (volt)**	**phase angle down (volt)**	**amplitude up (volt)**
0.1	49.48	42.24	0.36
0.5	42.59	46.69	1.88
1.0	37.28	50.88	3.07
frequency(MHz)	**amplitude down (volt)**	**width up (volt)**	**width down (volt)**
0.1	0.63	0.35	0.52
0.5	2.50	0.31	0.62
1.0	3.59	0.18	0.40

The signal plots of the crack with 20 degree under frequency 0.1, 0.5, 1.5MHz are shown in Figure 5.5, Figure 5.6, and Figure 5.7 respectively. The corresponding signal features are shown in Table 5.8.

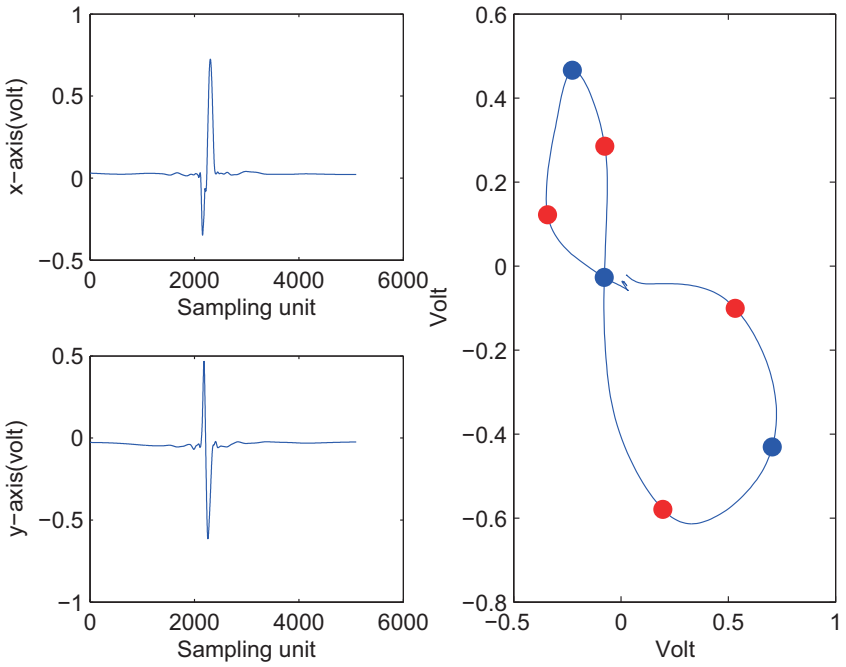

Figure 5.5: 20 degree with test frequency of 0.1MHz.

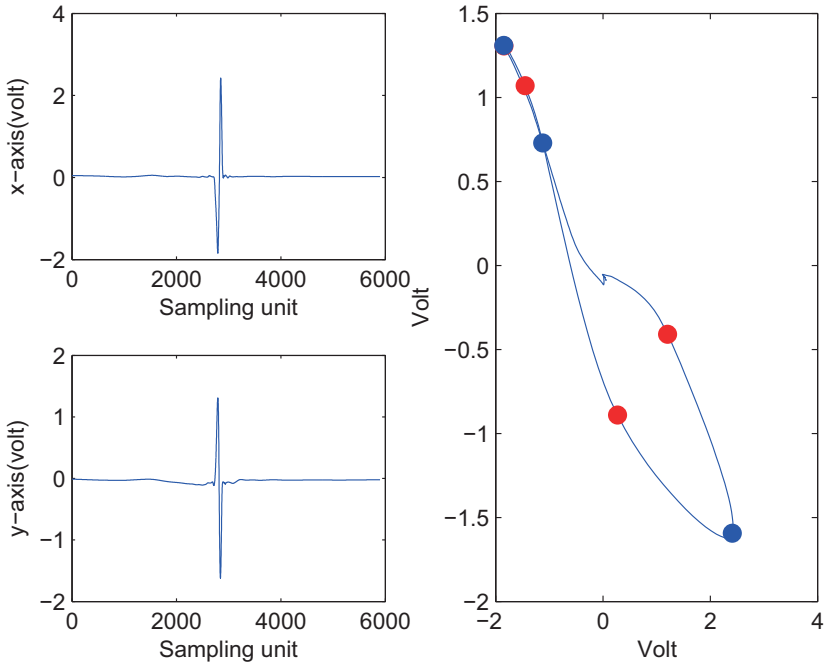

Figure 5.6: 20 degree with test frequency of 0.5MHz.

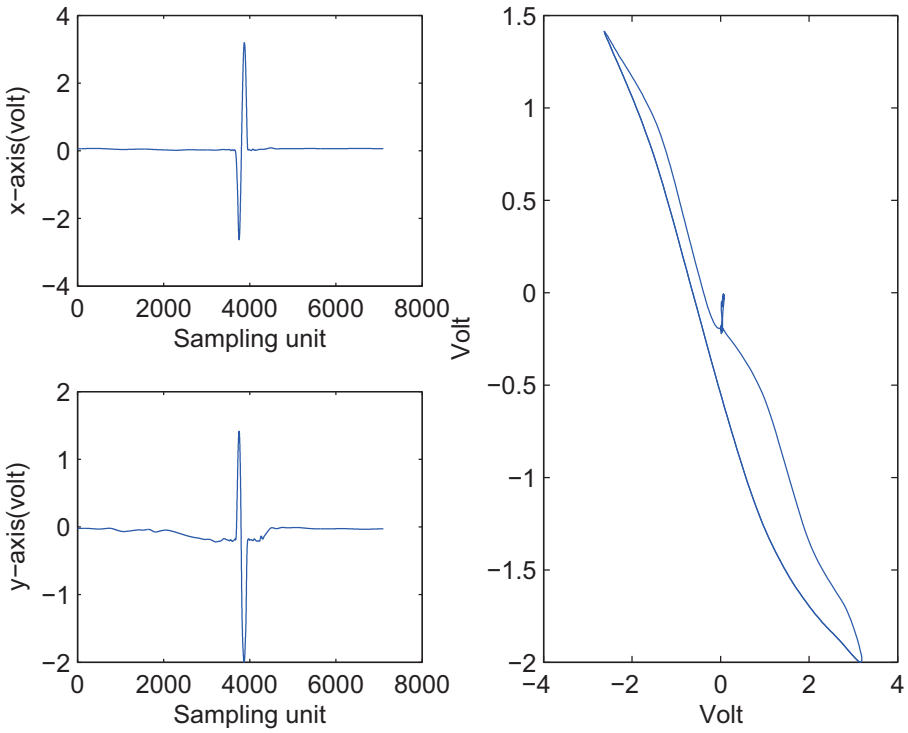

Figure 5.7: 20 degree with test frequency of 1.5MHz.

Table 5.8: ECT signal features of angled sample (20degree) with different frequencies

frequency(MHz)	**phase angle up (volt)**	**phase angle down (volt)**	**amplitude up (volt)**
0.1	36.35	48.04	0.27
0.5	15.70	64.55	2.58
1.0	no “8” shape	no “8” shape	no “8” shape
frequency(MHz)	**amplitude down (volt)**	**width up (volt)**	**width down (volt)**
0.1	0.66	0.27	0.67
0.5	3.14	0.06	0.91
1.0	no “8” shape	no “8” shape	no “8” shape

The signal plots of the crack with 40 degree under frequency 0.1, 0.5, 1.5MHz are shown in Figure 5.8, Figure 5.9, and Figure 5.10 respectively. The corresponding signal features are shown in Table 5.9.

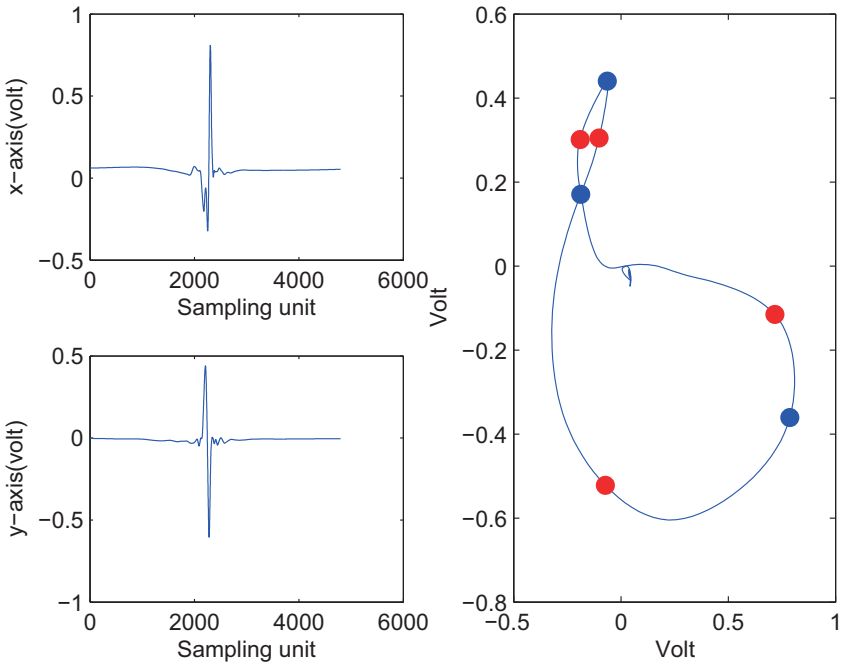

Figure 5.8: 40 degree with test frequency of 0.1MHz.

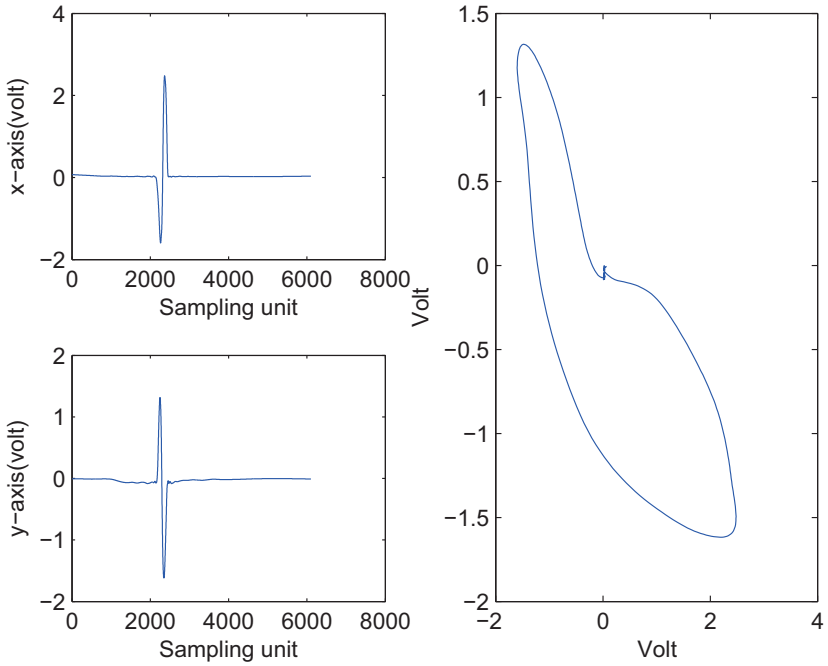

Figure 5.9: 40 degree with test frequency of 0.5MHz.

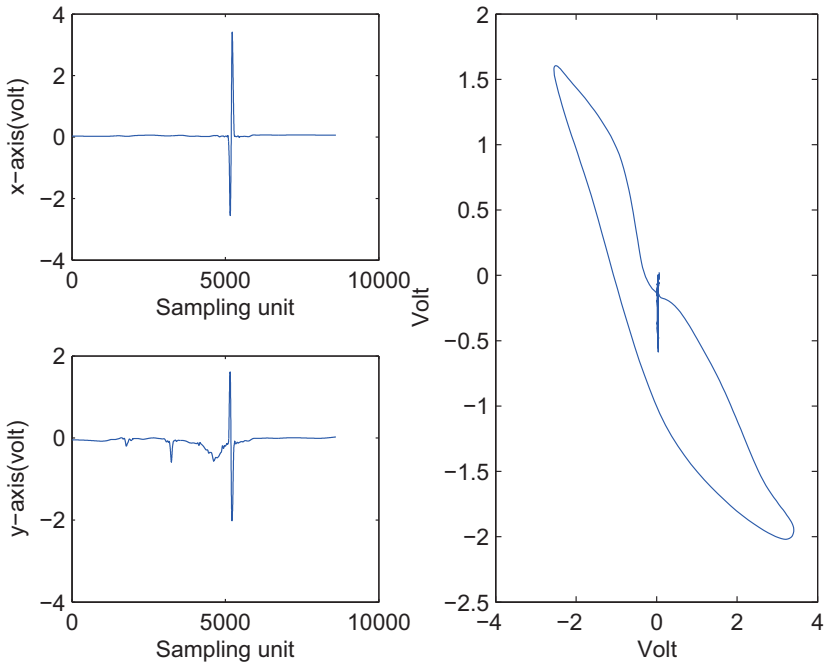

Figure 5.10: 40 degree with test frequency of 1.5MHz.

Table 5.9: ECT signal features of angled sample (40degree) with different frequency

frequency(MHz)	**phase angle up (volt)**	**phase angle down (volt)**	**amplitude up (volt)**
0.1	-32.42	56.92	0.22
0.5	no “8” shape	no “8” shape	no “8” shape
1.0	no “8” shape	no “8” shape	no “8” shape
frequency(MHz)	**amplitude down (volt)**	**width up (volt)**	**width down (volt)**
0.1	0.92	0.07	0.69
0.5	no “8” shape	no “8” shape	no “8” shape
1.0	no “8” shape	no “8” shape	no “8” shape

According to above signal plot and features, it is observed that the crack angle have relationship with the ratio of upper loop width and down loop width which will be investigated in the future.

It is known that the accuracy of the intelligent detection system largely depends on the fuzzy logic rules. A complete set of fuzzy rules are expected to include as many as cracks that could exist in the inspection parts. Hence, large amount of data on smaller cracks are needed in this study.

5.3 Conclusion

In this chapter,extensive experiments have been carried out to test the developed intelligent ECT crack detection system. The experimental results demonstrate that the developed intelligent detection system can detect the crack and predict the crack depth with reasonable accuracy (above 90 %). The future works include detecting

the smaller cracks and the cracks with more complicated shapes and improving the user interface for real industrial application.

Chapter 6

Conclusion

6.1 Summary of research work

In this thesis, ECT test and ECT signal processing techniques have been reviewed. User-friendly ECT data processing software is done based on current crack samples. In addition, a robot based analog to digital input and digital to analog output data acquisition system is built. The spring loaded ECT probe holder is designed and manufactured via 3D printing technology.

In the design of spring loaded probe and ECT data acquisition system, the research work is summarized as follows:

- A Simulink based data acquisition system is established. An online calculated threshold based on data mean value in first 2 (modifiable) seconds is used to generate pulse (+12V) signal in order to notify the robot controller when encountered with crack.

- Considering the constraints of cost and time and previous prototype holder design, a spring loaded probe is manufactured via 3D printer and installed on robot arm. The ball bearing slider is used to guarantee a smooth up and down motion. And spring loaded mechanism compensates robot calibration error, protects the probe from collision and avoid too much lift-off.

In the design of an advanced fuzzy based signal processing system, the research work is summarized as follows:

- A new feature–the width of crack along with the amplitude and phase angle are extracted based on 8 shaped signal of differential probe. A signal filter based on wavelet transform is developed and demonstrated with good noise removal ability.

- A set of ECT crack data is collected and fuzzy logic is trained based on ANFIS and the width of signal is found to be related to crack width and the crack angle.

- A user friendly interface is designed to show the original signal, perform the filter, fetch the useful signal and make final decision via trained fuzzy logic. Finally the depth of the crack can be displayed to assist the inspectors to make final decision.

- The accuracy rate of the crack detection is calculated and is accepted by two industrial partners.

6.2 Future work

The following research work can be investigated in the future:

- The communication through computer to robot controller needs to be done in order to record the robot arm coordinate. With this function in data acquisition system, the robot can perform online crack scan and after the scan the robot is able to go back to crack indications either to double check the crack or perform more detailed scan.

- The width of crack signal investigation is needed to be done since the current experiment indicates it could be related to crack opening as well as have relationship to the crack angle. In addition, theoretical inverse modeling based on ECT signal research as well as simulation is needed to verify the real relationship between features of signal and the crack geometry.

- More data collection is needed to train the fuzzy logic in order to find a universal membership function and numbers of membership function for one test frequency. Currently robot system is under development for scanning much smaller crack samples provided by Pratt & Whitney Canada.

6.3 Acknowledgements

This study is supported by CRIAQ, NSERC and industrial partner: CNRC Aerospace, Pratt & Whitney Canada, and L-3 Communications.

Bibliography

[1] A. Yashan, W. Bisle, and T. Meier, "Inspection of hidden defects in metal-metal joints of aircraft structures using eddy current technique with gmr sensor array," *Proc. 9th ECNDT, Berlin*, 2006.

[2] S. W. Smith, *Digital signal processing: a practical guide for engineers and scientists*. Newnes, 2003.

[3] N. D. T. recourse center, "Basic principles of eddy current inspection." `http://www.ndt-ed.org/EducationResources/CommunityCollege/EddyCurrents/Introduction/IntroductiontoET.htm`.

[4] W. Lord and R. Palanisamy, "Development of theoretical models for nondestructive testing eddy-current phenomena," in *Eddy-current Characterization of Materials and Structures: A Symposium*, no. 722, p. 1, ASTM International, 1981.

[5] N. D. T. recourse center, "Depth of penetration and current density." `http://www.ndt-ed.org/EducationResources/CommunityCollege/EddyCurrents/Physics/depthcurrentdensity.htm`.

[6] L.-X. Wang, "A course in fuzzy systems and control, 1997," *Prentice-Hall, Englewood Cliffs, New Jersey, ISBN 0*, vol. 13, no. 540882, p. 2.

[7] M. A. Boyacioglu and D. Avci, "An adaptive network-based fuzzy inference system (anfis) for the prediction of stock market return: the case of the istanbul stock exchange," *Expert Systems with Applications*, vol. 37, no. 12, pp. 7908–7912, 2010.

[8] J.-S. Jang, "Anfis: adaptive-network-based fuzzy inference system," *Systems, Man and Cybernetics, IEEE Transactions on*, vol. 23, no. 3, pp. 665–685, 1993.

[9] Y. E. corporation, "Motoman xrc operators manual user function," *YASKAWA Electric corporation*, no. MRS50070.

[10] U. W. website. `http://www.uniwest.com/US-454A_US-454-P4.aspx`.

[11] O. website. `http://www.olympus-ims.com/en/500/`.

[12] N. Instruments. `http://sine.ni.com/nips/cds/view/p/lang/en/nid/14136`.

[13] N. Instruments. `http://sine.ni.com/nips/cds/view/p/lang/en/nid/201987`.

[14] "Motoman xrc instruction manual motoman-sv3x, -sv3xl," *YASKAWA Electric corporation*, no. MRS52050.

[15] M. S. data sheet. http://research.fit.edu/rassl/documents/SV3X.pdf.

[16] N. D. T. recourse center, "Nondestructive testing in the aerospace industry." `http://www.fermentas.com/techinfo/nucleicacids/maplambda.htm`.

[17] T. L. Adair, D. H. Wehener, M. G. Kindrew, H. I. Winter, and B. MacCracken, "Automated fluorescent penetrant inspection (fpi) system is triple a," in *AUTOTESTCON'98. IEEE Systems Readiness Technology Conference., 1998 IEEE*, pp. 498–529, IEEE, 1998.

[18] M. V. J. Zheng, W. Xie and L. Birglen, "Design of advanced automatic data fusion software for turbine blade fpi analysis," *39th Annual Review of Progress in Quantitative Non-destructive Evaluation*, July.

[19] J. García-Martín, J. Gómez-Gil, and E. Vázquez-Sánchez, "Non-destructive techniques based on eddy current testing," *Sensors*, vol. 11, no. 3, pp. 2525–2565, 2011.

[20] R. Palanisamy and W. Lord, "Prediction of eddy current probe signal trajectories," *Magnetics, IEEE Transactions on*, vol. 16, no. 5, pp. 1083–1085, 1980.

[21] J. Bowler, S. Jenkins, L. Sabbagh, and H. Sabbagh, "Eddy-current probe impedance due to a volumetric flaw," *Journal of Applied Physics*, vol. 70, no. 3, pp. 1107–1114, 1991.

[22] S. J. Norton and J. R. Bowler, "Theory of eddy current inversion," *Journal of applied physics*, vol. 73, no. 2, pp. 501–512, 1993.

[23] B. Auld, S. Jefferies, and J. Moulder, "Eddy-current signal analysis and inversion for semielliptical surface cracks," *Journal of Nondestructive Evaluation*, vol. 7, no. 1-2, pp. 79–94, 1988.

[24] M. Cacciola, F. C. Morabito, D. Polimeni, and M. Versaci, "Fuzzy characterization of flawed metallic plates with eddy current tests," *Progress In Electromagnetics Research*, vol. 72, pp. 241–252, 2007.

[25] B. Silwal *et al.*, "Computation of eddy currents in a solid rotor induction machine with 2-d and 3-d fem," 2012.

[26] P. E. Mix, *Introduction to nondestructive testing: a training guide*. John Wiley & Sons, 2005.

[27] B. Auld and J. Moulder, "Review of advances in quantitative eddy current nondestructive evaluation," *Journal of Nondestructive Evaluation*, vol. 18, no. 1, pp. 3–36, 1999.

[28] B. Auld, F. Muennemann, and D. Winslow, "Eddy current probe response to open and closed surface flaws," *Journal of Nondestructive Evaluation*, vol. 2, no. 1, pp. 1–21, 1981.

[29] J. R. Jang, *MATLAB: Fuzzy Logic Toolbox User's Guide: Version 1.* Math Works, 1997.

[30] L. A. Zadeh, "Fuzzy sets," *Information and control*, vol. 8, no. 3, pp. 338–353, 1965.

[31] L. A. Zadeh, "The concept of a linguistic variable and its application to approximate reasoningi," *Information sciences*, vol. 8, no. 3, pp. 199–249, 1975.

[32] D. Nauck, "Neuro-fuzzy systems: review and prospects," in *In Proceedings of Fifth European Congress on Intelligent Techniques and Soft Computing (EUFIT97)*, pp. 1044–1053, 1997.

[33] R. Grimberg, A. Savin, L. Iancu, and S. Chifan, "Fuzzy inference system used for a quantitative evaluation of the material discontinuities detected by eddy current sensors," *Sensors and Actuators A: Physical*, vol. 81, no. 1, pp. 248–250, 2000.

[34] R. Sikora and P. Baniukiewicz, "Reconstruction of crack profile using fuzzy logic," *COMPEL: The International Journal for Computation and Mathematics in Electrical and Electronic Engineering*, vol. 25, no. 3, pp. 616–626, 2006.

[35] S.-J. Song and Y.-K. Shin, "Eddy current flaw characterization in tubes by neural networks and finite element modeling," *NDT & E International*, vol. 33, no. 4, pp. 233–243, 2000.

[36] L. A. N. M. Lopez, D. K. S. Ting, and B. R. Upadhyaya, "Eddy-current signal interpretation using fuzzy logic artificial intelligence technique," in *IV Pan American Conference, Buenos Aires*, Citeseer, 2007.

[37] T. Chady, M. Enokizono, and R. Sikora, "Neural network models of eddy current multi-frequency system for nondestructive testing," *IEEE transactions on Magnetics*, vol. 36, no. 4, pp. 1724–1727, 2000.

[38] N. Yusa, W. Cheng, Z. Chen, and K. Miya, "Generalized neural network approach to eddy current inversion for real cracks," *NDT & E International*, vol. 35, no. 8, pp. 609–614, 2002.

[39] M. Misiti, Y. Misiti, G. Oppenheim, and J.-M. Poggi, "Matlab wavelet toolbox user\'s guide. version 3.," 2004.

[40] T. Takagi, J. R. Bowler, and Y. Yoshida, *Electromagnetic nondestructive evaluation*, vol. 1. IOS Press, 1997.

[41] B. Upadhyaya, W. Yan, M. Behravesh, and G. Henry, "Development of a diagnostic expert system for eddy current data analysis using applied artificial intelligence methods," *Nuclear engineering and design*, vol. 193, no. 1, pp. 1–11, 1999.

[42] Y. E. corporation, "25. motocom sdk function manual," *YASKAWA Electric corporation*, no. MRS50070.

Appendices

Appendix A

UniWest® US-454

Figure A.1: UniWest US-454 [10]

Equipment Features: [17] [18]

- Dual-frequency capability
- Frequency Range: 10 Hz to 10 MHz
- Bright, 6.5" flat panel LCD display
- High Speed Scanner connection
- Video input for camera or borescope

- Digital strip chart recorder
- Toggle between eddy current, video & strip chart recorder
- High Speed Scanner connection
- Sequential smart battery charger
- Programmable push button function keys
- Weight: 5lbs with battery, 4 lbs without battery
- Dimensions: 11.5” long X 7.5” high X 3” deep
- Used in industrial air conditioning inspection

Olympus® Nortec 500S

Figure A.2: Olympus Nortec 500S [11]

Equipment features [19]:

- Frequency Range: 50 Hz - 12 MHz
- Gain: 0 - 90 dB in 0.1 dB steps. The horizontal and vertical gains may be adjusted separately or together.
- Rotation: Variable 0 - 359 in 1 steps.
- Sweep: Variable from 0.005 - 4 seconds per division.
- Low Pass Filter: 10 - 500 Hz and wide band.
- High Pass Filter: Off or 2 to 500 Hz, 2 pole response.
- Probe Drive: 2, 6, 12 volts.
- Variable Persistence: 0.1 - 5 seconds.
- Trace Storage: Up to 200 traces can be stored for recall. The traces can be static or frozen and can contain up to 60 seconds of movement. The traces are stored with the date and time of capture.
- Program Storage: Up to 200 instrument set-ups may be stored and recalled. The date and time of storage is recorded with each set-up.

Appendix B

NationalInstruments® NI PCI-6229

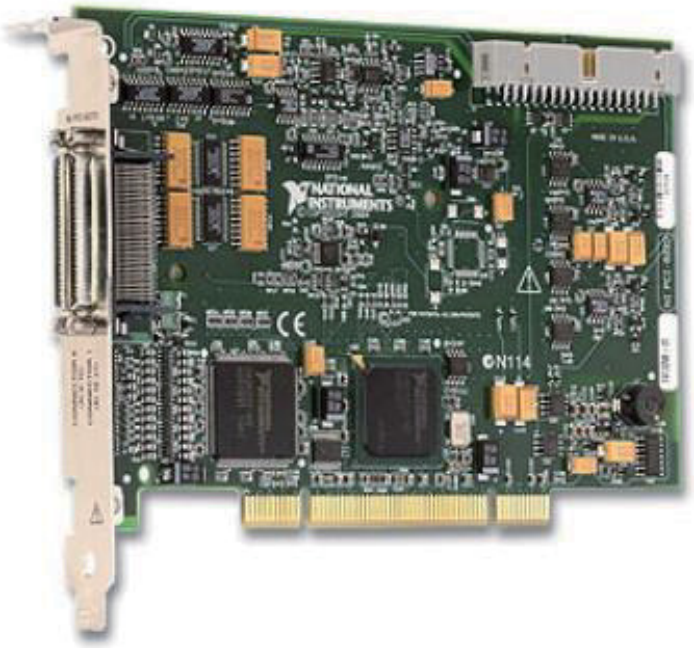

Figure B.1: National Instruments NI PCI-6229 [12]

Equipment features [20]:

- Four 16-bit analog outputs (833 kS/s)
- 48 digital I/O; 32-bit counters; digital triggering.
- Correlated DIO (32 clocked lines, 1 MHz).
- NIST-traceable calibration certificate and more than 70 signal conditioning options.

- Select high-speed M Series for 5X faster sampling rates or high-accuracy M Series for 4X resolution.
- NI-DAQmx driver software and NI LabVIEW SignalExpress interactive data-logging software.

NationalInstruments® NI USB-6009

Figure B.2: National Instruments NI USB-6009 [13]

Equipment features [21]:

- 8 analog inputs (14-bit, 48 kS/s).
- 2 analog outputs (12-bit, 150 S/s); 12 digital I/O; 32-bit counter.
- Bus-powered for high mobility; built-in signal connectivity OEM version available.
- Compatible with LabVIEW, LabWindows/CVI, and Measurement Studio for Visual Studio .NET.

Appendix C

$YASKAWA^{®}$ Motoman SV3X

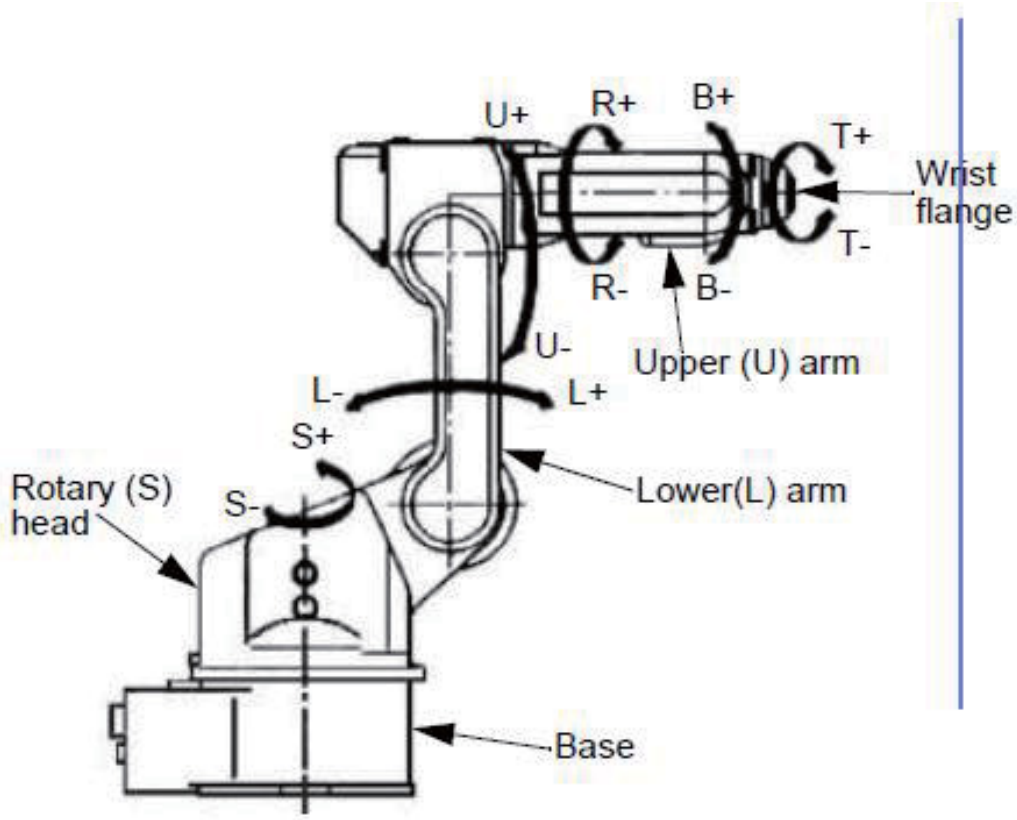

Figure C.1: SV3X robot arm axis [14]

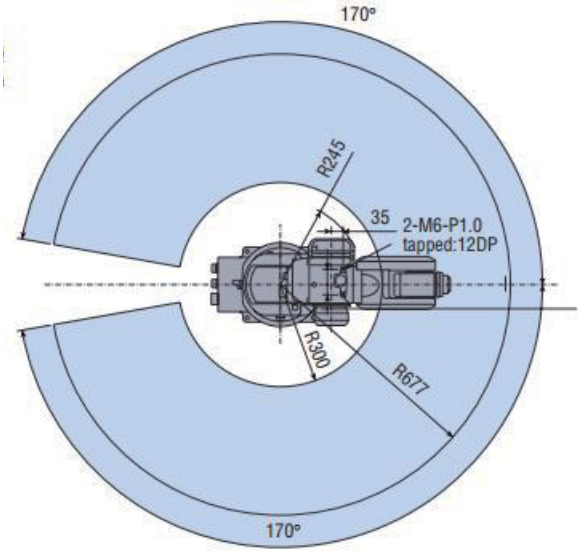

Figure C.2: SV3X robot arm operation area1 [15]

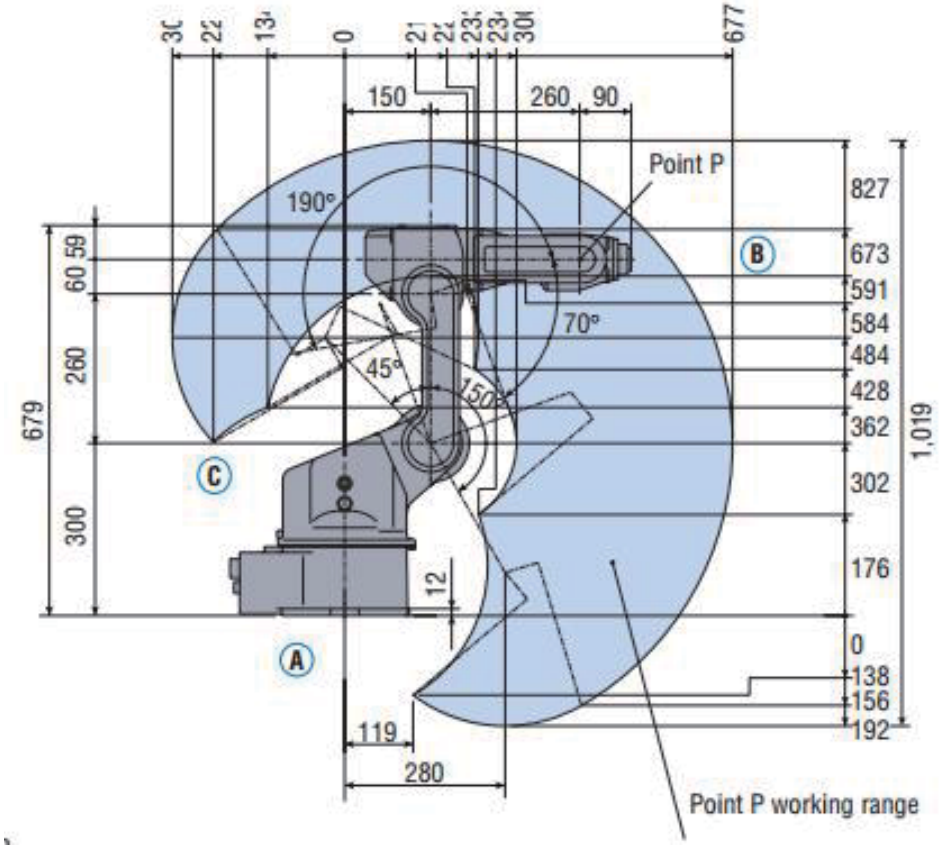

Figure C.3: SV3X robot arm operation area2 [15]